Lyle, M., Koizumi, I., Richter, C., and Moore, T.C., Jr. (Eds.), 2000
Proceedings of the Ocean Drilling Program, Scientific Results, Vol. 167

32. SEDIMENTARY RECORD OF THE CALIFORNIA CURRENT SYSTEM, MIDDLE MIOCENE TO HOLOCENE: A SYNTHESIS OF LEG 167 RESULTS[1]

Mitchell Lyle,[2] Itaru Koizumi,[3] Margaret L. Delaney,[4] and John A. Barron[5]

ABSTRACT

During Ocean Drilling Program Leg 167, the California continental margin was drilled from about 30°N to 42°N to sample high-resolution paleoceanographic and paleoclimatic records in the California Current system. Because of typically high sedimentation rates along the margin (80 to >200 m/m.y.), drilling has proved necessary to collect late Pleistocene sedimentary records that usually are sampled by standard piston cores in other oceanic regions. Triple piston coring on Leg 167 enabled us to construct continuous submillennial paleoceanographic records to about 2 Ma. In the offshore drill sites, continuous records were constructed into the Miocene. The oldest sediments recovered on Leg 167 have an age of ~14 Ma.

The California margin has an active diagenetic system driven by the degradation of organic matter. Leg 167 drilling provided a means to quantify the diagenetic processes within the deep sediment column and to study the links between sediment diagenesis and primary productivity.

This synthesis chapter also documents the oceanographic variability along the California margin at all time scales, from 10^3 to 10^6 yr. Millennial-scale variability is found in Santa Barbara Basin (drilled during Leg 146) and in nearby basins drilled during Leg 167. Leg 167 cores also captured millennial-scale variability in the northern and central California margin. Orbitally forced insolation changes invoke a strong response throughout the California margin. Sea-surface temperature (SST) measured by the alkenone $U^{k'}_{37}$ paleothermometer is highly coherent with the oxygen isotope record, being cold in glacials and much warmer in interglacials. Faunal and floral plankton assemblages vary strongly on the glacial–interglacial scale. Coastal plant communities show a glacial–interglacial variability that is most pronounced in the north, near the Cordilleran Ice Sheet.

Major changes in the sediments prior to the Pleistocene mark major late Neogene oceanographic events. Opaline silica burial in the middle and upper Miocene sections have step-like drops from high opal deposition in the middle Miocene. One major drop occurs at ~11 Ma and is roughly correlative with the eastern equatorial Pacific Miocene carbonate crash. A second major drop occurs at about 8 Ma, equivalent in age to the end of the Monterey Formation. A third drop occurs slightly younger than the end of the Miocene.

A lower Pliocene interval, roughly from 5 to 4.2 Ma, is low in all biogenic components. It separates the Miocene high-opal sediments from upper Pliocene high-carbonate sediments. High $CaCO_3$ deposition occurred all along the entire California margin in the late Pliocene, but $CaCO_3$ burial dropped abruptly with the beginning of Northern Hemisphere glaciation (2.6 Ma).

INTRODUCTION

The modern California Current system has well-known physical dynamics, chemical structure, biological standing stocks, and biogeochemical fluxes, but on paleoceanographic time scales (10^2–10^7 yr) its dynamics are poorly understood. Drilling during Ocean Drilling Program (ODP) Leg 167 was designed to explore the evolution of the California Current system and to study how the North Pacific Ocean has interacted with the global climate system from about 12 Ma to the present (Fig. 1). Many of the Leg 167 scientific party are also studying the effect of northeast Pacific paleoceanographic change on the regional climate of western North America, and how productivity along the California margin has evolved with changes in the California Current system.

Other Leg 167 priorities are to improve regional stratigraphy of the sediment column, to understand how paleoceanographic signals can be preserved or modified by diagenesis in a highly productive sedimentary system, and to understand how paleomagnetic signals are preserved on a rapidly sedimenting continental margin.

In this synthesis we will describe briefly what we have accomplished toward the Leg 167 objectives and then describe further work that should prove fruitful. With the immediate postcruise studies we have already profoundly improved our understanding of the California Current system and its variability on paleoceanographic time scales. The true synthesis work is just beginning, however. We are only just beginning to compare data between drill sites to study water column structure and are only just beginning detailed studies of the sedimentary record prior to the last 150 k.y. We have noted major changes in sediment deposition since the end of the middle Miocene but so far have only done reconnaissance-scale study of Neogene events (Ravelo et al., 1997). The prospects for future study are bright, however. The high quality of the Leg 167 sedimentary records will make it possible to study important climate transitions since 12 Ma in very high resolution.

Description of the Modern Environment

The California Current system is the eastern expression of the North Pacific subtropical gyre (Fig. 2). It carries cold, relatively fresh surface water out of the subarctic North Pacific and mixes it into warmer more saline water of the subtropical and tropical regions. The northern edge of the Leg 167 California margin drilling is roughly aligned with the modern position of the northern edge of the North Pacific subtropical gyre. Here the North Pacific Current flows across the Pacific, separating the cold nutrient-rich waters of the subarctic Alaska Gyre from the warm nutrient-depleted waters to the south. The southern Leg 167 drill sites reach into the southern reaches of the California current to permit latitudinal study of changes in strength of the California Current through time.

Because the California Current is an eastern boundary current, the region of southward flow is diffuse, especially when compared to the

[1]Lyle, M., Koizumi, I., Richter, C., and Moore, T.C., Jr. (Eds.), 2000. *Proc. ODP, Sci. Results,* 167: College Station TX (Ocean Drilling Program).

[2]Center for Geophysical Investigation of the Shallow Subsurface, Boise State University, Boise ID 83725, USA. mlyle@cgiss.boisestate.edu

[3]Division of Earth and Planetary Sciences, Graduate School of Science, Hokkaido University, Sapporo 060, Japan.

[4]U.S. Geological Survey, MS 910, Menlo Park CA 94025, USA.

[5]Ocean Sciences/Institute of Marine Sciences, University of California, Santa Cruz, Santa Cruz CA 95064, USA.

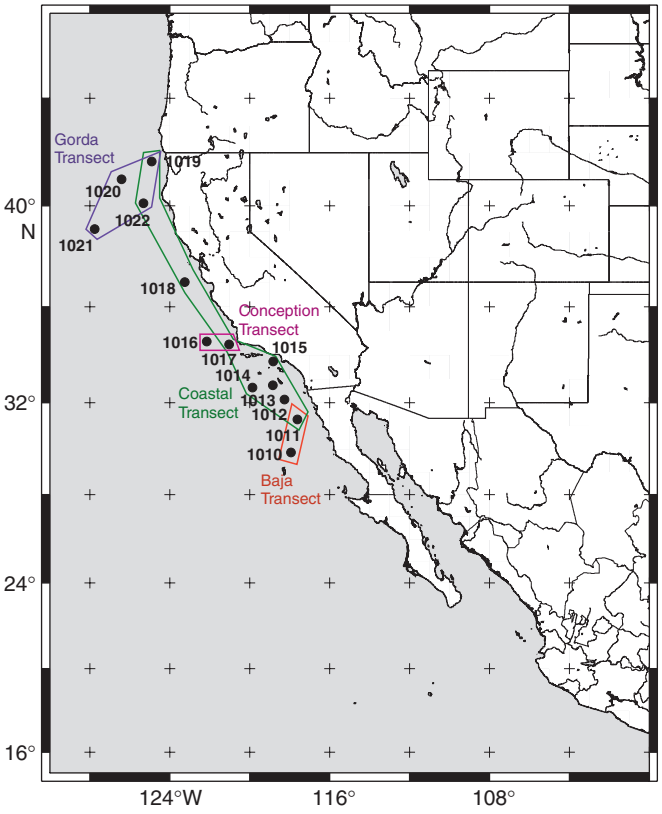

Figure 1. Sites drilled on Ocean Drilling Program Leg 167 along the Pacific coast of North America. The different transects are marked by boxes.

northward flow in the Kuroshio, the cognate western boundary current. Embedded within this diffuse flow are southward jets that separate nutrient-rich upwelled waters from the relatively barren offshore waters (e.g., Huyer et al., 1991). The core of the offshore California Current flow is located approximately 250–350 km from the coast of Oregon (~45°N) to as far south as Point Conception (~35°N; Hickey, 1979; Lynn and Simpson, 1987).

The California Current system has strong seasonal and interannual cycles. The pattern of winds along the coast controls seasonal variations in the current strength and position (Fig. 3), whereas changes in the dynamic topography of the North Pacific Gyre produce interannual variability in the current (Fig. 4, after Roessler and Chelton, 1987). The importance of both local and remote forcing in California Current flow has been emphasized by modeling efforts like that of Pares-Sierra and O'Brien (1989), who found that the local wind field in the northeastern Pacific is adequate to drive the annual cycle of the current system and to create the general features of its structure. They could model interannual variations of the California Current only by coupling the local model with one driven by equatorial winds. Kelvin waves generated during El Niño events in the equatorial Pacific propagate up the western coast of North America and strongly affect the California Current. California Current structure thus reflects both the local winds along the west coast of North America and basinwide events within the north and equatorial Pacific Ocean.

In the much longer climatic cycles that are observable by paleoceanographic studies, the location and strength both of trade winds and of westerlies should probably have a major impact on mean transport in the California Current. Shifts of the mean wind patterns (e.g., a shift in the position of the North Pacific high at 18 ka; Kutzbach, 1987; Kutzbach et al., 1993a) should also strongly affect the structure of the California Current flow as well as the locations of maximum coastal upwelling.

Coastal California Upwelling: Upwelling along coastal California is driven by equatorward winds that roughly parallel the coast (Huyer, 1983). Ekman transport of surface waters by these winds moves them away from the coast and causes upwelling of nutrient-rich waters from below. The upwelling waters are restocked by shallow flow inward toward the shelf beneath the surface ocean layer. The seasonality of northerly winds in Northern California causes strong upwelling in the summer but downwelling in the winter (Fig. 5, after Huyer, 1983). South of San Francisco there is coastal upwelling the year around. Because of the coastal embayment of the Southern California Bight, coastal upwelling is low all year round (Fig. 5). Instead upwelling occurs offshore near Sites 1012, 1013, and 1014, driven by the curl of wind stress (Bray et al., 1999).

The seasonal cycle of winds and upwelling is a direct result of the annual migration of the North Pacific high-pressure regime. The North Pacific high migrates between its southerly limit at 28°N in February and its most northerly limit, 38°N, in July (Fig. 3; Huyer, 1983). Using paleoceanographic data to monitor the strength and the seasonality of coastal upwelling along coastal California also is an indirect monitor of wind strength and seasonality along the margin. This in turn gives information about the strength and position of the North Pacific high.

SYNOPSIS OF DRILLING

The Quaternary and Neogene paleoceanography of the California margin is poorly understood, primarily because the marine sedimentary record is poorly sampled for sediments older than about 50 ka. Typically, the high sedimentation rates along the margin limit the recovery to <130 ka for even the longest piston cores from standard oceanographic vessels. For this reason, the highest priority objective on Leg 167 was the collection of continuous high-resolution sediment records from the initiation of Northern Hemisphere glaciation (2.6 Ma) to the present. We also needed to collect more slowly deposited sediments from the seaward sites of the onshore-offshore transects for a longer Neogene perspective. These drill sites (Fig. 1; Sites 1010, 1016, and 1021) formed the anchors for the development of a new biostratigraphic framework tied to the paleomagnetic chronology (Cande and Kent, 1992, 1995). They have also given us major insight into oceanographic conditions along the California margin since the latest middle Miocene.

It has been hypothesized from the Santa Barbara Basin drilling (Site 893; Kennett and Ingram, 1995) that major changes have occurred in the upper intermediate waters along the southern California margin. In particular, they suggested that a more oxygenated source of intermediate waters appeared in glacial intervals, perhaps from the North Pacific. Sites 1011–1014 were drilled in the California Borderlands, and Site 1017 was drilled off Point Conception to better study the evolution of Pacific intermediate waters through the Pleistocene. The California Borderlands basins have sill depths that range from about 1500 to 450 m. The bottom waters of each basin are samples of discrete intermediate waters taken from the sill depth into that basin (Fig. 6). Ultimately the data from the different drill sites can be combined to study a water-column depth transect through much of the Pleistocene.

Along the central and northern California margin there is a general lack of long paleoceanographic records, and a high priority was to collect both intermediate- and deep-water records where submillennial paleoceanographic events could be documented. For this reason, we drilled Sites 1019 (980 m), 1018 (2476 m), and 1020 (3038 m), all of which have high average sedimentation rates (Table 1).

Because high-resolution continuous records were a priority, all sites were triple cored with the advanced piston core (APC), and a continuous splice of the sediment section was assembled aboard the *JOIDES Resolution* (Lyle, Koizumi, Richter, et al., 1997). The continuous records are being used for high-resolution sedimentological

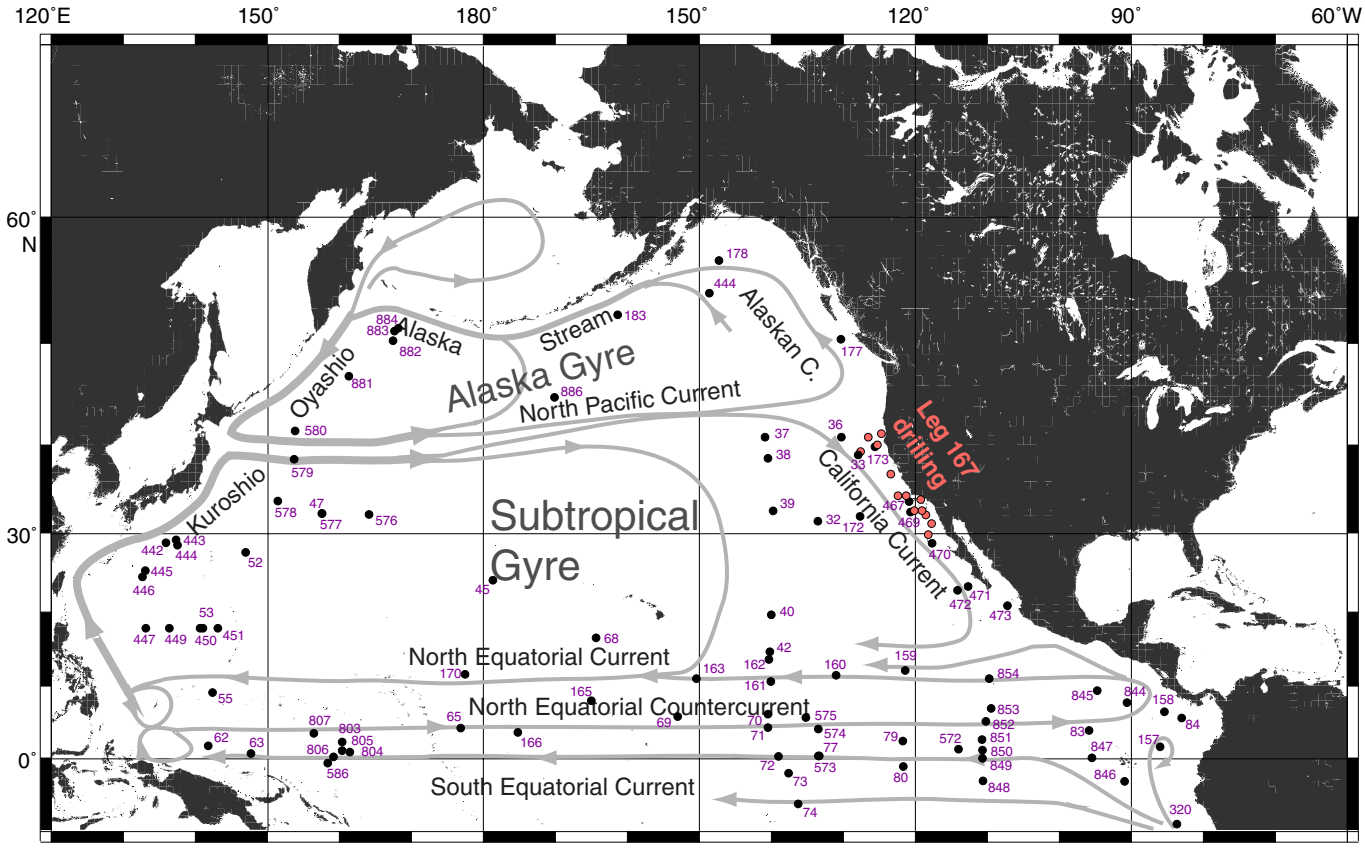

Figure 2. Surface currents in the modern North Pacific shown with Leg 167 drill sites (lightly shaded circles) and DSDP and ODP drill sites used to define Neogene Pacific carbonate flux (solid circles; Lyle, 1998). Other sites have been drilled in the Pacific but are not useful for paleoceanographic studies.

and paleoceanographic studies. Table 1 is a synopsis of the results of Leg 167 drilling. It contains the locations of the Leg 167 drill sites and pertinent information about the length and age of continuous sediment records. For the most part, the continuity is based upon shipboard correlations, but the ages incorporate new stratigraphic information generated since the cruise has ended (Fornaciari, Chap. 1, this volume; Kennett et al., Chap. 2, this volume; Maruyama, Chap. 3, this volume; Barron, Chap. 4, this volume; Hayashida et al., 1999). Because the California margin typically has high deposition of organic matter, we were also interested in diagenesis within the sediment column. We designed our sampling of interstitial waters to be of higher resolution than the average ODP sampling in the upper sediment column (one whole round per core for the first six cores followed by every third core thereafter; see "Explanatory Notes" chapter in Lyle, Koizumi, Richter, et al., 1997). Some sites had higher sampling (Site 1010 for oxygen isotope analysis, and Site 1019 to study gas hydrates).

THE MODERN ENVIRONMENT: INTERSTITIAL WATER GEOCHEMISTRY OF CALIFORNIA MARGIN SEDIMENTS

Leg 167 drilling afforded the unique opportunity to investigate interstitial water geochemistry at sediment depths accessible only by scientific ocean drilling (to hundreds of meters sub-bottom depth). Leg 167 sites covered a latitudinal range of ~10°, a water depth range from ~970 to ~4200 m, and distance offshore from ~50 to ~360 km. The sites were arrayed in three onshore-offshore transects and along a north-south transect of coastal sites (Fig. 1), allowing comparisons along gradients of factors controlling sediment supply (e.g., upwelling and primary productivity, terrestrial sediment sources) and those affecting regeneration processes in the water column and near the sediment-water interface (e.g., site water depth).

Previous studies of interstitial water geochemistry in this region, with depth of penetration often limited by coring techniques, generally covered the upper tens to hundreds of centimeters of the sediment. These studies, benefiting from high to very high sampling resolution, yielded great insight into early diagenetic processes, especially with regard to organic matter degradation and related redox reactions, early mineral authigenesis, and transition metal cycling (e.g., Brooks et al., 1968; Sholkovitz, 1973; Shaw et al., 1990; Kastner, 1995; Reimers et al., 1996; McManus et al., 1997). Previous scientific ocean drilling in this region yielding interstitial water profiles is summarized in Table 2. Leg 167 analyses cover significantly greater geographic and depth ranges with a comprehensive suite of geochemical analyses.

We focus on an overview of the interstitial water geochemistry from Leg 167 sites. Interstitial water samples from all sites were analyzed aboard ship for pH, salinity (by refractometer), chlorinity, sodium, alkalinity, sulfate, phosphate, ammonium, silicate, calcium, magnesium, strontium, lithium, and potassium (Lyle, Koizumi, Richter, et al., 1997; see "Explanatory Notes" chapter for details of methods and analytical figures of merit and see respective site chapters for results for individual sites). We discuss the observations in the context of the three onshore-offshore transects (Gorda, Conception, and Baja Transects, from north to south) and the north-south coastal transect (Fig. 1; Table 2). We focus on organic matter diagenesis (sulfate, alkalinity, phosphate, ammonium), on highlights of major element chemistry (chloride at the Eel River Basin site; Ca and Mg in the coastal transect sites), and on opaline silica dissolution and diagenesis (dissolved silicate coupled with thermal gradients).

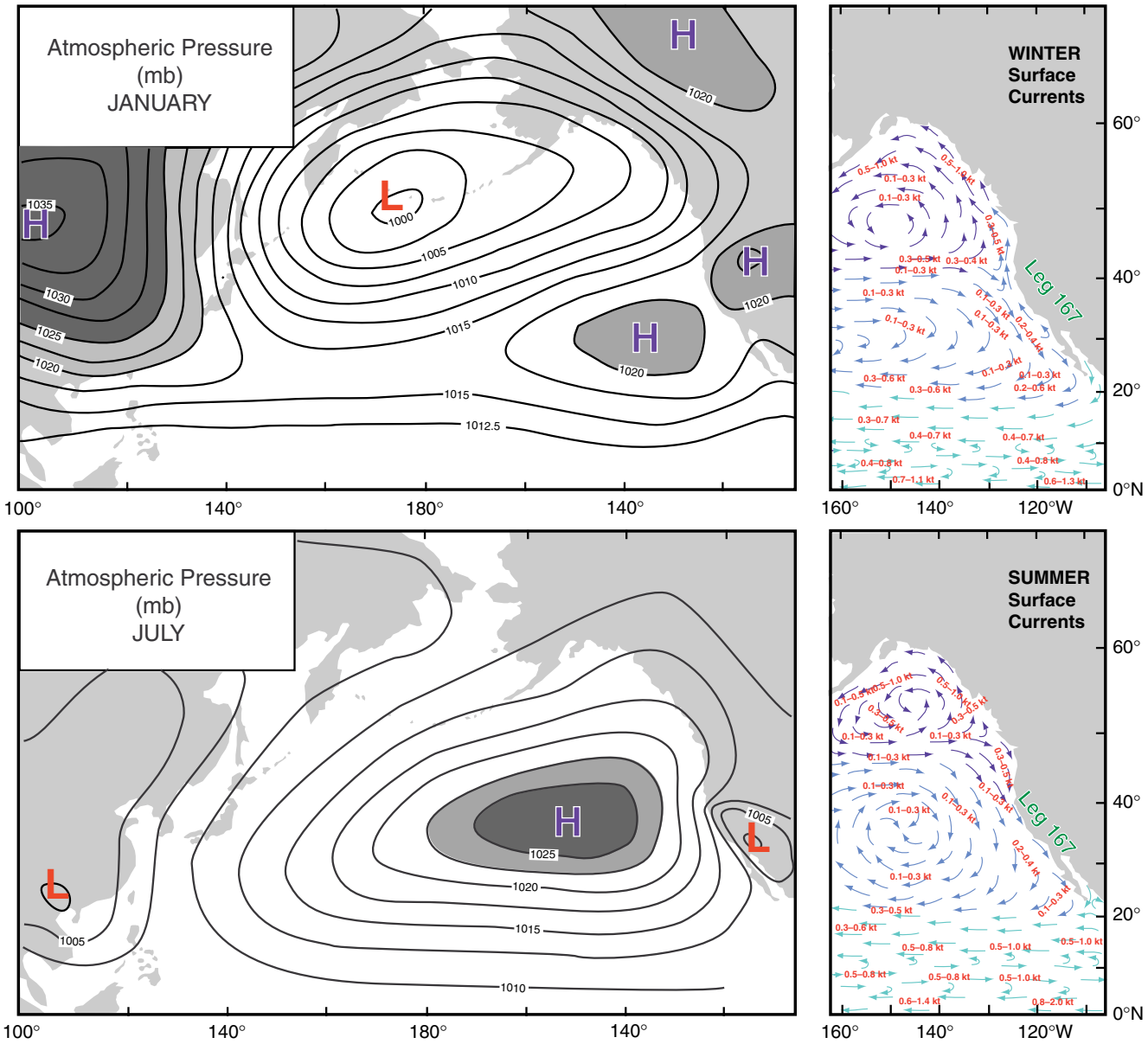

Figure 3. Surface atmospheric pressure, winter and summer, from Huyer (1983) compared to seasonal changes in northeast Pacific surface currents (Defense Mapping Agency Hydrographic/Topographic Center, 1989). Surface winds approximately parallel atmospheric pressure gradients. Seasonal variation in current patterns is driven by northeastern Pacific winds.

Organic Matter Diagenesis

A major control on the interstitial water geochemistry of the California margin sites is the oxidation of organic matter by the sequence of reactions typically observed in marine sediments (e.g., Froelich et al., 1979; aerobic respiration, denitrification, manganese reduction, iron reduction, sulfate reduction, etc.). Interstitial water sampling at these sites was geared toward capturing large-scale gradients with depth, and therefore did not have the high resolution near the sediment-water interface typical of shallower coring studies. Nevertheless, these profiles allow us to define the depth range of sulfate reduction, its regional variation, and the accompanying geochemical changes in a way not possible with shorter cores.

Sulfate reduction is an important process in many of these sites, marked by the consumption of sulfate and the production of alkalinity, dissolved phosphate, and dissolved ammonium from the oxidation of organic matter (Table 3). In all except the two deepest water sites farthest offshore (Sites 1021 and 1010), sulfate concentrations drop below the analytical detection limit (typically ~1 mM) within the upper 10–100 m sub-bottom depth (Fig. 7; Table 3). One site, Site 1011, displayed a reappearance of sulfate deeper in the sediment column. Presumably, early in the history of sediment accumulation at this site, the entire depth range was in diffusive communication with seawater, limiting the extent of sulfate reduction. After sufficient sediment thickness accumulated, sulfate reduction initiated. Sulfate reduction in the mid-depth range of the sediment is presently consuming sulfate from above, as well as residual sulfate at depth.

The depth to sulfate depletion is shallowest in sites closer to shore and increases with distance offshore in the three transects (Fig. 7A–C). Sulfate depletion is incomplete at Site 1021 (with sulfate decreasing from seawater values around 28 mM to 19 mM at depth) and at Site 1010 (decreasing to 25 mM), with most of the decrease in the upper 100 m at both sites. Along the coast there is no simple north–south pattern in the depth to sulfate depletion. All of the

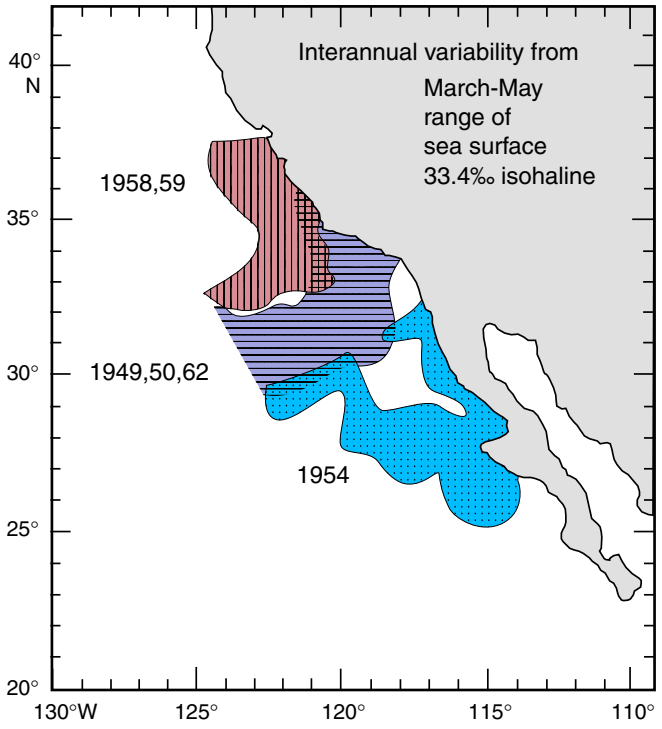

Figure 4. Illustration of strong interannual variation in California Current transport, from the CalCOFI data set (after Roessler and Chelton, 1987). Cold years (e.g., 1954) are typified by strong equatorward transport of subarctic (low salinity) water. Warm years (1958, 1959) are typified by weak equatorward transport. Most of the interannual variation is coupled to ENSO events in the equatorial Pacific (Pares-Sierra and O'Brien, 1989).

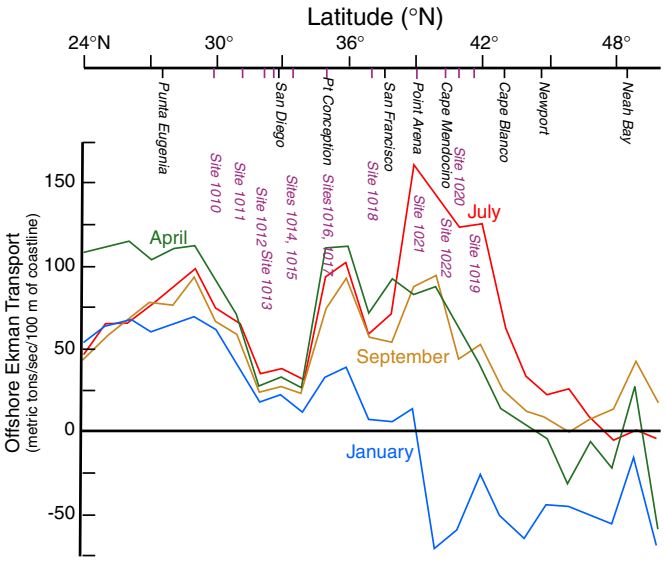

Figure 5. Offshore Ekman transport along the western coast of North America computed from long-term mean wind stress data for 1° squares adjacent to the coast, for January, April, July, and September (after Huyer, 1983). Leg 167 drill sites have been marked on the figure. Low upwelling in the California Borderlands coastal region (~30°–35°N) is because the coast retreats inland relative to the rest of the California margin and the stronger northerly winds remain offshore.

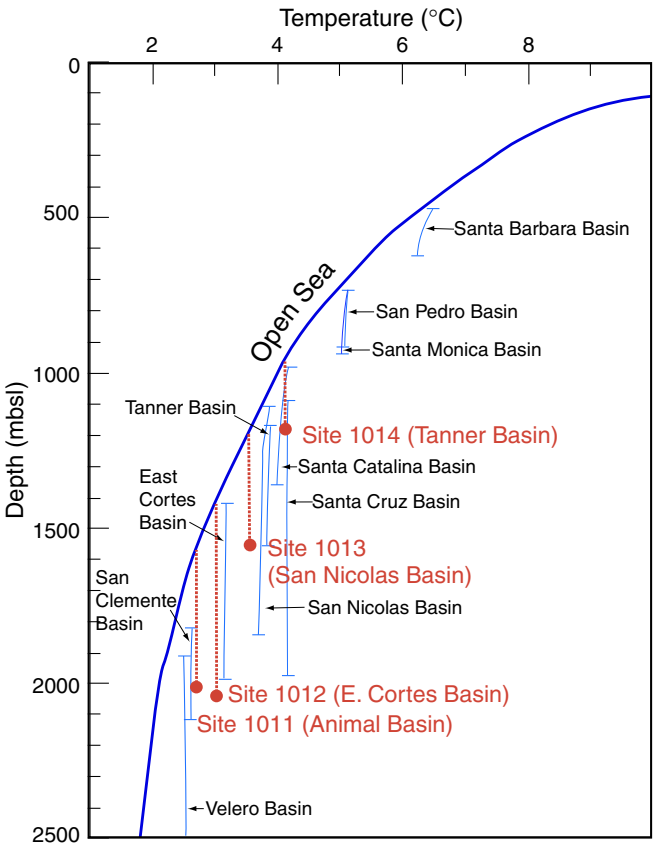

Figure 6. Temperature profiles below the sill depth (marked by the shallow horizontal line) in the California Borderlands Basins, after Emery (1960). Superimposed are Leg 167 drill sites, each located at its bathymetric depth and by the bottom-water temperature measured for sediment heat flow (Lyle, Koizumi, Richter, et al., 1997). Sill depths based upon matching bottom-water temperatures to the ocean temperature profile match the sill depths of the basins.

coastal transect sites reach nondetectable sulfate levels shallower than 50 m (Fig. 7D). These decreases in dissolved sulfate are accompanied by increases in alkalinity, dissolved phosphate, and dissolved ammonium.

Dissolved alkalinity profiles are influenced by alkalinity production during organic matter oxidation by sulfate reduction and by alkalinity consumption in authigenic mineralization reactions. Dissolved alkalinity reaches peak concentrations in depth zones coincident with, and extending deeper below, the depth of sulfate disappearance (Fig. 8; Table 3). Maximum alkalinity values are highest in the coastal transect sites and lowest in the sites in deepest water farthest offshore. The highest alkalinity is reached in the Eel River Basin site (Site 1019), where chloride and salinity profiles indicate a significant, although not well understood, influence of gas hydrate formation and dissociation processes on the interstitial water profiles (phosphate and ammonium are also strikingly high for this site; see following section for discussion of the chlorinity profile). Below the zone of maximum concentration, alkalinity typically decreases with increasing depth. Alkalinity profiles can also be influenced by ion exchange reactions and authigenic mineralization processes.

Dissolved phosphate is produced by organic matter degradation and by release during iron reduction and can be consumed by authigenic mineralization reactions. Phosphate profiles show substantial increases with depth, to concentrations as high as 200 µM in coastal transect sites, and up to 10–15 µM in the deepest water sites (Fig. 9; Table 3). Phosphate concentrations for the Eel River Basin site (Site

Table 1. Drill site statistics for Leg 167.

Site	Location	Latitude (°N)	Longitude (°W)	Water depth* (mbsl)	Distance from shore (km)	Total depth drilled (mbsf)	Age at base of sediments (Ma)	Depth of continuous sediment section (mbsf)	Depth of continuous sediment section (mcd)	Age at base of continuous section (Ma)	Age of paleomagnetic control (Ma)
1010	Seaward site, Baja transect	29°57.91′	118°06.05′	3465	209	210	14	180	196	13	6.9
1011	Coastal transect and Baja transect	31°16.82′	117°38.01′	2020 [1600]	85	276	9.3	165	177	6.7	—
1012	Coastal transect, California Borderlands	32°16.97′	118°23.02′	1773 [1415]	105	273	4.0	132	138	2.0	2.0
1013	Coastal transect, California Borderlands	32°48.04′	118°53.92′	1564 [1106]	115	146	3.1	94	97	1.8	1.8
1014	Coastal transect, California Borderlands	32°50.05′	119°58.88′	1166 [1166]	155	449	7.0	153	150	2.2	1.1
1015	Coastal transect, California Borderlands	33°42.92′	118°49.15′	901 [737]	31	150	0.1?	34	34	0.03?	—
1016	Seaward site, Conception transect	34°32.42′	122°16.59′	3835	148	317	6.1?	154	173	4.2	—
1017	Coastal transect and Conception transect	34°32.09′	121°06.42′	956	52	204	1.6	117?	130?	0.6	—
1018	Coastal transect	36°59.30′	123°16.65′	2476	76	426	3.5	158†	175†	1.2	—
1019	Coastal transect and Gorda transect	41°40.97′	124°55.98′	980	59	248	1.7	89	95	0.7	—
1020	Gorda transect	41°00.05′	126°26.07′	3038	167	279	3.7	118	126	1.3	1.1
1021	Seaward site, Gorda transect	39°05.25′	127°46.99′	4213	310	310	12	164	179	5.8	5.2
1022‡	Coastal transect	40°04.85′	125°20.56′	1926	87	388	5.8	157	170	3.5	—

Notes: Ages updated from Lyle, Koizumi, Richter, et al. (1997) for all sites except Site 1015; see text for references. mbsl = meters below sea level; mbsf = meters below seafloor; mcd = meters composite depth (from spliced continuous section). * = the basin sill depths for California Borderland basins are in [ ] and give the effective water depth for the sites for studies of water column structure. † = there is one minor break in the continuous record at 108 mbsf (119 mcd). ‡ = there is a hiatus at the top of Site 1022 from 0 to 2.3 Ma. — = no paleomagnetic data.

Table 2. Previous interstitial water studies by scientific ocean drilling in the Leg 167 region.

Leg	Site name (latitude)	Site number	Analyses (total depth range sampled)	Observations	Reference
DSDP Leg 63, California Borderland sites:					
	San Miguel Gap (34°N)	467	pH, alkalinity, salinity, chloride, sulfate, Ca, Mg (795 mbsf)	Sulfate depletion by 63 mbsf; alkalinity maximum of 50 mM at 158 mbsf; Ca minimum of 4.2 mM at 63 mbsf; sharp decrease in Mg in shallow portion; chloride depletion with depth	Gieskes et al. (1981)
	Patton Escarpment (32.5°N)	468	pH, alkalinity, salinity, chloride, sulfate, Ca, Mg (341 mbsf)	No sulfate depletion; small changes in Ca and Mg with depth	
	Foot of Patton Escarpment (32.5°N)	469	pH, alkalinity, salinity, chloride, sulfate, Ca, Mg plus ammonium, silicate, strontium, manganese, lithium, and potassium (390 mbsf)	Sulfate depletion to ~20 mM by 63 mbsf; alkalinity maximum of 5 mM at 63 mbsf; ammonium maximum of 0.46 mM at 109 mbsf; Ca increases, Mg decreases with depth; silicate increases to >1000 mM at 185 mbsf, then decreases to 54 mM at 390 mbsf	
	East of Guadalupe Island (29°N)*	470	pH, alkalinity, salinity, chloride, sulfate, Ca, Mg plus ammonium, silicate, strontium, manganese, lithium, and potassium (165 mbsf)	No sulfate depletion, minor increase in Ca, minor decrease in Mg with depth	
ODP Leg 146:	Santa Barbara Basin	893	pH, alkalinity, salinity, chloride, sulfate, Ca, Mg, silicate, sodium, lithium, and potassium (58 mbsf)	Sulfate depleted to <1 mM by 21 mbsf; alkalinity >40 mM; Ca below seawater values throughout, with 4.5 mM at 1.5 mbsf, decreasing to 2.1 mM at 58 mbsf; dissolved silicate >1000 mM by 58 mbsf	Kastner (1995)

Note: * = data compared well to data from the Mohole site (from Siever et al., 1965, as quoted in Gieskes et al., 1981).

Table 3. Interstitial water chemical signatures of organic matter diagenesis.

Site name (latitude)	Site	Water depth* (m)	Distance from shore (km)	Depth range of IW sampling (mbsf)	Sulfate "zero" depth† (mbsf)	Alkalinity maximum		Phosphate maximum		Ammonium maximum	
						Concentration (mM)	Depth (mbsf)	Concentration (mM)	Depth (mbsf)	Concentration (mM)	Depth (mbsf)
Gorda Transect (~40°N):											
Eel River Basin‡	**1019**	989	59	242	13	95	78-147	>340 (to 400)	61-137	>13	165
Delgada Slope	**1022**	1927	87	161 or 326**	37	>15	37-161	>65	28-47	5.7	161 (still increasing)
Eastern flank, Gorda Ridge	1020	3050	167	260	107	≥20	31-136	≥55	12-50	>3	164-193
Outer Delgada Fan	1021	4215	364	305	—	≥9	136-165	>15	3-79	>0.5	79-189
Conception Transect (~35°N):											
Santa Lucia Slope	**1017**	967	52	180	19	>40	19-48	>100 (to 161)	10-48 (at 19)	8.5	76-180
Pelagic site, off Point Conception	1016	3846	148	274	79	>17	40-50	57	31-40	2.3	79-274
Baja Transect (~30°N):											
Animal Basin	**1011**	2033 [~1600]	85	247	41††	>20	30-90	>40	10-60	>2.5	50-150
Ocean crust, near Guadalupe Island	1010	3465	209	170	—	>4	50	Always <10	—	0.13	170
Coastal Transect (other sites):											
Sediment drift, south of Guide Seamount (~37°N)		1018	2476	76	402	9	>50	19-76	>165 (to 182)	19-47(at 38)	>6.5 to 7.5104-257
Tanner Basin (~33°N)	1014	1177 [1165]	155	444	17	>100	137-222	>150 (up to 200)	27-191 (108-137)	>35	347-444
San Nicolas Basin (~33°N)	1013	1575 [1106]	115	131	27	>50	46	>170	19	>13	Increasing throughout
East Cortes Basin (~32°N)	1012	1783 [1415]	105	267	19	67	162	≥100	7-38	>14	131

Notes: Site numbers in bold in the onshore-offshore transects indicate sites that are also part of the north–south Coastal Transect. * = numbers in brackets indicate basin sill depth. IW = interstitial waters. † = depth of the shallowest sample with nondetectable sulfate concentrations (generally <1 mM). ‡ = this site has major decreases in chlorinity, salinity, and sodium in its interstitial water (IW) profiles; see site chapters in Lyle, Koizumi, Richter, et al. (1997). ** = samples from below 161 mbsf for Site 1022 were analyzed shipboard only for alkalinity, pH, and salinity, because of time limitations imposed by the end of the cruise. †† = sulfate increases again at depth at this site.

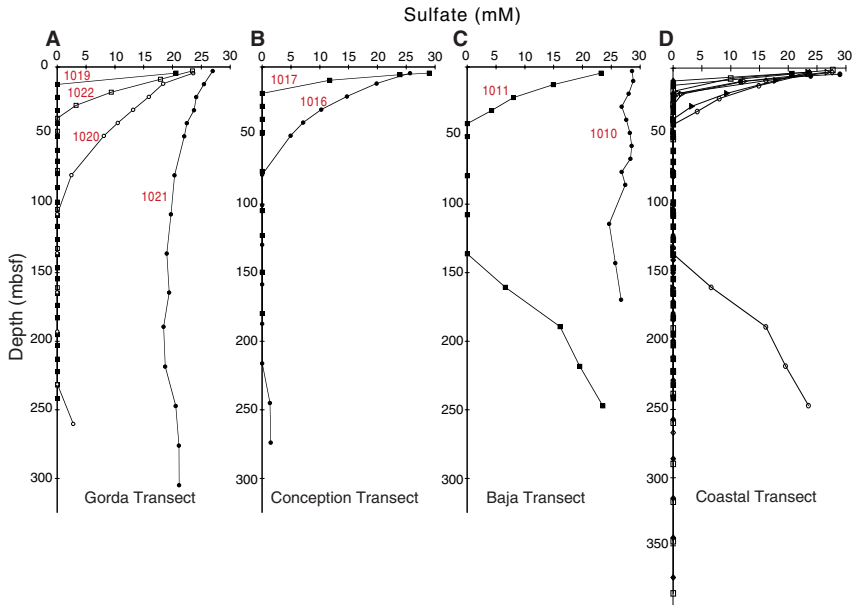

Figure 7. Sulfate vs. sediment depth. **A.** Gorda Transect. Symbols (from onshore to offshore) are solid square = Site 1019; open square = Site 1022; open circle = Site 1020; and solid circle = Site 1021. **B.** Conception Transect. Symbols are solid square = Site 1017 and solid circle = Site 1016. **C.** Baja Transect. Symbols are solid square = Site 1011 and solid circle = Site 1010. **D.** Coastal Transect. The inshore sites of the three onshore–offshore transects are included in this panel as well. Symbols (from north to south) are solid square = Site 1019; solid triangle = Site 1022; solid diamond = Site 1018; solid circle = Site 1017; open square = Site 1014; open triangle = Site 1013; open diamond = Site 1012; and open circle = Site 1011. Note that the slight increases in sulfate in the deepest samples of Sites 1020 and 1016 are likely because of a small proportion of contamination by drilling fluid.

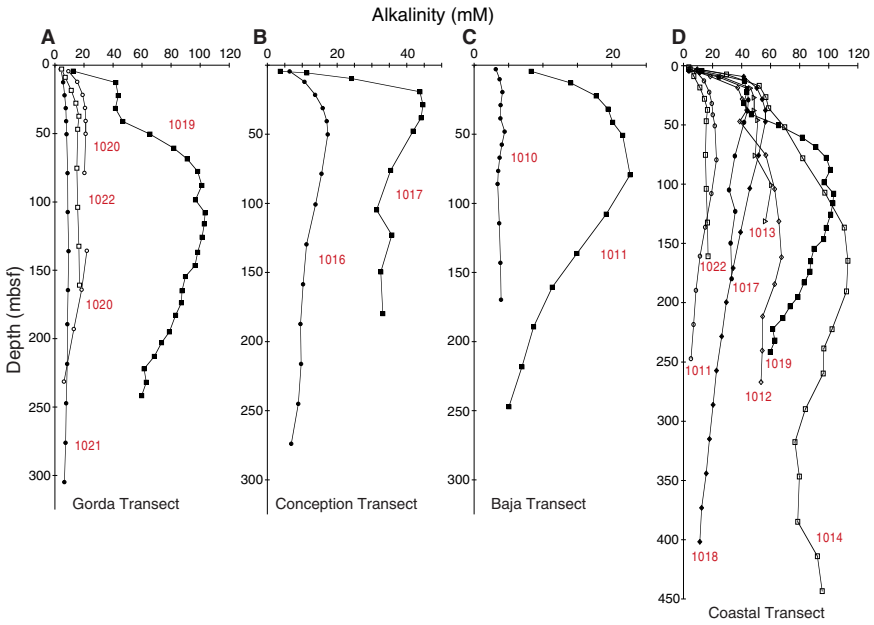

Figure 8. Alkalinity vs. sediment depth. **A.** Gorda Transect. **B.** Conception Transect. **C.** Baja Transect. **D.** Coastal Transect. Symbols for each panel are as in Figure 7.

1019) increase to 340–400 µM. Depth zones for maximum phosphate concentrations are generally shallower than, or coincident with, the shallowest portions of the maximum alkalinity zones (Table 3). After reaching these maxima, phosphate concentrations decrease with increasing depth to values <10 µM and as low as 2–3 µM below 150–200 m in the offshore sites (Fig. 9A–C). Phosphate profiles in all the coastal transect sites behave similarly to the more offshore sites, although the range of concentrations below 150–200 m is much larger for the coastal sites (Fig. 9D). Generally, larger phosphate maxima result in higher phosphate concentrations at depth. Presumably, phosphate uptake with increasing sediment depth below the depth zone of its maximum release by organic matter degradation is related to authigenic mineralization of phosphate-rich phases like carbonate fluorapatite, demonstrated to be significant in even the uppermost sediments of the Santa Barbara Basin (Reimers et al., 1996).

Ammonium is produced from organic matter regeneration by sulfate reduction, and its profiles can be influenced by ion exchange processes. Ammonium concentrations generally increase with increasing depth, to maximum values >5 mM and up to >35 mM in the Coastal Transect sites, and up to 3 mM in the deeper water sites (Fig. 10). The depth zone of maximum ammonium concentrations is generally deeper than the zone of maximum alkalinity values. A few sites show small decreases in ammonium at greater depth, and the Animal Basin site (Site 1011) shows a substantial decrease coincident with increasing sulfate concentrations in that site below 150 m (see Table 3 footnote). There is no simple relationship between ammonium and phosphate in interstitial waters throughout the depth range sampled because of the changing balance of influences of organic matter regeneration, ion exchange, and authigenic mineralization processes and their differing effects on the two nutrient element profiles.

The significance of organic matter supply to the sediments in driving organic matter regeneration is demonstrated by a comparison of peak alkalinity values with average organic carbon mass accumulation rates (C_{org} MAR; Fig. 11) over the drilled interval. There is a

quasi-linear relationship between peak alkalinity and C_{org} MAR, with the two sites with the lowest values for these (Sites 1010 and 1021) being the two sites where sulfate reduction did not go to completion (Table 2). The Eel River Basin site (Site 1019) has higher alkalinity relative to C_{org} MAR than the other sites, and the Santa Lucia Slope site (1017) and Delgada Slope site (Site 1022) have relatively low alkalinity values. Site 1022 is characterized by a very thin Pleistocene section (~1 m), underlain by upper Pliocene sediments. Thus, the interstitial chemistry at this site may reflect a continued influence of diffusive exchange with seawater, reducing the maximum alkalinity value observed compared to other sites with comparable C_{org} MAR.

Calcium and Magnesium Gradients

Calcium and magnesium profiles at these sites reflect the varying influence of basalt alteration in the underlying oceanic crust (resulting in linearly correlated Ca increases and Mg decreases with depth), authigenic mineral precipitation (possibly including calcium carbonate, dolomite, and carbonate fluorapatite), and ion exchange reactions, especially for Mg. Most Ca profiles decrease to a minimum and then increase deeper in the section (Fig. 12A). Minimum Ca concentrations are reached at depths close to or just below the depths at which sulfate is reduced to nondetectable levels. Minimum Ca concentrations are generally shallower than or at the top of the depth zone of maximum alkalinity values (Table 4). In general, the larger the peak alkalinity value (Table 3), the lower the minimum Ca concentration. The minimum in dissolved Ca near the depth of the alkalinity maximum is consistent with calcite precipitation. The deeper portions of the Ca profiles, with Ca increases correlated with Mg decreases, reflect the diffusional influence of alteration reactions in the underlying basaltic crust.

Mg profiles are considerably more complex than Ca profiles, reflecting the competing influences of ion exchange reactions, authigenic mineral precipitation, and the diffusional influence of alteration reactions in the underlying basaltic crust. As a consequence, depending on the site, Mg profiles display a variety of patterns (Fig. 12B). However, in the majority of sites, below the depth zone of the Ca minimum, increases in Ca are linearly correlated with decreases in Mg, consistent with alteration reactions in the underlying basalt and with the conservative behavior of Ca and Mg in these portions of the profiles. Ca gradients range from 1.2 to 11 mM/100 m, compared to the mean pelagic site gradient of ~3–4 mM/100 m (Lawrence and Gieskes, 1981); Mg gradients range from –0.87 to 12 mM/100 m, with $\Delta Ca/\Delta Mg$ ratios from –0.13 to –1.30 (Table 4).

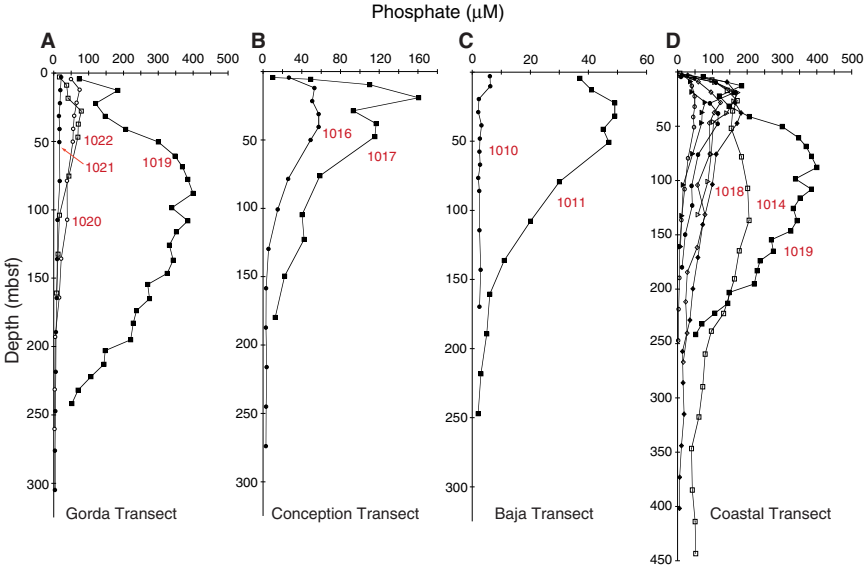

Figure 9. Dissolved phosphate vs. sediment depth. **A.** Gorda Transect. **B.** Conception Transect. **C.** Baja Transect. **D.** Coastal Transect. Symbols for each panel are as in Figure 7.

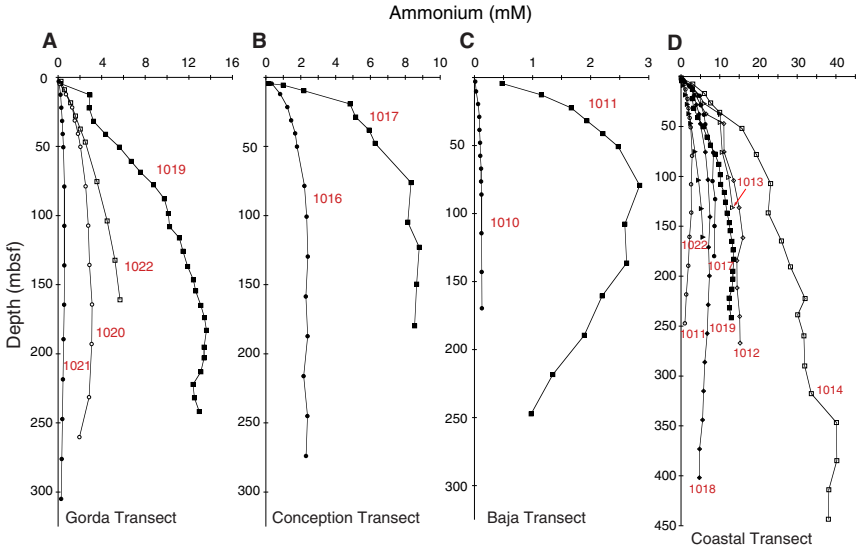

Figure 10. Dissolved ammonium vs. sediment depth. **A.** Gorda Transect. **B.** Conception Transect. **C.** Baja Transect. **D.** Coastal Transect. Symbols for each panel are as in Figure 7.

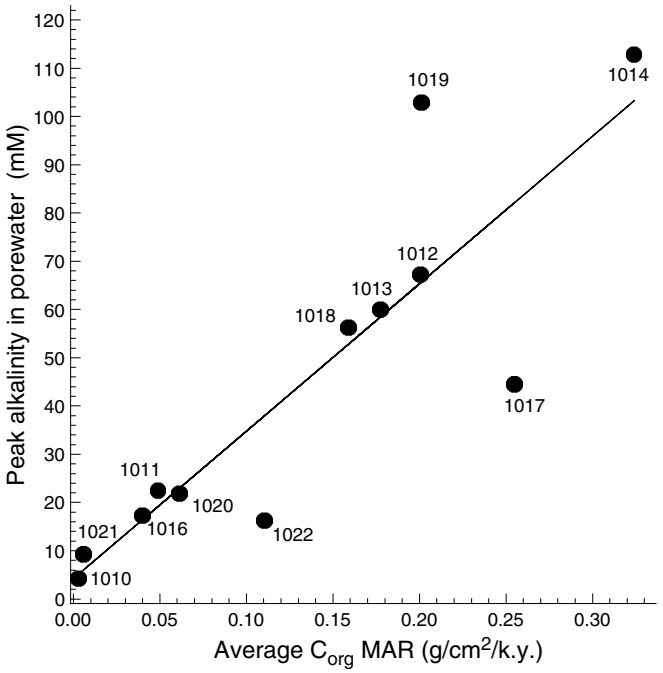

Figure 11. Peak interstitial water alkalinity vs. organic carbon mass accumulation rate. There is a general linear correlation between the two parameters. Three sites are the furthest from the trend: Site 1022, the only drill site with a >2 m.y. hiatus at the top; Site 1019, with gas hydrates; and Site 1017.

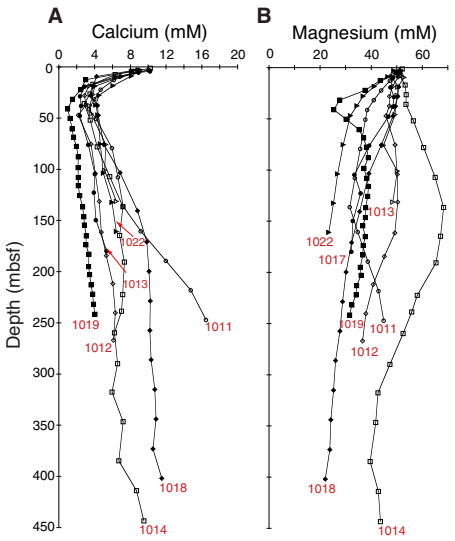

Figure 12. **A.** Calcium vs. sediment depth for the Coastal Transect. **B.** Magnesium vs. sediment depth for the Coastal Transect. Symbols are as in Figure 7.

Opaline Silica Dissolution and Diagenesis

All sites show an increase in dissolved silicate to values >1000 mM with increasing depth, consistent with the solubility of biogenic opal (Fig. 13A). There is a wide spread in dissolved silicate at any given depth across the range of sites. Downhole temperature measurements taken during Leg 167 at each drill site allowed the construction of a thermal gradient for each site. The site with the highest thermal gradient (Site 1020; 189°C/km) has the highest dissolved silicate at any given depth >50 mbsf, and the site with the lowest thermal gradient (Site 1018; 32°C/km) has the lowest dissolved silicate concentration. Using the bottom-water temperatures and these gradients, we can define modern sediment temperature.

The dissolved silicate gradients vs. temperature for the different sites (Fig. 13B) cluster much more tightly than those vs. depth, especially in the deeper sediment sections. This indicates the first-order control of temperature on biogenic opal solubility as an influence on the interstitial water geochemistry. The different behavior of silicate vs. temperature <10°C, with two apparent clusters, may indicate the further influence of sediment lithology on opal dissolution.

Paleotemperature and Chertification

The temperature history of the sites gives further insight into diagenetic alteration of biogenic opal to porcellanite and chert. Knowing the modern heat-flow gradient and thermal conductivity at each site lets us use the decay in conductive heat flow through time to hindcast the temperature of a sediment layer in the drill holes (Fig. 14). Conductive heat flow, like ridge-crest topography, decreases proportional to the square root of the crust age (Anderson and Hobart, 1976) for ocean crust. Continental heat-flow patterns are more complicated, but similar $t^{1/2}$ behavior should occur since the last major rifting event or volcanic episode for drill sites in the California Borderlands or on a continental margin. Knowing the modern geothermal gradient, one can hindcast the gradient in the past, provided that most of the heat loss was conductive. The temperature of any particular sediment layer depends upon its burial depth at the time of interest and the geothermal gradient.

We have hindcast the sediment temperature at the first diagenetic silica layer (opal-CT or chert) based upon the burial history and the change in heat flow (Fig. 14). Cherts or porcellanite are only found where sediment temperatures become higher than 24°–25°C (Sites 1010, 1011, 1016, 1020, and 1022). Site 1021 has no cherts but high dissolved silicate in pore waters and high biogenic opal contents. The base of the drilled sediment section at Site 1021 has never been warmer than 19°C, however. This would suggest that ~25°C is a critical temperature range for chertification of sediments.

At many of the drill sites there is a significant depth offset between the first chert or porcellanite and this hypothesized diagenetic horizon, suggesting that biogenic opal in the sediments shallower than the first chert should also be in the process of converting. There must either be a significant time lag between passage of the critical temperature and significant chertification, or other factors must also play a significant role. Earlier work has established that sediment composition likely plays a role (Kastner et al., 1977).

Gas Hydrates and Interstitial Water Chemistry, Eel River Basin (Site 1019)

The California and Cascadia margins are an important observatory to study gas hydrates, because although there is high methane production all along the margin, gas hydrates are only known to occur north of the Mendocino Fracture Zone (Field and Kvenvolden, 1985; Brooks et al., 1991; MacKay et al., 1994; Hovland et al., 1995; Kastner et al., 1995; Spence et al., 1995; Tréhu et al., 1995; Yuan et al., 1996). For this reason, we looked for geophysical signatures of gas hydrates during the site surveys for Leg 167 and prepared a small-scale geochemical sampling program for any drill site where we found evidence for their existence.

One of the surprising features of the California margin is the lack of any bottom-simulating reflector (BSR) south of the Mendocino Fracture Zone despite high burial rates of organic matter and high methane contents of the sediments (Lyle, Koizumi, Richter, et al., 1997). During the Leg 167 site survey cruise (EW9504) we specifically looked for any evidence of BSRs, yet located a BSR only at Site 1019, in the Eel River Basin to the north of the Mendocino Fracture Zone. Nevertheless, high methane occurred at all the coastal sites, ranging up to 160,000 ppm in headspace samples at Site 1017 (Con-

Table 4. Overview of calcium and magnesium gradients.

Site name (latitude)	Site	Calcium minimum: Concentration (mM)	Calcium minimum: Depth (mbsf)	Gradients at depth: Comments on Ca and Mg gradients and Ca vs. Mg regression	ΔCa (mM/100 m)	ΔMg (mM/100 m)	ΔCa/ΔMg*	r^2
Gorda Transect (~40°N):								
Eel River Basin	**1019**	0.97	41	Deepest 14 points, from where Mg increase ends	+1.5	–5.9	–0.24	0.87
Delgada Slope	**1022**	4.1	31	Deepest 6 points, from Ca minimum	+1.9	–8.8	–0.21	0.88
Eastern flank, Gorda Ridge	1020	5.1	50	Deepest 8 points, below Ca minimum	+11.4	–11.8	–0.82	0.94
Outer Delgada Fan	1021	8.7	107	Deepest 8 points, from Ca minimum	+1.9	–0.87	–2.1	0.78
Conception Transect (~35°N):								
Santa Lucia Slope	**1017**	2.4	29-48	Deepest 8 points, from Ca minimum	+2.3	–11.0	–0.16	0.82
Pelagic site, off Point Conception	1016	5.2	79	Deepest 8 points, from Ca minimum	+4.1	–8.9	–0.80	0.92
Baja Transect (~30°N):								
Animal Basin	**1011**	3.4	41	Mg increases deeper than minimum at 136 mbsf	—	—	—	—
Ocean crust, near Guadalupe Island	1010	—	—	Ca decreasing throughout entire depth sampled (n = 13)	+4.2	–3.3	–1.3	0.96
Coastal Transect (other sites):								
Sediment drift, south of Guide Seamount (~37°N)	1018	3.6	28	Deepest 15 points, from Ca minimum	+2.1	–7.6	–0.28	0.97
Tanner Basin (~33°N)	1014	2.8	36	Mg increases to a maximum at 137 mbsf	—	—	—	—
San Nicolas Basin (~33°N)	1013	3.5	38	No inverse relationship between Ca and Mg observed (shallow total sediment thickness)	—	—	—	—
East Cortes Basin (~32°N)	1012	2.2	47	Deepest 6 points, below Ca minimum	+1.2	–10.2	–0.13	0.95

Notes: Site numbers in bold in the onshore-offshore transects indicate sites that are also part of the north–south Coastal Transect. * = the correlation coefficients for the linear regressions of Ca vs. Mg are all significant at the 99% confidence level, except for regressions at Sites 1021 and 1017, where the correlation coefficient is significant at the 95% confidence level. — = not applicable.

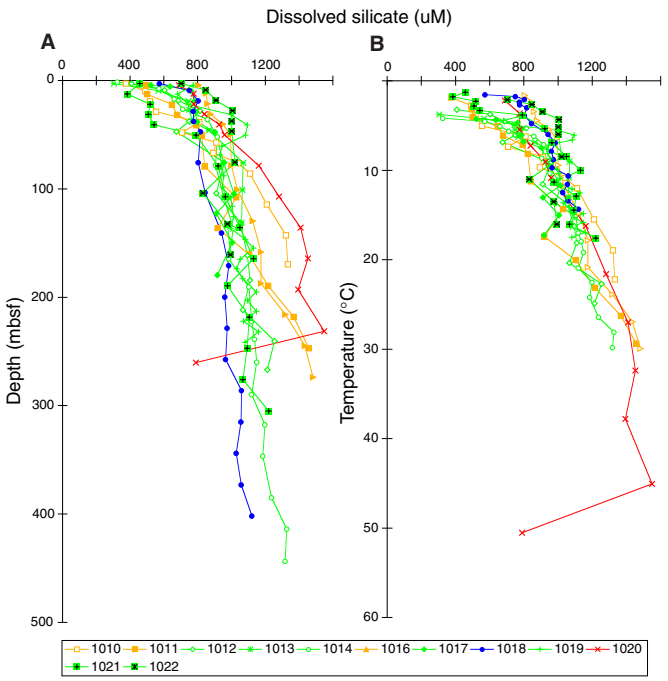

Figure 13. **A.** Dissolved silicate vs. sediment depth. **B.** Dissolved silicate vs. modern temperature, based on bottom-water temperature and geothermal gradient determined for each site. Symbols, in order of increasing site thermal gradient, are solid circle = Site 1018; gray-shaded plus = Site 1021; plus = Site 1019; open circle = Site 1014; star-like symbol = Site 1013; solid diamond = Site 1017; open diamond = Site 1012; gray-shaded star-like symbol = Site 1022; open triangle = Site 1016; solid square = Site 1011; open square = Site 1010; and cross = Site 1020.

ception Transect; Lyle, Koizumi, Richter, et al., 1997). Although enough methane was present at both Sites 1014 and 1017 to cause a stressed APC core to blow apart on recovery, no BSRs were detected at either site. Nor did we find any evidence for gas hydrates at these drill sites from the logging or the shipboard pore-water geochemical program.

We can speculate that gas hydrates only occur north of the Mendocino Fracture Zone because of the lack of a concentrating mechanism for methane to the south, most likely the lack of strong focused fluid flow through the sedimentary section. North of the Mendocino Fracture Zone the sediments are exposed to compression and dewatering because of convergence between the Gorda/Juan de Fuca Plates and North America, which could cause methane to flow to the hydrate formation zone. The BSR region we drilled at Site 1019 is at the continental slope break, and the sediments beneath the western edge of the basin have been compacted and dewatered. South of the Mendocino Fracture Zone, compression is lower because most of the margin has now been incorporated into the Pacific Plate.

Gas Hydrates and the Bottom-Simulating Reflector in the Eel River Basin

The Eel River Basin has long been known to contain gas hydrates (Field and Kvenvolden, 1985; Brooks et al., 1991). We picked a drill-site location for Site 1019 in a region known to have a BSR. Because of safety considerations Site 1019 was not located on the strongest BSR but on an area with a weak reflector on both seismic crosslines (Fig. 15, after Gallaway, 1997). Based on a 266-ms two-way traveltime to the BSR from the seafloor and an average sedimentary seismic velocity of 1600 m/s, the base of the hydrate layer should be around 212 mbsf. Because the site was moved for safety reasons, the

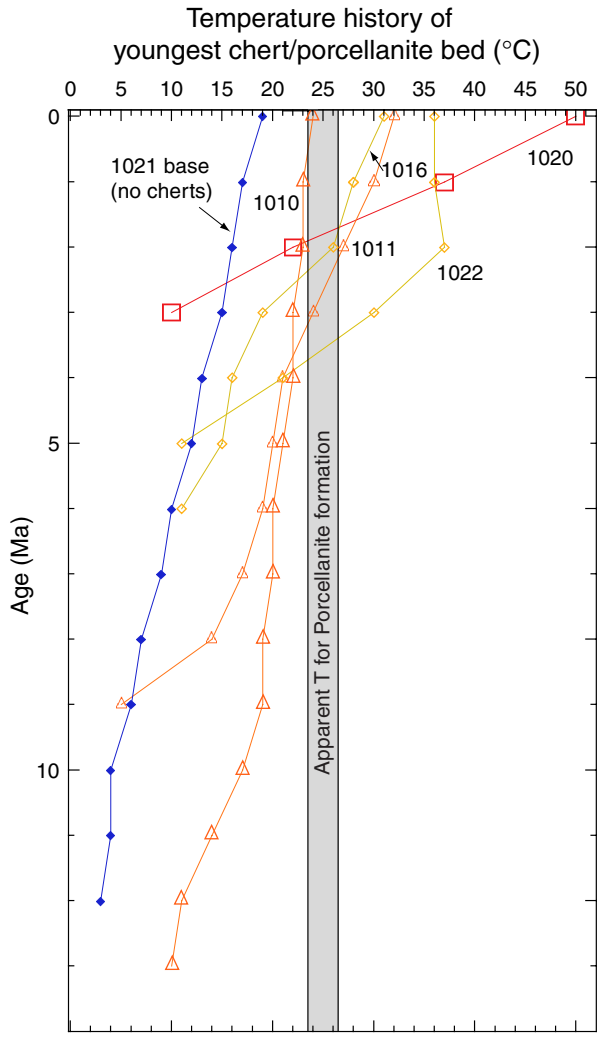

Figure 14. Temperature history of youngest chert bed vs. age for various sites. The temperature was hindcast by assuming a $T^{1/2}$ decrease in heat flow with time since crustal formation. Site 1021 does not have cherts even though the deepest sediments recovered contain about 30% opal (Janecek, Chap. 16, this volume). The basal sediments of Site 1010 do have cherts with similar silica contents. The two would suggest that chert conversion increases rapidly at a temperature of about 25°C.

BSR was slightly deeper than we had planned when we originally designed the drilling and the strength of the BSR was weaker.

One of the important features from the seismic survey is the patchiness of the BSR (Fig. 15). We do not observe large areas with consistent amplitude on the BSR near Site 1019 but instead observe small areas (on the order of a few square kilometers) with high-amplitude reflections separated by areas of low reflection strength or no BSR. Transitions from a high-amplitude BSR and no BSR can be abrupt. Because the BSRs drilled on Leg 146 in other parts of the Cascadia Subduction Zone are caused by trapped free gas under the clathrates (MacKay et al., 1994), the patchiness should be caused by variability in the amount of trapped methane. We do not know why there should be patchiness but suspect a highly variable supply of methane to the clathrate-forming regions, implying a variable fluid-flow regime, and/or an episodic mode of formation, where individual gas release events from deeper in the section randomly occur in space and time. Further work to resolve this issue should include a high-resolution, three-dimensional seismic survey in the region around Site 1019.

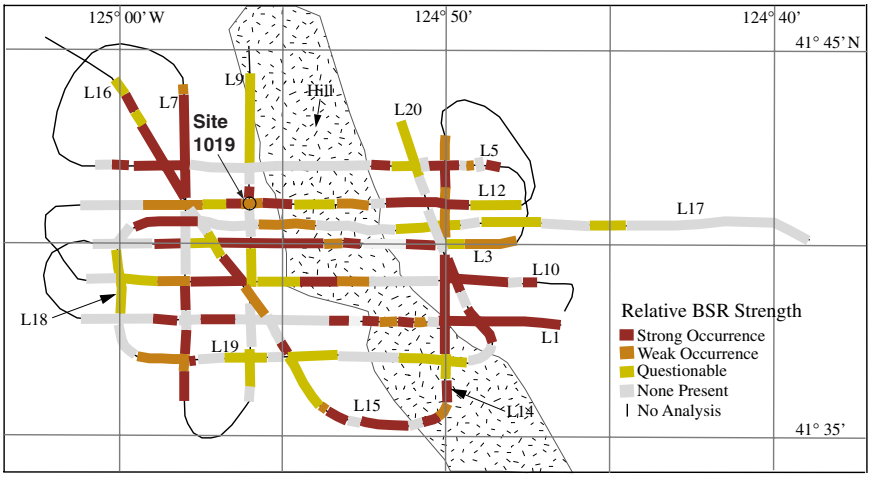

Figure 15. Relative strength of the bottom-simulating reflector (BSR) around Site 1019 from the site survey cruises (W9406 and EW9504) after Gallaway (1997). BSR strength should be a semiquantitative indicator of the amount of gas hydrate present. The BSR is very patchy and would suggest a nonsteady-state formation process.

Chloride

Because of the presence of the BSR at about 212 mbsf, we sampled the deeper sediment section at Site 1019 at a resolution of one interstitial water sample per core, or about three times the normal resolution. One of the primary geochemical tracers of the influence of methane hydrate dissociation below the BSR is a general freshening of the interstitial water with depth, and the presence of methane hydrates in sediments above the BSR can be marked by anomalously low chlorinity spikes as a consequence of methane hydrate dissociation during recovery (e.g., Blake Ridge Sites 994, 995, 997; Paull, Matsumoto, Wallace, et al., 1996). The Eel River Basin site interstitial water chemistry displays a striking decrease in chlorinity with increasing depth (Fig. 16), with correspondingly large reductions in salinity and sodium. Chlorinity values decrease to ~356 mM, about 65% of normal seawater values below 125 m, significantly lower than the background values of ~500 mM in the methane hydrate zone of the Blake Ridge sites.

There is no significant change in the Cl profile near the estimated depth of the BSR, nor were any unusually low-chlorinity spikes observed as artifacts of hydrate decomposition during recovery. The Cl profiles are remarkably similar to those from other drill sites along the Cascadia Subduction Zone (Leg 146, Yuan et al., 1996). At Sites 889/890, with a strong BSR, chlorinity decreased from seawater concentrations around 550 mM to about 350 mM. Assuming that this represents dilution by the volume of hydrate dissociating during recovery, Yuan et al. (1996) calculated that hydrate as a percentage of pore space varied from near 0 at the top of the section to up to 35% by the BSR. One of the features they noted, which is also apparent at Site 1019, is a lack of change in the Cl profile across the BSR. They attributed this phenomenon to an upward migration of the base of the hydrate stability field associated with a deglacial change in water temperatures.

Defining the influence of methane hydrate dissociation as the source of freshening with depth at Site 1019, as opposed to the contribution of other low-chlorinity sources, will require other isotopic (deuterium and oxygen isotopes) and elemental (iodide and bromide) profiles on these samples.

BSR from Borehole Logging

We attempted to log in situ physical properties across the BSR zone as part of the downhole logging program at Site 1019 but achieved ambiguous results. Part of the problem was because the hole depth was designed for a shallower BSR region than the actual Site 1019 location. We do not know if we completely logged the critical region of the BSR.

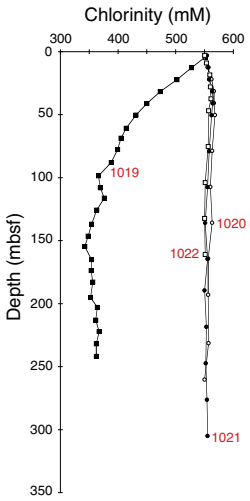

Figure 16. Chloride vs. sediment depth for the Gorda Transect. Symbols as in Figure 7. Note the low values in the Eel River Basin site (Site 1019).

Figure 17 shows the Cl profile compared to the resistivity log and reprocessed seismic velocity log (M. Lyle, unpubl. data). The seismic velocity log had inconsistent traveltimes, and only the traveltimes from the two longest paths were used, corrected for borehole size, to determine the traveltime within the formation. A formation velocity was also computed from the difference in traveltimes between these two paths. All are shown in Figure 14. The two separate logging passes over Hole 1019C agreed in detail.

The corrected seismic velocity does not show any obvious major increase over the supposed hydrate interval (the interval where Cl is near its minimum) as would be expected if gas hydrates were cementing the formation. Instead there are small variations on the order of 50–100 m/s throughout the Cl-minimum zone. There is a major drop in velocity on both passes near the start of the logging runs (below 200 mbsf), which might represent the base of the hydrate zone but could also be an artifact from beginning the log.

Because hydrates are nonconductive, a massive hydrate layer appears as a high-resistivity and high-velocity layer in logs (Mathews and von Huene, 1985; Mathews, 1986). Although we find significant resistivity anomalies in the logs, they are not associated with velocity anomalies. The major resistivity anomaly occurs at the beginning of the Cl minimum, which suggests a common factor controlling both.

The lack of high-velocity anomalies within the hydrate layer and the lack of significant changes in resistivity is similar to the logging

data from Sites 889 and 892 on the Cascadia Subduction Zone (MacKay et al., 1994). The BSR was difficult to locate with standard logs but was very apparent with a vertical seismic profile (VSP). The Eel River Basin BSR is thus in a common class with others found along the Cascadia Subduction Zone—it has a distinct seismic signature and a strong Cl anomaly, but is poorly defined by the standard shipboard logs. We assume that vertical seismic profiles would detect the base of the BSR at Site 1019.

Outstanding Questions to be Addressed by Further Study

There are several obvious areas for further exploration with the interstitial water data set. The profiles of alkalinity, phosphate, and ammonium can be compared within and across sites to examine the influence of organic matter degradation at each site, including investigating the rates of organic matter degradation and the relative patterns of behavior of carbon (alkalinity) and the nutrient elements P and N. This will help to address questions about the composition of organic matter being regenerated and the ultimate fate (e.g., retention in sediments, loss to the water column) of P with sedimentary redox state. The major element chemistry, especially that of Ca and Mg, points to the significance of authigenic mineralization reactions in influencing the geochemistry of these sites, including the profiles of alkalinity and phosphate. Development of records of other tracers (e.g., oxygen and deuterium isotopes, bromide, and iodide) would give greater insight into the geochemical environment, especially at the Eel River Basin site. The integration of the thermal properties of the sites with the interstitial water silicate distributions has helped to define the significance of temperature as a control on biogenic opal dissolution and its alteration. This topic deserves further consideration, including comparison to other regions with well-defined temperature gradients and interstitial silicate profiles.

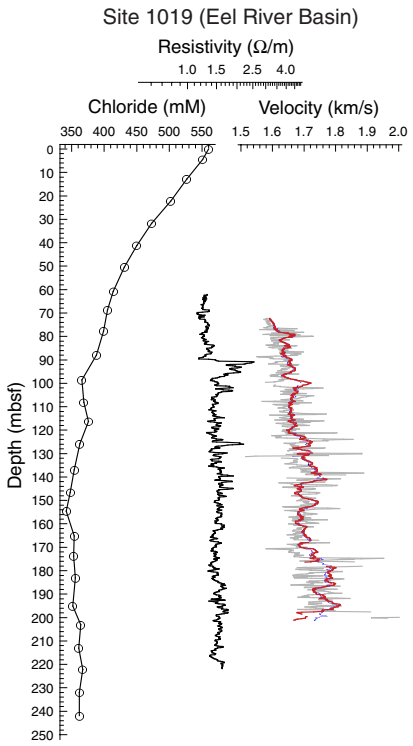

Figure 17. Velocity and resistivity profiles compared to Cl^- profile. No obvious indications of hydrates can be seen in the logged interval. The velocity profiles have been processed for this synthesis by using the few good traveltime recordings from the log. The light profile is velocity from a differential traveltime between 10′ and 12′ spaced source-receiver pairs. The two solid curves are calculated from the individual traveltime records and the smoothed caliper log, to calculate the extent of the water path within the borehole.

PLEISTOCENE MILLENNIAL- TO ORBITAL-SCALE PROCESSES IN THE CALIFORNIA MARGIN

Discovery of Millennial-Scale Variability Along the California Margin, Site 893

One primary objective of Leg 167 was to gain a better understanding of millennial-scale variability known to occur along the California margin. The drilling of the Santa Barbara Basin on Leg 146 (Site 893, Kennett, Baldauf, and Lyle, 1995) documented that significant millennial-scale variability exists along the Pacific coast of North America and that this variability is tied to the North Atlantic Dansgaard/Oeschger events, the weak and abrupt interstadials within marine isotope Stages (MIS) 2–5 (Behl and Kennett, 1996; Hendy and Kennett, 1999). The Younger Dryas interval at the MIS 2/1 boundary, a return to nearly full glacial conditions, is also prominent at Site 893. The last glacial stage and the Younger Dryas interval are marked by higher oxygenation of the basin and disappearance of laminated sediments, possibly because of strengthened production of North Pacific Intermediate Water in the glacial northwest Pacific.

One of the major questions that remained from the Site 893 studies in Santa Barbara Basin was the extent to which the Santa Barbara Basin is representative of regional conditions. The 120 m drop in sea level at the last glacial maximum significantly restricted the access of open ocean waters to the Santa Barbara Basin (Fig. 18). It is possible that some of the environmental changes recorded at Site 893 were caused by changes in the basin configuration because of changes in water depth. One of the goals of the Leg 167 drilling was to collect paleoceanographic records in the vicinity of the Santa Barbara Basin to compare to the Site 893 record. A second goal was to extend the

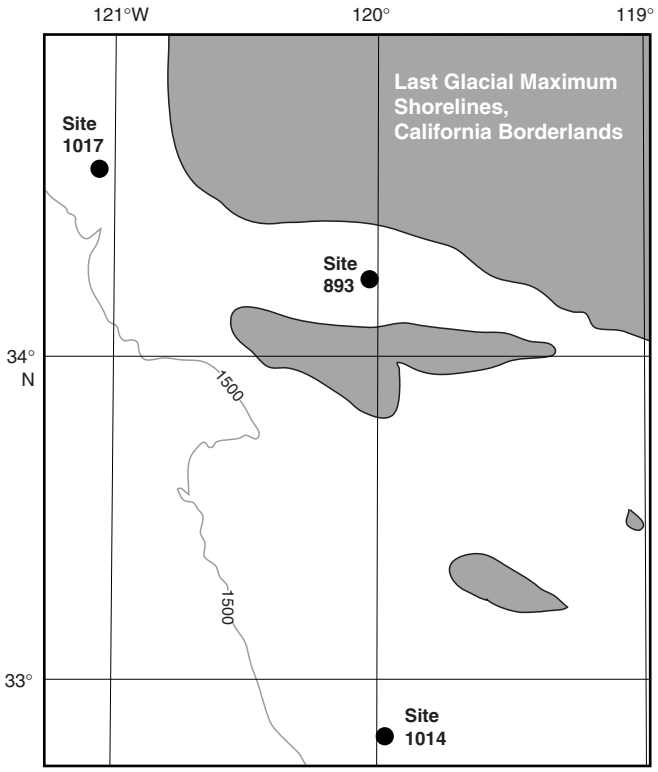

Figure 18. Santa Barbara Basin at the last glacial maximum with sea level 120 m lower than Holocene sea level. Sites 893, 1017, and 1014 are also shown.

record beyond that of Santa Barbara Basin and study more of the Pleistocene.

Leg 167 Drill Sites Compared to Santa Barbara Basin

Sites 1014 (Tanner Basin) and 1017 (Santa Lucia Slope) are both in the vicinity of Santa Barbara Basin (Fig. 18; Table 1) but are bathed by somewhat deeper waters. Bottom waters in Santa Barbara Basin originate from intermediate waters at a depth of 475 m below sea level (mbsl) because of the sill into the basin. Site 1017 was drilled at 956 mbsl, whereas Site 1014 was drilled at 1166 mbsl. Both drill sites are bathed by waters of the open eastern Pacific Ocean and so have minimal artifacts that could be caused by basin restriction.

We found that Dansgaard/Oeschger (D/O, Dansgaard et al., 1982; Oeschger et al., 1985; Dansgaard et al., 1993; McManus et al., 1994) interstadial events are indeed present at both sites, showing up most strongly in the planktonic oxygen isotope signal (Fig. 19; Kennett et al., Chap. 21, this volume; Hendy and Kennett, Chap. 7, this volume). They appear similar to events in the Santa Barbara Basin (Hendy and Kennett, 1999). Oxygen isotopes have been measured on *Globigerina bulloides* in all three sites, and the D/O events are strongest in Santa Barbara Basin (up to 2‰, Site 893, Hendy and Kennett, 1999), moderate near Point Conception (up to 1‰, Site 1017, Kennett et al, Chap. 21, this volume), and more poorly expressed in Tanner Basin (about 0.5‰, Site 1014, Hendy and Kennett, Chap. 7, this volume). The difference seems largely because of a sedimentary recording effect rather than a regionality in response: Site 893 has a sedimentation rate of about 1200 m/m.y. above the MIS 5/6 boundary, Site 1017 has a rate of about 185 m/m.y., and Site 1014 has a rate of around 112 m/m.y. Bioturbation should smooth the signal at Site 1014 much more completely than at Site 893, and aliasing of the signal by relatively coarse sampling becomes more important.

The D/O events as expressed by stable isotopes are primarily a surface-water phenomenon, in contrast to the strong response of the benthic community to anoxia during the events (Behl and Kennett, 1996; Cannariato et al., 1999). The strongest signals in oxygen and carbon isotopes are in planktonic foraminifers, and the plankton community has major compositional changes during these events. As Hendy and Kennett (1999) have pointed out, the strong surface-water expression of D/O events in the Santa Barbara Basin suggests an atmospheric connection to the source of the D/O oscillations. There are events in the subsurface ocean (e.g., Lund and Mix, 1998) but they are subdued relative to the surface signal. In addition, benthic and planktonic foraminiferal isotope signals do not strongly track each other, at least in the California Borderland. The lack of a strong intermediate D/O signal in carbon isotopes is troubling, if the signal is driven by intermediate-water source changes.

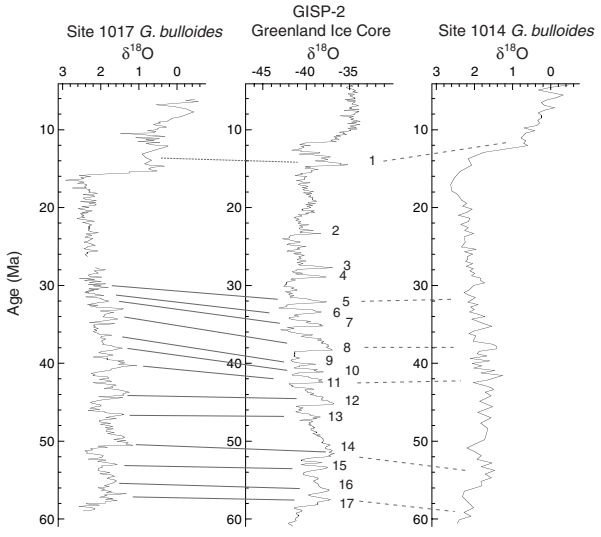

Figure 19. Dansgaard/Oeschger events in GISP-2 (oxygen isotopes from Grootes et al. [1993] and Stuiver et al. [1995]; time scale from Sowers et al. [1993] and Meese et al. [1994]) compared to planktonic $\delta^{18}O$, Sites 1014 and 1017, in the California Borderland. See Kennett et al. (Chap. 21, this volume) and Hendy and Kennett (Chap. 7, this volume), for more information about the oxygen isotope records.

When working with millennial-scale events, assigning ages is a significant problem. Compare, for example, age assignments for Sites 1017 (Kennett et al., Chap. 21, this volume) and 1014 (Hendy and Kennett, Chap. 7, this volume) in Figure 19. It is apparent that the preliminary age models used for these cores need revision assuming that the D/O events are chronostratigraphic between the GISP-2 ice core from Greenland and the California Borderlands drill sites. Because the D/O link is probably atmospheric, we expect little or no phase lag to the signal, which should make it possible to use the D/O events stratigraphically. Development of a D/O "tuned" time scale for the California margin will be highly important for the next level of study of millennial-scale processes and global climate. It will provide a means to study decadal to centennial oceaographic variability. Development of tuned time scales for the California Borderland drill sites must be done in a systematic manner, however, and more confirmation that the D/O events on the California margin are truly in phase with the Greenland ice cores would increase the confidence in this time scale.

Millennial-Scale Paleoceanographic Events—Central and Northern California Margin

During Leg 167, high-resolution records were recovered from central California (Site 1018, Fig. 1), the northern California Eel River Basin (Site 1019, Fig. 20), and the eastern Gorda Ridge (Site 1020, Fig. 20) to compare with the records from the California Borderlands. Millennial-scale events possibly linked to D/O cycles appear in these records (Lyle et al., Chap. 11, this volume; Fig. 21). In Figure 21 we compare the stacked MAR records from Site 1018, Site 1020, and two piston cores (EW9504-17 andW8709-13), normalized by standard deviations from the median. Construction of the stack is discussed in Lyle et al. (Chap. 11, this volume). Stacking smooths out events but also improves signal-to-noise characteristics of the record. The individual records of the stack can be studied in Lyle et al. (Chap. 11, this volume).

Detailed planktonic foraminiferal oxygen isotope records have yet to be constructed for any of the northern drill sites, so we do not know if there is a high-amplitude isotopic response in surface plankton similar to the response recorded at the California Borderlands. However, sedimentary time series of both C_{org} and $CaCO_3$ have millennial-scale variability. Lyle et al. (Chap. 11, this volume) argue that this variability represents variability in the production and rain of C_{org} and $CaCO_3$ from surface waters, not from rapid changes in dissolution. Lyle et al. (Chap. 11, this volume) reached this conclusion because there is no depth-dependent change in the events, because most of the events exceed the $CaCO_3$ burial expected from saturation of North Pacific deep waters, and because some of the events even exceed the modern $CaCO_3$ rain from the surface. Changes in production and/or the ratio of $CaCO_3$ to C_{org} in the particulate rain best explain the observations.

Millennial-Scale Events in the Last 25 k.y.: the Last Glacial Maximum, the Younger Dryas, and the Holocene

Because of the high precision of radiocarbon dating we have the best age control in the interval from about 25 ka to the present. Within this time window lies the last glacial maximum (LGM), a series of millennial-scale warmings and coolings during the deglaciation (including the return to near-glacial conditions in the Younger Dryas interval) and the Holocene. This is also the best known interval along

the California margin, having been sampled by numerous studies with long gravity cores and piston cores (Moore, 1973; Gardner et al., 1988; Lyle et al., 1992; Sancetta et al., 1992; Sabin, 1994; Prahl et al., 1995; Thunell and Mortyn, 1995; Dean et al., 1997; Doose et al., 1997; Gardner et al., 1997; Ortiz et al., 1997; Dean and Gardner, 1998).

From the earlier studies it is generally accepted that productivity was lowest in MIS 2 and highest in the Holocene, with MIS 3 being intermediate (Lyle et al., 1992; Dean and Gardner, 1998). There appears to be weaker coastal upwelling in the glacial half of this period, with a higher fraction of productivity derived during the spring bloom off southern Oregon (Sancetta et al., 1992). During the glacial period, nutrient injection into the surface waters may be dominated by diffuse offshore upwelling driven by the curl of the wind stress (Ortiz et al., 1997). Sea-surface temperatures (SST) were significantly colder during the last glacial maximum. Prahl et al. (1995) estimated 5°–6°C temperature difference between the last glacial maximum and modern SST off southern Oregon by both alkenone- and radiolarian-based regressions. Ortiz et al. (1997) estimated the LGM temperature by foraminiferans to be 3.3° ± 1.5°C colder along the same transect. The gradient in SST from north to south appears to have been highest at the LGM (Moore, 1973; Herbert et al., 1995; Prahl et al., 1995; Doose et al., 1997). This remains a controversy because other workers have used abundance of left-coiling *Neogloboquadrina pachyderma* as an indicator that the SST in the California Borderlands may have been about 8°C colder than modern at the LGM (a glacial SST of about 7°–8°C, about the same SST as southern Oregon; Thunell and Mortyn, 1995; Kennett and Venz, 1995), rather than the 2°–3°C difference measured from alkenone biomarkers (Herbert et al, 1995; Yamamoto et al., Chap. 12, this volume; Ostertag-Henning and Stax, Chap. 26, this volume; Manglesdorf et al., in press). It should be a priority to explore and settle this controversy. It is important to point out that Ortiz and Mix (1997) find 100% left-coiling *N. pachyderma* from core tops in waters as warm as 12°C. The late Holocene sediments at Site 1019 are also nearly 100% left-coiling *N. pachyderma* (Mix et al., 1999). Subpolar water is not required for a switch from right- coiling to left-coiling *N. pachyderma.*

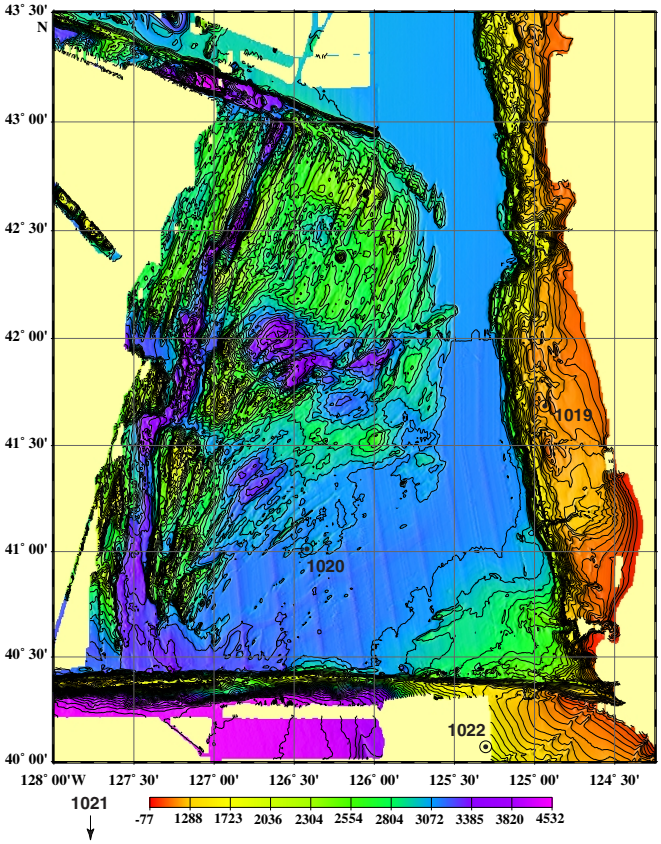

Figure 20. Locations of Sites 1019 and 1020. The base map was produced by the NOAA VENTS program in August 1998. Site 1019 (41°41′N, 124°56′W) is located in the actively deforming edge of the Eel River Basin, due west of Crescent City, California, at a water depth of 980 mbsl.

Deglaciation (~18–9 ka)

Northern California

ODP drilling is responsible for the highest resolution records from the LGM to the present along the California margin: Site 893 (LGM located about 30 mbsf; Kennett et al., 1995), Site 1017 (LGM at 4.5 mbsf, Kennett et al., Chap. 21, this volume), and Site 1019 (LGM at 11 mbsf, Lyle et al., Chap. 11, this volume; Mix et al., 1999). Site 1019 has the fastest sediment accumulation and highest time resolution of the northern sites drilled on Leg 167 (Fig. 20). This drill site is located just shoreward of the slope break in the Eel River Basin and is in a region of active deformation. A hill 220 m high lies just east of Site 1019 and is formed of late Pleistocene sediments. The major uplift of the hill occurred after 400 ka and perhaps as late as 160 ka (Gallaway, 1997). Sedimentation rates at the site are extremely high during the MIS 6/5 and MIS 2/1 deglaciations, averaging 550 m/m.y. during the MIS 2/1 deglaciation and 360 m/m.y. during the MIS 6/5 deglaciation (Mix et al., 1999; Lyle et al., Chap. 11, this volume).

Lyle et al. (Chap. 11, this volume) have analyzed late Pleistocene and Holocene sediments from Site 1019 for C_{org} and $CaCO_3$ at

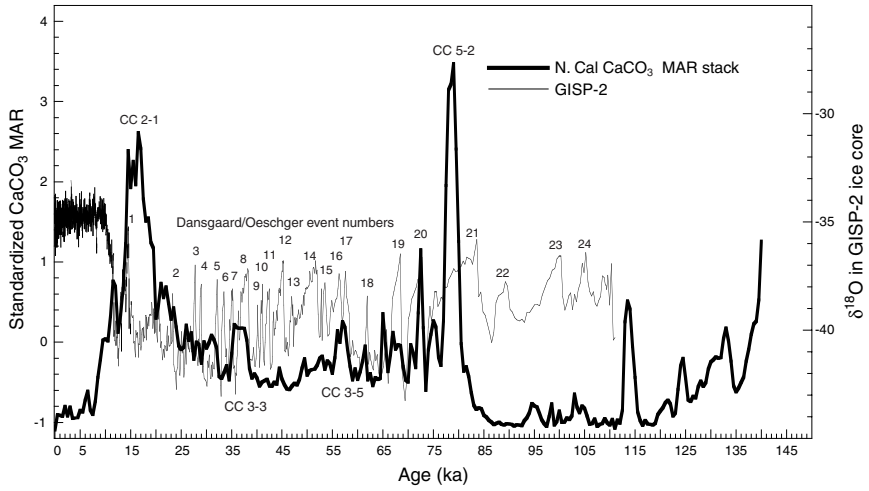

Figure 21. Comparison of Dansgaard/Oeschger events in GISP-2 (oxygen isotopes from Grootes et al. [1993] and Stuiver et al. [1995]; time scale from Sowers et al. [1993] and Meese et al. [1994]) to the Northern California $CaCO_3$ Mass Accumulation Rate stack (Lyle et al., Chap. 11, this volume). The stack is made from Sites 1018, 1020, and the piston cores EW9504-17 and W8709-13, as described in Lyle et al. (Chap. 11, this volume). Within MIS 2–4 there is a correspondence between D/O events and $CaCO_3$ events. The weakest coherence is in late MIS 3 (D/O Events 4–10).

roughly 100 yr intervals (Fig. 22) and find that the deglacial sequence is similar to the North Atlantic: records of both C_{org} and $CaCO_3$ mass accumulation rates (MAR) mimic the oxygen isotope record from the GISP-2 Greenland ice core until about 10 ka. The deglaciation has slightly higher C_{org} MAR than the Holocene, which is somewhat different than records offshore. This may in part be a preservation effect because of the high sedimentation rates. $CaCO_3$ MAR responds dramatically through the glaciation, marked by highs in late Stage 2 and the Bølling-Allerød (D/O Event 1), and immediately younger than the Younger Dryas interval. $CaCO_3$ becomes much more rare in the sediments of Site 1019 (as well as elsewhere in the northern California and southern Oregon region) at 8 ka.

At Site 1019, the Younger Dryas interval is more easily recognized in the C_{org} percentage data (Fig. 23). The Younger Dryas is marked by about a 0.5% C_{org} difference between it and the warm intervals on either side. There is also a major shift in coiling ratio of *N. pachyderma* to essentially 100% left-coiling specimens (Mix et al., 1999). The flanking C_{org} highs have three laminated intervals within them: 19.0–19.13 ka (9.52–9.61 mcd), 14.66–14.96 ka (7.04–7.25 mcd), and 10.9–11.65 ka (4.82–5.26 mcd; Pike et al., 1998). These laminated intervals appear to represent enhanced productivity, because they have high numbers of upwelling diatom flora and extensive benthic foraminiferal colonization, which would rule out anoxic conditions (Pike et al., 1998). Carbon isotope contents of the benthic foraminiferan *Uvigerina peregrina* are actually enriched in ^{13}C during the laminated intervals (Mix et al., 1999) arguing against a strongly oxygen-depleted water source at this time.

Southern California

It is clear that productivity plays a role in the appearance of laminations in the warmer deglacial stages in the Eel River Basin (Site 1019) in Northern California. This is a substantially different interpretation than that for the California Borderlands (Site 893, Santa Barbara Basin), where researchers have argued for changes in strength of the oxygen minimum as the primary driving force shaping the deglacial sedimentary record (Kennett and Ingram, 1995; Behl and Kennett, 1996; Cannariato et al., 1999). Leg 167 postcruise scientific research has concentrated heavily on the late glacial and Holocene record in Site 1017 to investigate the causes of glacial interglacial variability (Behl et al., Chap. 22, this volume; Irino and Pedersen, Chap. 23, this volume; Ishiwatari et al., Chap. 24, this volume; Kennett et al., Chap. 21, this volume; Ostertag-Henning and Stax, Chap. 26, this volume; Tada et al., Chap. 25, this volume). It appears that current activity and/or offshore transport of clastics is an important factor shaping the Site 1017 record.

Strong glacial/interglacial changes occur at Site 1017 but are complicated by active slope depositional processes. The sedimentation processes are an important component of the preserved sediment record here. Because one of the typical environments for high-resolution paleoceanographic records is the upper continental slope and because sedimentation here can be much more variable than in the deep sea, it is critical to understand how sedimentation can affect the paleoceanographic record to properly interpret paleoceanographic change.

Site 1017 is marked by a series of small turbidites (1–3 cm sand layers) in the glacial part of the record, including the Younger Dryas (Irino and Pedersen, Chap. 23, this volume). The likely cause of the turbidites is the lowered sea level and more proximal position of the drill site to the coast during glacial intervals. The provenance of the finer sediment fraction changed during the deglaciation from a more mafic source in MIS 2 and 3 to a more felsic source in the Holocene. Irino and Pedersen (Chap. 23, this volume) argue for a stronger glacial littoral and offshore transport from Franciscan sources to the north of Cape Conception in MIS 2 and 3 to be the cause of the change in provenance.

The glacial part of the record also has larger modal grain size in the nonturbidite intervals (Tada et al., Chap. 25, this volume) and oc-

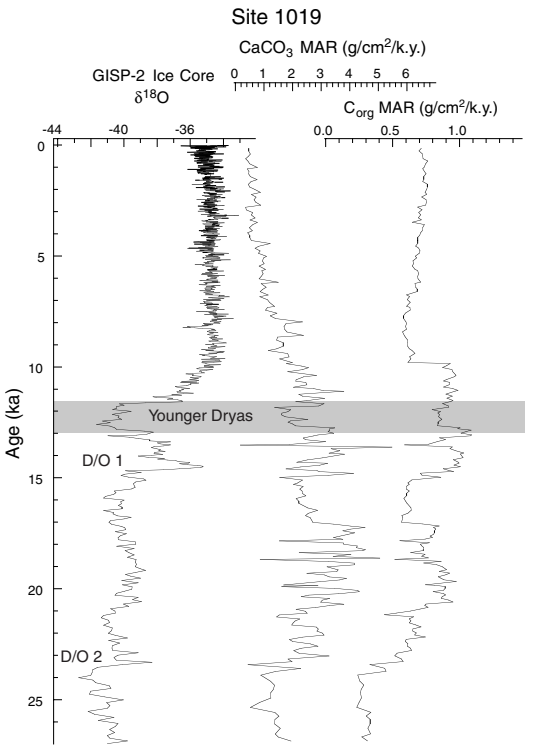

Figure 22. Comparison of Dansgaard/Oeschger events in GISP-2 (oxygen isotopes from Grootes et al. [1993] and Stuiver et al. [1995]; time scale from Sowers et al. [1993] and Meese et al. [1994]) to the MAR section of Site 1019 with radiocarbon age control (time scale from Mix et al., 1999; carbon data from Lyle et al., Chap. 11, this volume).

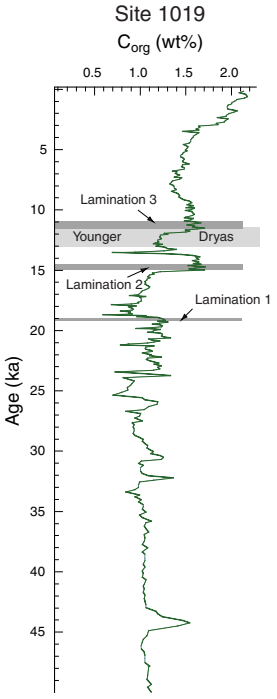

Figure 23. Organic carbon profile at Site 1019 (Eel River Basin) showing the Younger Dryas interval based upon the radiocarbon age model of Mix et al. (1999) and showing the positions of the three laminated intervals on the deglaciation.

casional faint laminations interpreted as contourites. Tada et al. (Chap. 25, this volume) argue that the northward-flowing California Undercurrent may have been stronger in MIS 2 and 3, or at least the energy of intermediate waters impinging upon the upper slope was stronger in the vicinity of Site 1017.

Tada et al. (Chap. 25, this volume) also show that the organic content of the sediment is primarily in the finer fraction and argue that any change in current strength will change the deposition of this fraction and the C_{org} profile. They also argue that C_{org} variation uncorrelated with the grain-size effect seems to relate to higher production. Sorting out the depositional control from the production control here is obviously of high importance to our ultimate understanding of paleoproductivity and upwelling along the California margin.

Comparison of High-Resolution Time Series

It will become increasingly important to compare high-resolution time series through the deglacial interval from a variety of sites along the North American margin to understand the dynamics of Pleistocene oceanographic change. In Figure 24 we make an initial comparison of the high-resolution $CaCO_3$ weight percentage time series from Site 893 (Santa Barbara Basin; data from Gardner and Dartnell, 1995), Site 1017 (Santa Lucia Slope; data from Ostertag-Henning and Stax, Chap. 26, this volume), and Site 1019 (Eel River Basin; data from Lyle et al., Chap. 11, this volume).

There is a fundamental difference in the records from near the California Borderlands and the northern California site: the Holocene has higher $CaCO_3$ overall than the Pleistocene at Sites 893 and 1017, whereas the inverse is true at Site 1019. Nevertheless, one of the prominent features in all the records is the $CaCO_3$ peak immediately after the Younger Dryas interval in the vicinity of 10–11 ka. This peak has roughly double the $CaCO_3$ percentage of the Younger Dryas at all sites. At Sites 1019 and 1017 on the open ocean margin, the Younger Dryas interval is bracketed by another $CaCO_3$ high during the early deglaciation. The early Holocene $CaCO_3$ peak at Site 1017 is largely composed of coccoliths and is primarily associated with deposition of small *Gephyrocapsa* species, an upwelling indicator (Tanaka and Tada, Chap. 27, this volume).

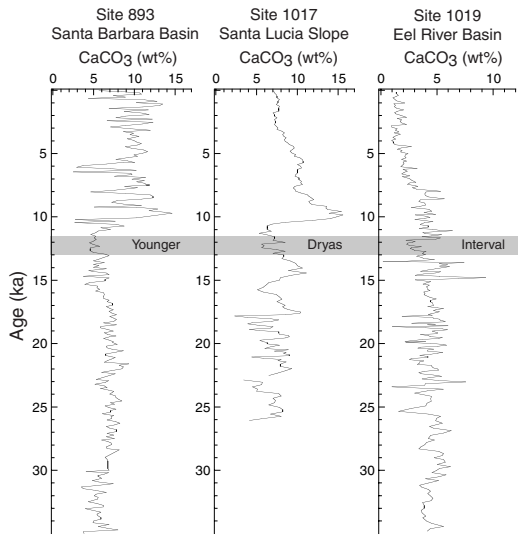

Figure 24. $CaCO_3$ profiles for the late Pleistocene and Holocene from Site 893 (Gardner and Dartnell, 1995; age model from Kennett, 1995), Site 1017 (Ostertag-Henning and Stax, Chap. 26, this volume; age model from Kennett et al., Chap. 21, this volume), and Site 1019 (Lyle et al., Chap. 11, this volume; age model from Mix et al., 1999) all in calendar years ka. The Younger Dryas Interval is a low carbonate interval all along the California margin, whereas there is a carbonate burial spike at 10–11 ka.

There is an apparent offset of about 1000 yr between the equivalent early Holocene $CaCO_3$ peak at Sites 1019 and 1017. It is very possible that the offset may be a dating artifact, and we encourage systematic detailed age models to be developed and intercalibrated at both sites. If the age offset is real, it may represent the propagation of a $CaCO_3$ production event from north to south along the California margin.

Late Pleistocene

Benthic Foraminiferal Oxygen Isotopes

A major postcruise research effort for Leg 167 consisted of measuring benthic foraminiferal oxygen isotopes for high-resolution Pleistocene stratigraphy and deep-water properties (Fig. 25; Andreasen et al., Chap. 8, this volume; deMenocal and Baker, Chap. 9, this volume; Hendy and Kennett, Chap. 7, this volume; Kennett et al., Chap. 21, this volume; Lyle et al., Chap. 11, this volume). As a result of these studies we now have benthic stable isotope data from seven Leg 167 drill sites to at least MIS 6 (>130 ka; Fig. 25). These data and that from Santa Barbara Basin (Site 893) not only allow us to develop age models for each of the drill sites but also to investigate the structure of the intermediate- and deep-water column (480 to >3000 mbsl).

Figure 26 shows a comparison of average benthic isotopic composition for the Holocene (MIS 1) plotted against measured modern bottom-water temperatures at each drill site. The bottom-water temperatures were measured while taking the sedimentary thermal gradient (Lyle, Koizumi, Richter, et al., 1997). The Santa Barbara Basin bottom-water temperature is from Emery (1960; Fig. 6). The modern

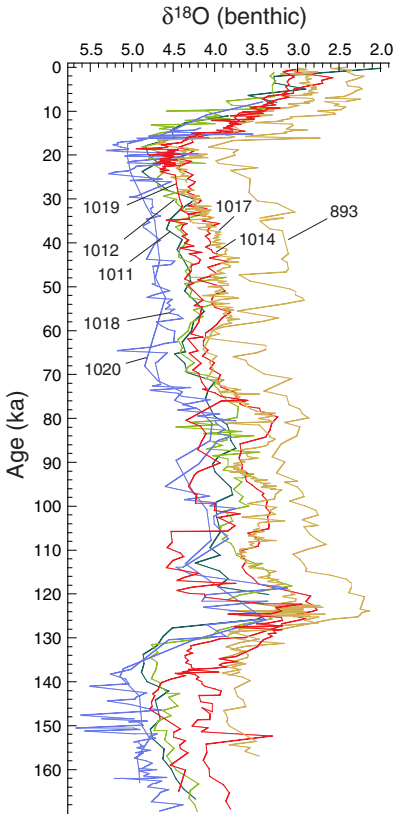

Figure 25. Benthic oxygen isotope profiles from ODP drill sites along the California margin. Site 893 data from Kennett et al., 1995; Site 1017 data from Kennett et al., Chap. 21, this volume; Site 1014 data from Hendy and Kennett, Chap. 7, this volume; Sites 1011, 1012, and 1018 data from Andreasen et al., Chap. 8, this volume; Sites 1019 and 1020 data from Lyle et al., Chap. 11, this volume. Offsets in the isotope curves are primarily because of the temperature profile through the thermocline.

profile of temperature vs. benthic foraminiferal oxygen isotope composition provides a simple internal calibration between temperature and isotopes for further isotopic temperature estimates. The change in isotope composition with depth is essentially a temperature function, because the modern salinity change is small in the intermediate and deep waters along the California margin (0.39 practical salinity units [PSU; 1 PSU approximately equals 1‰ change] between 500 and 6000 mbsl; Talley and Roemmich, 1991). The salinity gradient should cause minimal differences in oxygen isotope composition, because the oxygen isotope–salinity slope in the North Pacific is 0.322‰ per PSU (Lynch-Stieglitz et al., 1999).

Figure 26 also shows the MIS 2 average benthic foraminiferal isotopes plotted against modern bottom-water temperature. One would expect, if there were a major change in density gradient, to find the drill sites plot with a different slope or with a significant kink in the profile when compared to the modern profile. Instead, the sites plot along the same slope but with an offset of 1.55‰ from the Holocene profile. This is slightly less than the reported Pacific deep benthic oxygen isotope shift of 1.70‰ (Norton et al., 1997). The 0.15‰ difference, if real, is the equivalent to a 0.6°C average temperature increase relative to deep water, or a 0.5 PSU average decrease in salinity relative to deep water. Because surface temperatures at the last glacial maximum were 2°–5°C colder along the California margin (Doose et al., 1997), it is more likely that the average intermediate-water salinity dropped. Whether or not temperature or salinity was the more important factor, the intermediate-water density gradient appears to have been little affected by the glacial–interglacial climate changes.

Because Leg 167 investigators have thus far concentrated their efforts on individual drill sites, the ability to profile the intermediate-water column has not yet been strongly exploited. However, we expect that follow-up studies will more strongly focus upon this potentially powerful paleoceanographic tool.

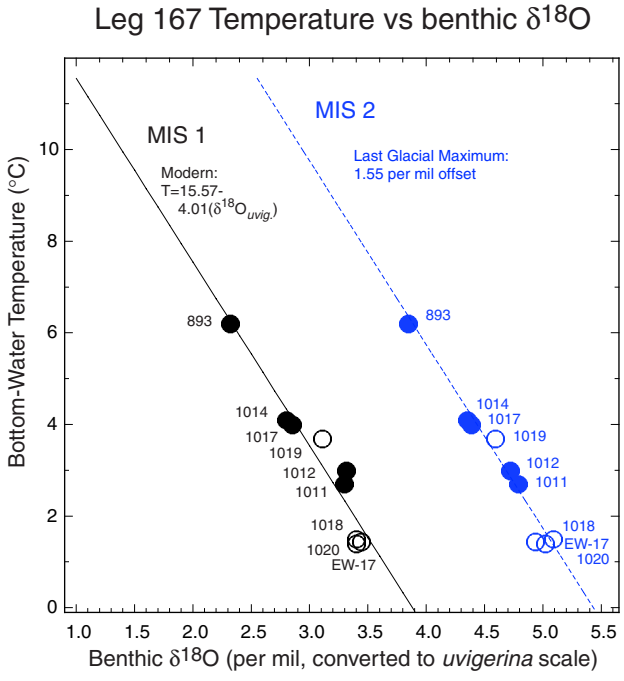

Figure 26. Benthic foraminiferal oxygen isotopes for Holocene (MIS 1) and last glacial maximum (MIS 2) plotted against modern bottom-water temperature measured on Leg 167. Site 893 (Santa Barbara Basin) bottom-water temperature is from Emery (1960). The bottom-water temperatures compare with WOCE profiles measured in the northeastern Pacific (Talley and Roemmich, 1991). Solid circles are California Borderlands drill sites, and open circles are drill sites from Northern and Central California. EW-17 marks the site survey core EW9504-17 (Lyle et al, Chap. 11, this volume). The glacial/interglacial change is an offset for all sites of 1.55‰. There is no evidence for a major change in density structure.

SST Records

One of the other major data sets collected during the initial post-cruise studies on Leg 167 is alkenone-derived SST records (Kreitz et al., Chap. 10, this volume; Ostertag-Henning and Stax, Chap. 26, this volume; Yamamoto et al., Chap. 12, this volume; Mangelsdorf et al., in press). The California margin is particularly well suited for these studies because of the significant number of biomarker calibration studies in the modern California Current system and by comparisons between alkenone SST, faunal SST, and oxygen isotope SST estimates (Prahl et al., 1993; Prahl et al., 1995; Doose et al., 1997; Herbert et al., 1998). The results of these calibration studies indicate that haptophyte production in slope and shelf locations (water depths <2 km) occurs <30 m deep and has no bias in SST from the mean annual SST, whereas farther from shore the haptophyte production occurs slightly deeper in the water column and there is a slight bias toward colder temperature estimates (Herbert et al., 1998). Relatively high abundance of the coccolithophorid *Emiliani huxleyi,* a major producer of the alkenones, occurs throughout at least the last 25 k.y. (Tanaka and Tada, Chap. 27, this volume). It is likely that modern SST calibrations are valid for at least the late Pleistocene. Comparisons between radiolarian and alkenone estimates of SST show that the two different estimates are essentially the same (Prahl et al., 1995).

All along the California margin the warmest SST coincides with maximum interglacials but the coldest SST occurs before maximum glaciation (Kreitz et al., Chap. 10, this volume, Herbert et al., 1995). This is true at all Leg 167 drill sites studied (Site 1017, Ostertag-Henning and Stax, Chap. 26, this volume; Site 1016, Yamamoto et al., Chap. 12, this volume; Site 1020, Kreitz et al., Chap. 10, this volume; Sites 1017, 1018, and 1019, Mangelsdorf et al., in press) and Site 893 (Herbert et al., 1995). The SST record for the last 150 k.y. from a northern California drill site (Site 1020; Kreitz et al., Chap. 10, this volume) and a southern California drill site (Site 1016; Yamamoto et al., Chap. 12, this volume) are shown in Figure 27. Because both sites are away from the coast and well out into the California Current (Fig. 1), similar SST time series are found at both sites. The SST record of Site 1020 is offset from that of Site 1016 by ~3°C throughout the last 160 k.y. Site 1018, which is approximately midway between Sites 1020 and 1016 (Fig. 1), has an SST profile that lies mid-

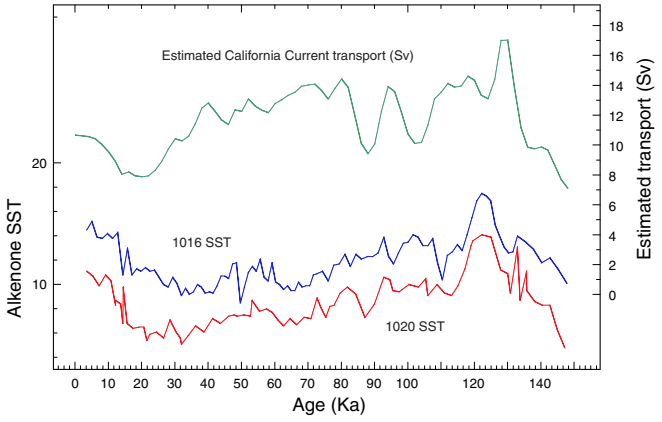

Figure 27. A comparison of SST changes for the last 150 k.y. in the northern California Current (Site 1020; Kreitz et al., Chap. 10, this volume) and the southern California Current (Site 1016; Yamamoto et al., Chap. 12, this volume), showing the coherence of alkenone-estimated SST along the California margin. Changes in California Current transport (sverdrups [Sv], 10^6 m^3/s) calculated from a simple temperature difference model (Doose et al., 1997) are also shown. If the model is correct, lowest California Current flow rates are at the glacial maxima, and highest flow rates are in interglacials.

way between them (Mangelsdorf et al., in press). The 3°C temperature difference between Sites 1016 and 1020 is slightly larger than the modern annual gradient of about 1.5°C but is the same as the spring seasonal temperature gradient (Levitus and Boyer, 1994).The temperature gradient should become smaller if the California Current gains strength.

The glacial maxima are marked by the largest alkenone SST differences between the north and south (about 5°C), even though the minimum alkenone SST does not coincide with this time. Doose et al. (1997) have interpreted the alkenone SST difference between north and south to be a measure of California Current strength, where maximum difference in SST equates to minimum flow in the current. Using this model, California Current flow at the glacial maxima (MIS 2 and 6) is around 60% of the flow at other times. If other data sets confirm a weak California Current at glacial maxima, this represents a major decrease in heat exchange between the subarctic and subtropical Pacific. Ultimately this may help to end glaciation: low import of heat into the North Pacific lowers evaporative water loss from the North Pacific, perhaps curtailing water supply to North American glaciers.

Longer Pleistocene Time Series: an Example from Site 1020

Longer time series that cover more than the last glacial–interglacial cycle are still uncommon for the Leg 167 drill sites because of the high sedimentation rates and the thickness of sedimentary sections that must be analyzed. We now have the most information about multiple glacial cycles from Site 1020 from Northern California (Figs. 21 and 28; SST from Kreitz et al., Chap. 10, this volume; pollen data from Heusser et al., Chap. 17, this volume; oxygen isotopes and carbon measurements from Lyle et al., Chap. 11, this volume; biogenic silica from Kuroda et al., Chap. 14, this volume). The longer records illustrate some of the possible directions for future research.

MIS 12/11 Transition

One of the important features in the Site 1020 time series is a transition at roughly the MIS 12–11 boundary (~423 ka on the Imbrie et al. [1984] time scale) apparent in SST, $CaCO_3$, and biogenic silica (Fig. 28). The glacial stages prior to MIS 12 are marked by relatively small glacial/interglacial changes in alkenone SST—around 3°–4°C for the maximum difference between glacials and interglacials. Beginning with the MIS12–11 glacial–interglacial pair, the alkenone SST difference between glacials and interglacials doubled and the SST variance strongly increased at higher frequencies. The MIS12/11 boundary roughly marks the end of a relatively high $CaCO_3$ interval and a high biogenic silica interval. Part of the decrease may result from higher terrigenous input in the younger section (Kuroda et al., Chap. 14, this volume). Lower terrigenous dilution in the section older than MIS 11 may explain part but not all of the elevated biogenic contents of the pre-MIS 11 interval. Sedimentation rates were 20% lower in the section older than MIS 11 based upon the stage boundaries in Figure 28, but biogenic silica and $CaCO_3$ contents average a factor of 2 higher. The older sediments have significantly higher biogenic MAR's as well as somewhat lower terrigenous dilution than post-MIS 11 sediments.

The biogenic silica record (Kuroda et al., Chap. 14, this volume) indicates that the period of high biogenic deposition may have lasted only for about 200 k.y. and began at about the MIS 15/16 boundary. We have only coarse-scale shipboard measurements of $CaCO_3$ and C_{org} along with reflectometry records through the interval from MIS 11 to 16 to estimate the length of the high $CaCO_3$ burial interval (Lyle, Koizumi, Richter, et al., 1997). Both would suggest that high

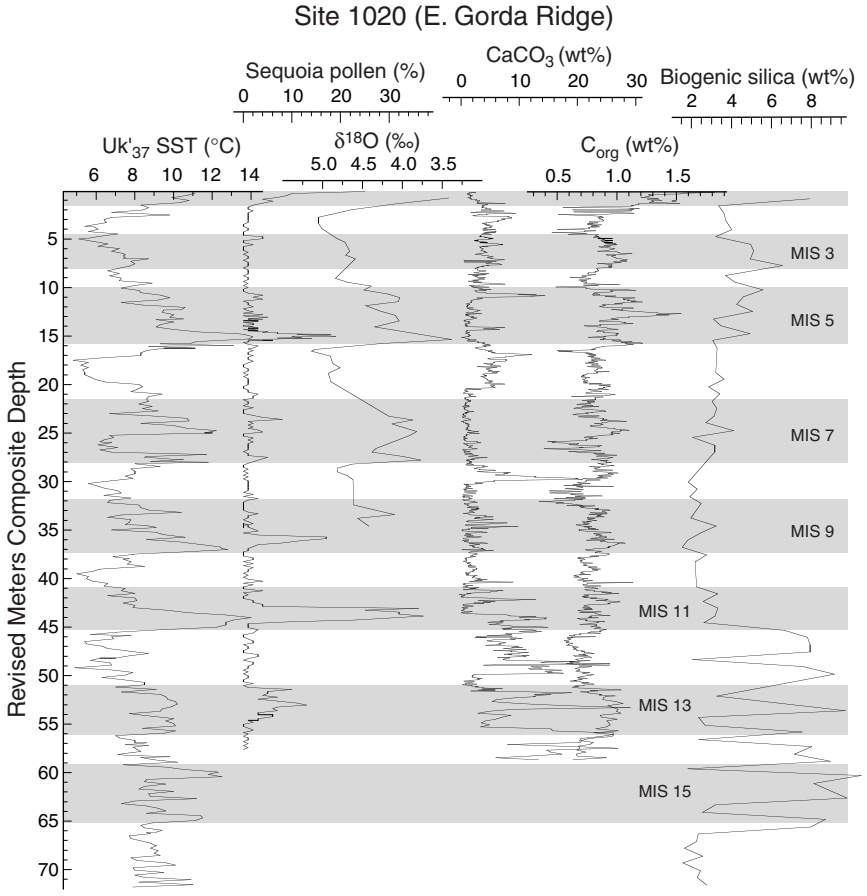

Figure 28. Time series from Site 1020 on the East Gorda Ridge, off Northern California (Fig. 20). SST data from Kreitz et al. (Chap. 10, this volume); *Sequoia* pollen data from Heusser et al. (Chap. 17, this volume); oxygen isotopes, $CaCO_3$ and C_{org} from Lyle et al. (Chap. 11, this volume); biogenic silica from Kuroda et al. (Chap. 14, this volume). High *Sequoia* (redwood) abundance is associated with only the major interglacials, as marked by both isotopes and alkenone SST. High $CaCO_3$ generally occurs in glacial periods, but lowest values lag the glacial–interglacial transition. There is a major transition in alkenone SST, $CaCO_3$, and biogenic silica records occurring through MIS 12 and 11. Depth is shown in revised meters composite depth from Lyle et al. (Chap. 11, this volume).

$CaCO_3$ burial began nearly coincident with the beginning of the high biogenic silica burial, near the MIS 15/16 boundary. Lyle et al. (Chap. 11, this volume) have noted a similar $CaCO_3$ high prior to MIS 10 at Site 1021, but no detailed records exist to the south. The estimated $CaCO_3$ percent from reflectometry for the California Borderlands sites (Sites 1011, 1012, 1013, and 1014) would suggest that this event is much less prominent in the southern California margin. Detailed longer records from the California Borderlands need to be analyzed and compared to the records from the north.

Alkenone SST records would suggest that the period of relatively warm glacial intervals in the North Pacific may have lasted from the Brunhes/Matuyama boundary to MIS 12. We do not yet understand why the temperate North Pacific Ocean remained relatively warm during this period; nor do we understand why there was high biogenic deposition in the period from MIS 15 to 11, although it may be related to the 400-k.y. orbital forcing. Obviously we need to analyze more long time series to better understand the evolution of North Pacific oceanographic conditions during the Pleistocene. Most of the Leg 167 drill sites have the potential for time series of 1000 k.y. or longer.

Tantalizing comparisons can be made with time series from other regions in the Pacific. In the eastern equatorial Pacific at Site 847, Murray et al. (1995) noted peak $CaCO_3$ percent and MAR for the last 1 m.y. at about 400 ka. The interval between 0.35 and about 1.1 Ma has higher than average $CaCO_3$ percentages and $CaCO_3$ MAR. In the Peru Basin in the southeastern Pacific, high $CaCO_3$ percentages and $CaCO_3$ MAR are also found in the interval 0.4–1.1 Ma (Weber et al., 1995). These intervals are somewhat longer than the Site 1020 record. It is not yet clear if there is any significance to the coincidence of high $CaCO_3$ around 400–600 ka in the eastern Pacific, but better regional comparisons are clearly needed.

$CaCO_3$ and C_{org} Records

High-resolution records of carbon burial for the last 500 k.y. are being generated for Sites 1020, 1018, and 1012 (Lyle et al., Chap. 11, this volume; M. Lyle, unpubl. data). Figure 28 shows the record from Site 1020. Whereas the general Pacific pattern of high $CaCO_3$ in glacial intervals typically occurs, the Site 1020 time series is much more spiky than a typical orbitally forced record—it has high variance in frequencies higher than the orbitally forced ones. The $CaCO_3$ events can be correlated to other northern California drill sites (Sites 1019 and 1018; Lyle et al., Chap. 11, this volume) and show the potential for millennial-scale correlation between sedimentary records within the region throughout the late Pleistocene.

C_{org} has a tendency to be higher in the interglacial periods, in contrast to $CaCO_3$. The level of variability of C_{org} is significantly smaller than $CaCO_3$, however, and has a two-times range vs. a ~10-times range for $CaCO_3$. Surprisingly, the $CaCO_3$ spikes tend to also be high C_{org} events. C_{org} has a slight tendency to lead a $CaCO_3$ burial spike, however.

Lyle et al. (Chap. 11, this volume) have suggested that the orbital-scale glacial–interglacial variation in $CaCO_3$ may be driven in part by changes in the saturation state of $[CO_3]^=$ in Pacific deep water, but that the majority of the variance in the record is driven by changes in the production of $CaCO_3$ in surface waters combined with change in $CaCO_3/C_{org}$ in the particulate rain to the seafloor. This hypothesis implies that the surface of the North Pacific Ocean is highly sensitive to millennial-scale climate processes.

One of the lines of evidence that the $CaCO_3$ record is driven by the surface ocean depends upon the SST record. Highest $CaCO_3$ deposition is not inversely correlated with SST but instead occurs when SST is in the range of about 7.5°–9°C. Even the prominent $CaCO_3$ spike in the middle of MIS 8 occurs after the minimum SST and in the shoulder of moderate SST immediately prior to the first MIS 7 interglacial event. The 7.5°–9°C temperature range marks one in which sediment trap experiments record high $CaCO_3$ rain with high $CaCO_3/C_{org}$ leaving modern North Pacific surface waters (Lyle et al., Chap. 11, this volume). High $CaCO_3$ rain and high $CaCO_3/C_{org}$ maximizes the delivery of $CaCO_3$ to the ocean floor and minimizes the C_{org}-mediated dissolution at the bottom.

Further work linking the biogenic sedimentary records (including biogenic silica) to specific high-resolution micropaleontological and stable isotope records will be crucial to establish the change in the surface North Pacific Ocean through the Pleistocene and will provide a better understanding of the implications of these changes for climate and biogeochemical cycles.

The Terrestrial–Marine Connection

One of the other priorities from Leg 167 is to better understand the linkages between the oceanographic conditions along the California margin and terrestrial climate. Some researchers have been studying the provenance and mass accumulation rates of terrestrial aluminosilicate detritus in the Leg 167 cores (Irino and Pedersen, Chap. 23, this volume; Hovan et al., Chap. 18, this volume) to understand changes in continental erosion and transport. In northern and central California (Sites 1018 and 1020), Hovan et al. (Chap. 18, this volume) note a link between terrigenous MAR and orbital-scale climate variability. Highest terrigenous MARs are associated with glacial periods, indicating increased supply from source regions, because of exposure of continental shelves and/or increased fluvial sediment discharge. Provenance of the material suggests a primary source region from the Klamath Mountains or Cape Mendocino region to Site 1020 during glacial intervals. In the south, Tada et al. (Chap. 25, this volume) and Irino and Pedersen (Chap. 23, this volume) also show a glacial–interglacial change, suggesting higher offshelf transport or fluvial discharge for the period MIS 3–2.

Pollen from coastal plant communities is also buried in sediments along the California margin and provides a way to link changes in the terrestrial climate to changes in paleoceanographic conditions offshore (Heusser, 1998; Heusser et al., Chap. 17, this volume). In Northern California, peak interglacials are marked by a distinctive floral succession. On deglaciations, alder (*Alnus*) pioneers reforestation by the interglacial community, followed by lowland oak (*Quercus*), and finally by redwood (*Sequoia*). Redwood is typically found in the late stages of strong interglacial periods. We only have information about the last 160 k.y. from southern California (Site 893, Heusser, 1995), but see a strong glacial–interglacial signal alternating between oak and nonarboreal pollen in the interglacials and *juniperus* or pine in the glacials. Pine most strongly appears at the glacial maximum in MIS 2.

Figure 28 allows the comparison of the *Sequoia* record with that of the benthic foraminiferal oxygen isotopes and the alkenone SST record at Site 1020. *Sequoia* pollen is only present in significant quantities when the SST goes above 10°C. For greater than 90% of the last 500 k.y. in Northern California, *Sequoia* has been a rare genus and not the dominant tree type. If one looks closely at the record it becomes apparent that the peak *Sequoia* pollen percentages lag peak SST. It also is clear that the highest abundance of *Sequoia* pollen is found during intervals when SST remained for the longest time above 10°C (e.g., MIS1 and 11). Short intense SST warmings (e.g. MIS 5e) don't seem to allow time for the *Sequoia* forest to reach its maximum extent. The very short SST warmings in MIS 7 lead to a small response by *Sequoia*.

The response in the plant community to glacial–interglacial cycles is complex, being a response to temperature, insolation, precipitation, seasonality, and competition. Nevertheless, there is a typical response to the glacial cycle that should eventually provide an important means to understand how insolation changes affect these factors on the adjacent continent. There is not only a typical response to each glacial–interglacial change but also a unique response specific to individual glacial–interglacial pairs (Heusser et al., Chap. 17, this volume) that implies an evolution to the system through time or some inherent instabilities that we do not yet understand.

By lumping the pollen data from genera that are common in the Holocene coastal region from Northern California to Canada into an 'interglacial lowland forest' community (sitka spruce, western red cedar, western hemlock, redwood, oak, ferns; Fig. 29) and comparing the aggregate to SST we find a more linear response from the group than from any of the individual genera. It appears that changes in SST cause a relatively consistent expansion or contraction of the community as a whole, even though there are also important shifts in importance of species within the community.

MST Records and Color Reflectometry

It is now typical within ODP to measure wet bulk density, magnetic susceptibility, natural gamma-ray activity, and *P*-wave velocity at high resolution using the shipboard multisensor track (MST). On Leg 167, we also measured color reflectometry by two systems: the ODP digital color imaging system (Nederbragt et al., Chap. 29, this volume) and the Oregon State University (OSU) SCAT spectral reflectometer (see "Explanatory Notes" chapter in Lyle, Koizumi, Richter, et al., 1997; Harris et al., 1997). Nederbragt et al. (Chap. 29, this volume) took combined data from three-channel (RGB) video images to make 1-cm color averages downcore, using the L*a*b* system (lightness, green-red, and blue-yellow). The OSU system, in contrast, measures 1000 channels of color information from the near-infrared to near-ultraviolet wavelengths at discrete 2 cm spots downcore.

The most useful records for the high-resolution stratigraphic correlation proved to be the color data, because sediments with fast sedimentation rates tend to be rich in C_{org} and gassy. Gaps and expanded sections caused significant artifacts in GRAPE (gamma-ray attenuation porosity evaluator) bulk density data at many sites, whereas diagenesis highly attenuated the magnetic susceptibility signal after ~20 mbsf, except when diagenetic sulfides were formed in high quantities. The GRAPE density and magnetic susceptibility records are extremely good offshore at sites with more moderate sedimentation rates (e.g., Sites 1010, 1016, and 1021), as we will show when discussing the Neogene sediments.

Color changes in sediments are caused by a change in the relative abundance of different sedimentary phases. The best known example is $CaCO_3$, where changes in its abundance change the lightness of the sediment color. Color changes can also occur when other minerals change abundance. When hematite concentration changes in equatorial Atlantic sediments, for example, the amount of red color in the sediment changes (Balsam et al., 1995).

The resolution of video images and the rapidity at which they can be collected makes this an attractive tool to study sedimentary core material. Significant problems are encountered when using video images quantitatively, however, because of nonuniform illumination and the changing color of the light source over time. These require postcruise processing before use (Nederbragt et al., Chap. 29, this volume). Figure 30 shows the processed profiles for the four drill sites in the California Borderlands. Also included are benthic oxygen isotope time series (where available) for independent correlation between sites (Andreasen et al., Chap. 8, this volume; Hendy and Kennett, Chap. 7, this volume). The L* curves have extremely high resolution and provide a simple way to correlate between drill sites or to other cores from the California Borderlands region. They also may provide a high-resolution analytical tool if we can understand the cause of the signal observed.

We have $CaCO_3$ and C_{org} data from Site 1011 at 10-cm resolution (Lyle et al., Chap. 11, this volume) to compare to the L* curve and test if the change in sediment lightness is essentially a measure of $CaCO_3$ content (Fig. 31). A quick comparison shows that the L* and $CaCO_3$ time series have significant differences. The intervals that are most anomalous in the L*–$CaCO_3$ comparison also happen to be extremes in the C_{org} record. High C_{org} is a major factor causing a darker average sediment color. A simple linear model can be created to estimate L* by subtracting 85% of the C_{org} variation (expressed as percentage of C_{org} range in the intervals) from $CaCO_3$ in percentage of its range. Because L* is a mixed signal nearly equally weighted to both $CaCO_3$ and C_{org} variability, one cannot use the L* time series as a proxy for either $CaCO_3$ or C_{org} in the California Borderlands, even though it is highly useful for correlations. Further work must be done to use the other color information recorded by the digital imaging system to distinguish between C_{org} and $CaCO_3$.

The OSU SCAT spectral reflectometer, which takes 1024 channels of reflection data, has a stronger ability to distinguish between sedimentary components by their color spectra. To get the spectral resolution, one trades off depth resolution. Maximum resolution on the SCAT is 20 mm vs. ~0.25 mm for the digital imaging technology. Typical spacing of SCAT measurements on Leg 167 were 4–6 cm. The use of this data is still in its infancy because of the lack of good calibration data sets. Independent high-quality data sets of sedimentary components must be measured on the core material to determine the spectral response of each component.

Some calibration has been done using shipboard data, with impressive results. Figure 32 shows a comparison between an estimate of C_{org} by the SCAT reflectometer on Hole 1019C (Eel River Basin) and the splice C_{org} data from Lyle et al. (Chap. 11, this volume), which is a combination of data from Holes 1019C and 1019E. None of the data used for the reflectometry calibration is from this data set. The estimated and measured C_{org} profiles overlay each other except for the interval between about 21 and 30 mcd. The discrepant interval is one with essentially no $CaCO_3$ in the section, as compared to an av-

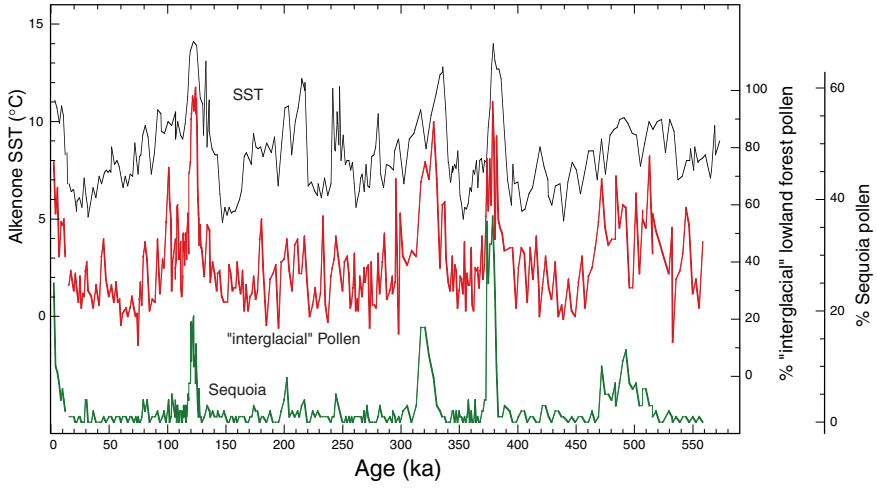

Figure 29. Comparison of alkenone SST from Site 1020 to "interglacial lowland forest" pollen percentages. This represents the sum of sitka spruce, western red cedar, western hemlock, redwood, oak, and fern pollen. It is evident that this aggregate basically responds to SST or they both respond to a common outside factor. However, individual plant groups within the interglacial community respond to much more specific needs (e.g., *Sequoia*) and have significantly different time series.

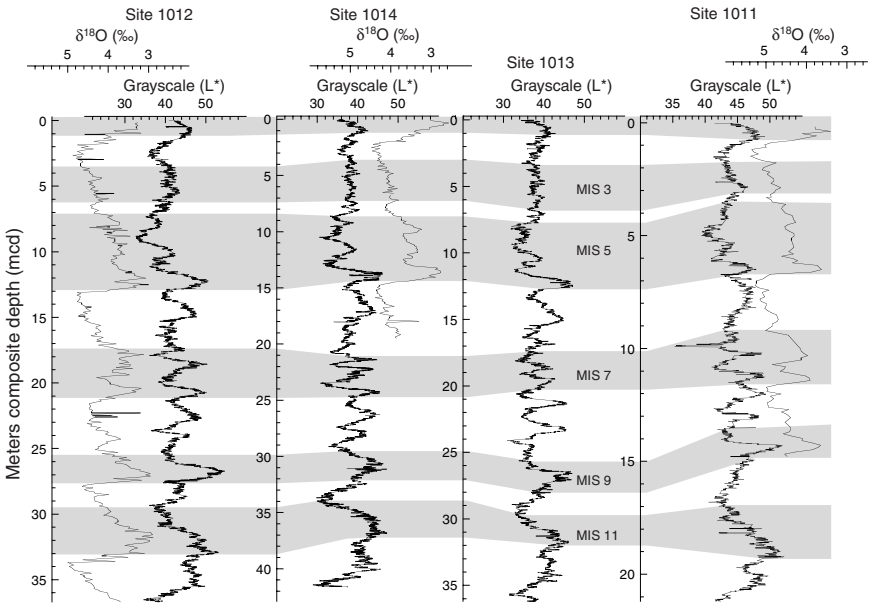

Figure 30. Plots of L*, the grayscale measure in the L*a*b* system vs. depth, and benthic foraminiferal oxygen isotopes at each of the four California Borderlands drill sites. L* data is from Nederbragt et al. (Chap. 29, this volume). Benthic oxygen isotope data are from Andreasen et al. (Chap. 8, this volume) for Sites 1011 and 1012, and Hendy and Kennett (Chap. 7, this volume) for Site 1014. L* ranges between 0 when the color is black to 100 when the color is white. There is clearly a strong and correlatable signal throughout the California Borderlands, providing a fast, simple stratigraphic correlation tool.

erage of about 5% elsewhere, so it is abnormally darker than the average sediment. For this reason, the C_{org} was overestimated. The C_{org} estimate can probably be improved by a recalibration with sediments expressing a full range of sediment variability.

NEOGENE

The Neogene sedimentary record along the California margin is somewhat familiar because the outlines of the Neogene history have been assembled from earlier drilling (Deep Sea Drilling Project [DSDP] Legs 5, 18, and 63; Barron,1989, 1998). The discontinuous nature of the DSDP drilling recovery, the scattered positions of the older drilling sites, and the lack of good stratigraphic control meant that detail was lacking prior to Leg 167 drilling and that much of the structure within the sedimentary record could not be studied. Much of the potential usefulness of the Leg 167 records has yet to be exploited because of Pleistocene research had the priority in initial post-cruise studies. So far, most of the Neogene research has focused upon development of better regional stratigraphic control.

We describe only a reconnaissance of major paleoceanographic developments along the margin, but even at this early stage we note that major changes in paleoceanographic conditions since 14 Ma have relationships, unsurprisingly, to exposed sedimentary sections of equivalent age in coastal California; for example, the Miocene Monterey and Sisquoc formations. We also identified a major $CaCO_3$ depositional event in the late Pliocene that abruptly ended or strongly diminished in strength at 2.6 Ma with the beginning of Northern Hemisphere glaciation (Ravelo et al., 1997). Fine-scale structure of these events still needs to be measured and the implications for paleoceanography, the biogeochemical cycle, and climate need to be understood.

Neogene Stratigraphy

One of the primary goals of Leg 167 was to collect magnetostratigraphic records of the Quaternary and Neogene that could be used to provide a good chronostratigraphic framework to evaluate the isochroneity of biostratigraphic events along the California margin. Prior to Leg 167, magnetostratigraphic studies in the middle-latitude northeastern Pacific were limited to relatively fragmentary onshore records (e.g., Madrid et al., 1986; Omarzai et al., 1993).

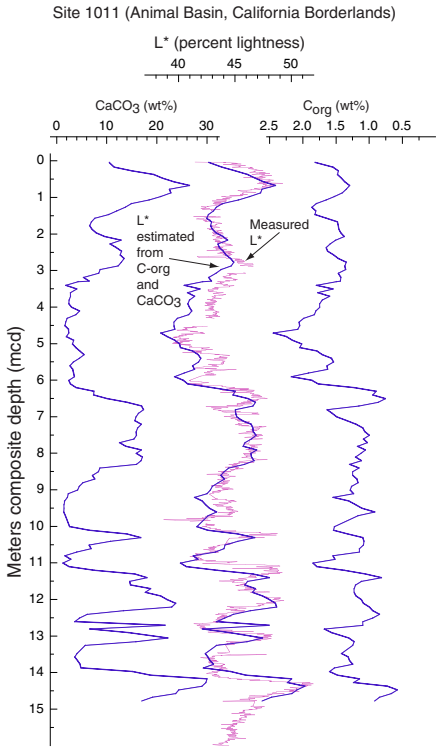

Figure 31. A comparison of the L* signal (Nederbragt et al., Chap. 29, this volume) to $CaCO_3$ and C_{org} (Lyle et al., Chap. 11, this volume) shows that the L* depth series is significantly different from the $CaCO_3$ series. $CaCO_3$ is not the only sedimentary phase controlling the lightness of the sediment. High C_{org} is a significant factor that makes the sediment darker. Note that C_{org} is plotted reversed to $CaCO_3$ in order that it have the same sense of change with respect to L*. Using a simple linear combination of C_{org} and $CaCO_3$ time series it is possible to reconstruct the L* signal.

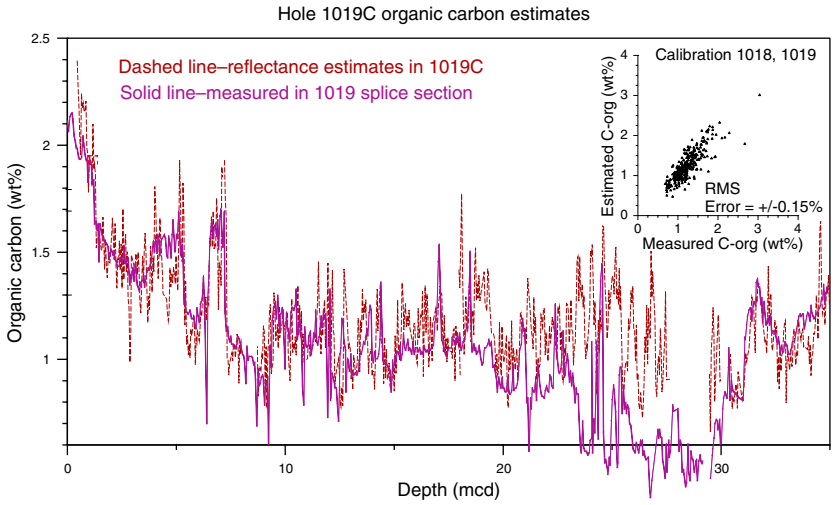

Figure 32. A comparison of the spliced C_{org} data from Site 1019 (Holes 1019C and 1019E, Lyle et al., Chap. 11, this volume) to an estimate of C_{org} in Hole 1019C from the OSU SCAT reflectometer. The reflectometer estimate was calibrated with shipboard $CaCO_3$ and C_{org} analyses.

Leg 167 provided excellent magnetostratigraphic records of the last 6.3 m.y. The longest one is from the composite section of Holes 1010C and 1010E (Hayashida et al., 1999), which yielded a high fidelity record from C1n (Brunhes) to C3A.n2 (latest Miocene; Table 5; Fig. 33). The magnetostratigraphic reversal record from Site 1021 is also lengthy, extending from C1n (Brunhes) to C3n.4n (5.23 Ma; earliest Pliocene). The magnetostratigraphic records at other Leg 167 sites—Sites 1012, 1013, and 1014—are excellent for the Quaternary, but unfortunately they do not extend back beyond the Olduvai (1.195 Ma; see Table 1 of Lyle, Koizumi, Richter, et al., 1997).

Calcareous Nannofossil Biostratigraphy

The study of Fornaciari (Chap. 1, this volume) represents the first real attempt since Bukry's (1981) study of DSDP Leg 63 to refine calcareous nannofossil biostratigraphy along the California margin. Fornaciari (Chap. 1, this volume) has evaluated the reliability of 50 calcareous nannofossil biostratigraphic events (biohorizons) by considering their mode of occurrence, ranking, and spacing. Four biohorizons in the Pleistocene are considered good and apparently synchronous (Table 5; Fig. 34): the last occurrence (LO) of *Pseudoemiliania lacunosa*, the LO and first occurrence (FO) of large *Gephyrocapsa*, and the FO of *G. oceanica* s.l. All these biohorizons can be recognized across the entire Leg 167 latitudinal transect in the California margin (Table 5; Fig. 33).

The Pliocene calcareous nannofossil assemblage is generally poorly diversified and badly preserved. The following six biohorizons are considered reliable in the Pliocene interval: the LO of *Discoaster pentaradiatus*, the LO of *D. surculus*, the LO of *D. tamalis*, the LO of *Reticulofenestra pseudoumbilicus*, the LO of *Amaurolithus delicatus*, and the paracme beginning (PB) of *D. pentaradiatus* (Table 5; Fig. 34).

The late Miocene calcareous nannofossil assemblages are distinctive, as discoasterids are generally rare to scarce because the area was affected by high productivity conditions that are unfavorable for discoasterids. In particular, the standard zonal marker species of Okada and Bukry (1980) are quite rare. Based on their occurrences at ODP Sites 1010, 1011, and 1021, ten late Miocene calcareous nannofossil datum levels appear to be useful for correlation (Table 6; Figs. 34, 35): the LO of *D. quinqueramus/berggrenii*, the FO of *A. primus*, the FO of *D. quinqueramus/berggrenii*, the LO of *D. hamatus*, the FO of *D. bellus*, the FO of *Catinaster coalitus*, the LO of *Cyclicargolithus floridanus*, the FO of *D. kugleri*, the LO of *Calcidiscus premacintyrei*, and the LO of S*phenolithus heteromorphus*. Additional older middle and early Miocene calcareous nannofossil datum levels that have proven to be useful for correlation in the California area (Bukry, 1981; pers. comm., 1999) are included on Figure 35.

Diatoms

Previous work on diatom biostratigraphy along the California margin is summarized in Barron (1981, 1992a, 1992b). Correlation of diatom datum levels to magnetostratigraphy in the mid-latitude North Pacific has been poor, especially below the latest Pliocene. Maruyama (Chap. 3, this volume) identifies at least 31 middle Miocene through Pleistocene diatom datum levels (biohorizons) that allow precise correlation along the California Current from Sites 1010 to 1022. He identifies six biohorizons that appear to be nearly synchronous through the interval from Pliocene to Pleistocene sediments recovered from the California margin: the FO and LO of *Proboscia curvirostris*, the FO of *Fragilariopsis doliolus*, the LO of *Thalassiosira convexa*, the LO of *Neodenticula kamtschatica*, and the FO of *Neodenticula seminae* (Table 5; Figs. 33, 34). Within the northern region, the FOs of *N. koizumii* and *Stephanopyxis dimorpha* may also be useful for stratigraphic correlation (Table 5; Figs. 33, 34). Because of dissolution or poor preservation in the southern sites and the cool-water character of the northern sites, subtropical age-diagnostic species are scarce in the Pliocene and Pleistocene sediments recovered by Leg 167.

Maruyama (Chap. 3, this volume) identifies 11 biohorizons that are essentially synchronous through Miocene interval of Leg 167: FO of *Thalassiosira oestrupii*, the last common occurrence (LCO) of *Rouxia californica*, the first common occurrence (FCO) and LCO of *Thalassionema schraderi*, the FCO and LCO of *Denticulopsis simonsenii*, the FO and LO of *D. dimorpha*, and the FO and LCO of *D. praedimorpha* (Tables 5, 6; Figs. 33–35). All these biohorizons have been recognized to be of the essence of various North Pacific diatom zonations (Koizumi, 1992; Barron and Gladenkov, 1995). Additional older middle and early Miocene diatom datum levels that have proven to be useful in the California region (Barron, 1992a) are included on Figure 35.

An interval of poor diatom preservation containing only rare and poorly preserved diatoms is present from the late Miocene (7.0 Ma) through the early Pliocene (2.6 Ma) (Maruyama, Chap. 3, this volume). Diatom stratigraphy reveals the diatomaceous interval from middle to late Miocene, but in the overlying units prior to 2.6 Ma diatoms quickly disappear due to the increase of terrigenous component. Maruyama (Chap. 3, this volume) interpreted the poor diatom preservation to be a result first of rapid cooling, which is also indicated by a global fall in sea level, followed by a warming that should have caused a decline in diatom abundance in the surface waters.

Table 5. Summary of biohorizons from Leg 167 drill sites with magnetostratigraphic age control.

Code	Event (CK95)	Age (Ma)	Depth (mcd)											
			Site 1010	Site 1011	Site 1012	Site 1013	Site 1014	Site 1016	Site 1017	Site 1018	Site 1021	Site 1022	Site 1020	Site 1019
D17	LO *P. curvirostris*	0.30		NR	NR	NR	NR	32.75	NR	73.68	NR	—	43.67	44.16
P8	LO *P. lacunosa*	0.46	4.70	21.98	37.08	13.57	39.21	25.00	104.40	96.78	16.91	—	49.98	52.49
F8	LO *N. pachyderma* A		NR	26.19	54.96	62.25	62.75	NR	NR	117.61	NR	—	69.75	NR
	Cln. "Brunhes" (o)	0.78	9.52	NR	61.85	56.64	65.66	NR	>110	>116.24	27.16	—	84.83	>85.72
	Clr. ln "Jaramillo" (t)	0.79	12.28	NR	75.95	65.97	81.58	NR	NR	NR	33.23	—	100.68	NR
	Clr. ln "Jaramillo" (o)	1.07	13.08	NR	83.18	69.27	87.62	NR	NR	NR	NR	—	108.81	NR
	Clr. 2r. ln "Cobb Mtn." (t)	1.20	14.78	NR	87.64	76.37	NR	NR	NR	NR	NR	—	NR	—
	Clr. 2r. ln "Cobb Mtn." (o)	1.21	14.93	NR	89.75	78.65	NR	NR	NR	NR	NR	—	NR	—
P5	LO large *Gephyrocapsa*	1.24	16.67	NR	90.97	NR	95.83	NR	186.55	177.57	NR	—	123.51	—
F7	FO *N. pachyderma* B		NR	46.48	93.50	74.04	99.73	NR	NR	194.59	NR	—	123.44	—
P3	FO large *Gephyrocapsa*	1.46	18.28	NR	105.68	84.41	113.92	NR	193.33	193.18	NR	—	148.17	—
D16	FO *P. curvirostris*	1.50	NR	NR	NR	NR	NR	63.84	—	207.47	NR	—	151.03	—
F6	FO *N. pachyderma* A		NR	46.48	126.98	89.85	116.64	NR	—	225.67	NR	—	188.94	—
P2	FO *G. oceanica* s.l	1.64-1.77	20.53	60.62	114.62	98.89	123.08	65.47	—	224.97	53.98	0.87	165.60	—
	C2n "Olduvai" (t)	1.77	22.50		124.57	92.44	NR	NR	—	NR	55.33	NR	NR	—
F5	LO *N. kagaensis*		NR	72.47	126.98	102.74	140.51	NR	—	268.47	NR	NR	188.88	—
	C2n "Olduvai" (o)	1.95	24.21	NR	132.57	104.81	NR	NR	—	NR	61.63	NR	NR	—
F4	LO *N. asanoi*		NR	86.77	143.06	120.40	186.06	NR	—	321.44	NR	NR	191.61	—
	FO *N. pachyderma* C		NR	92.52	NR	123.05	197.02	NR	—	299.84	NR	NR	227.02	—
D15	FO *F. doliolus*	2.00	NR	NR	NR	NR	NR	NR	—	Diachronous	NR	NR	NR	—
D14	LO *T. convexa*	2.35	NR	NR	NR	NR	214.15	102.63	—	315.99	79.25?	37.85	247.50	—
Pl14	LO *D. pentaradiatus*	2.44-2.51	31.84	93.04	173.52	132.12	195.11	110.05	—	338.28	83.33	22.48	242.43	—
Pl13	LO *D. surculus*	2.54-2.55	33.32	101.95	183.03	132.12	201.34	110.05	—	341.58	84.94	22.48	242.43	—
	C2An. ln "Gauss" (t)	2.58	34.05	NR	NR	NR	NR	NR	—	NR	86.03	NR	NR	—
D13	LO *N. kamtschatica*	2.61-2.68	NR	NR	NR	NR	Diachronous	Diachronous	—	383.54	NR	86.29?	247.40?	—
D12	FO *N. seminae*	2.68	NR	Diachronous	NR	NR	NR	120.46	—	421.94	65.48	69.91	260.47	—
Pl12	LO *D. tamalis*	2.97	37.97	108.45	204.32	138.33	249.77	132.00	—	376.99	102.20	74.22	255.76	—
	C2An. lr "Kaena" (t)	3.04	38.62	NR	NR	—	NR	NR	—	NR	105.18	NR	NR	—
	C2An. lr "Kaena" (o)	3.11	39.39	NR	NR	—	NR	NR	—	NR	107.16	NR	NR	—
	C2An. 2r "Mammoth" (t)	3.22	40.53	NR	NR	—	NR	NR	—	NR	109.62	NR	NR	—
	FO *G. inflata*	3.3	NR	133.95	245.41	—	299.02	NR	—	428.04	NR	NR	258.25	—
	C2An. 2r "Mammoth" (o)	3.33	41.79	NR	NR	—	NR	NR	—	NR	113.14	NR	NR	—
	FO *N. koizumii*	3.53	NR	Diachronous	NR	—	312.65	155.33	—	431.54	86.88	151.81	NR	—
F3	FO *N. asanoi*		NR	141.45	234.06	—	318.86	NR	—	428.04	NR	NR	268.07	—
	C2Ar "Gilbert" (t)	3.58	45.09	NR	NR	—	NR	NR	—	NR	121.80	NR	NR	—
	FO *S. dimorpha*	3.7	NR	NR	NR	—	NR	Diachronous	—	<445.20	99.48	190.58	NR	—
P19	LO *R. pseudoumbilicus*	3.83	Poor	147.39	269.46	—	332.41	174.89	—	—	127.76	NR	289.07	—
P18	LO *A. delicatus*	3.96	NR	147.39	269.46	—	340.94	174.89	—	—	130.76	NR	289.07	—
P17	PB *D. pentaradiatus*	4.06	NR	152.06	NR	—	352.69	177.25	—	—	133.01	NR	—	—
	C3n. ln "Cochiti" (t)	4.18	49.98	NR	NR	—	NR	NR	—	—	136.50	NR	—	—
	C3n. ln "Cochiti" (o)	4.29	50.82	NR	NR	—	NR	NR	—	—	140.00	NR	—	—
	C3n. 2n "Nunivak" (t)	4.48	52.33	NR	NR	—	NR	NR	—	—	143.15	NR	—	—
	C3n. 2n "Nunivak" (o)	4.62	53.50	NR	NR	—	NR	NR	—	—	151.39	NR	—	—
	C3n. 3n "Sidufjall" (t)	4.80	55.44	NR	NR	—	NR	NR	—	—	155.67	NR	—	—
	C3n. 3n "Sidufjall" (o)	4.89	56.22	NR	NR	—	NR	NR	—	—	NR	NR	—	—
	C3n. 4n "Thvera" (t)	4.98	58.01	NR	NR	—	NR	NR	—	—	NR	NR	—	—
	C3n. 4n "Thvera" (o)	5.23	60.59	NR	NR	—	NR	NR	—	—	168.84	NR	—	—
D11	FO *T. oestrupii*	5.49	NR	NR	NR	—	NR	302.75	—	—	160.20	<368.78	—	—
	LO *D. quinqueramus/berggrenii*	5.6	64.89	187.95	NR	—	400.17	301.86	—	—	189.48	NR	—	—
	C3A. nl (t)	5.89	70.08	NR	NR	—	NR	NR	—	—	NR	—	—	—
	C3A. nl (o)	6.17	74.29	NR	NR	—	NR	—	—	—	NR	—	—	—
	C3A. n2 (t)	6.27	76.40	NR	NR	—	NR	—	—	—	NR	—	—	—

Notes: Codes are used to identify biohorizons on Figures 33, 38, and 39. CK95 = age following Cande and Kent (1995). NR = not recorded. (t) = termination; (o) = onset. — = not recovered. Stratigraphic depths reported here represent a midpoint between constraining samples.

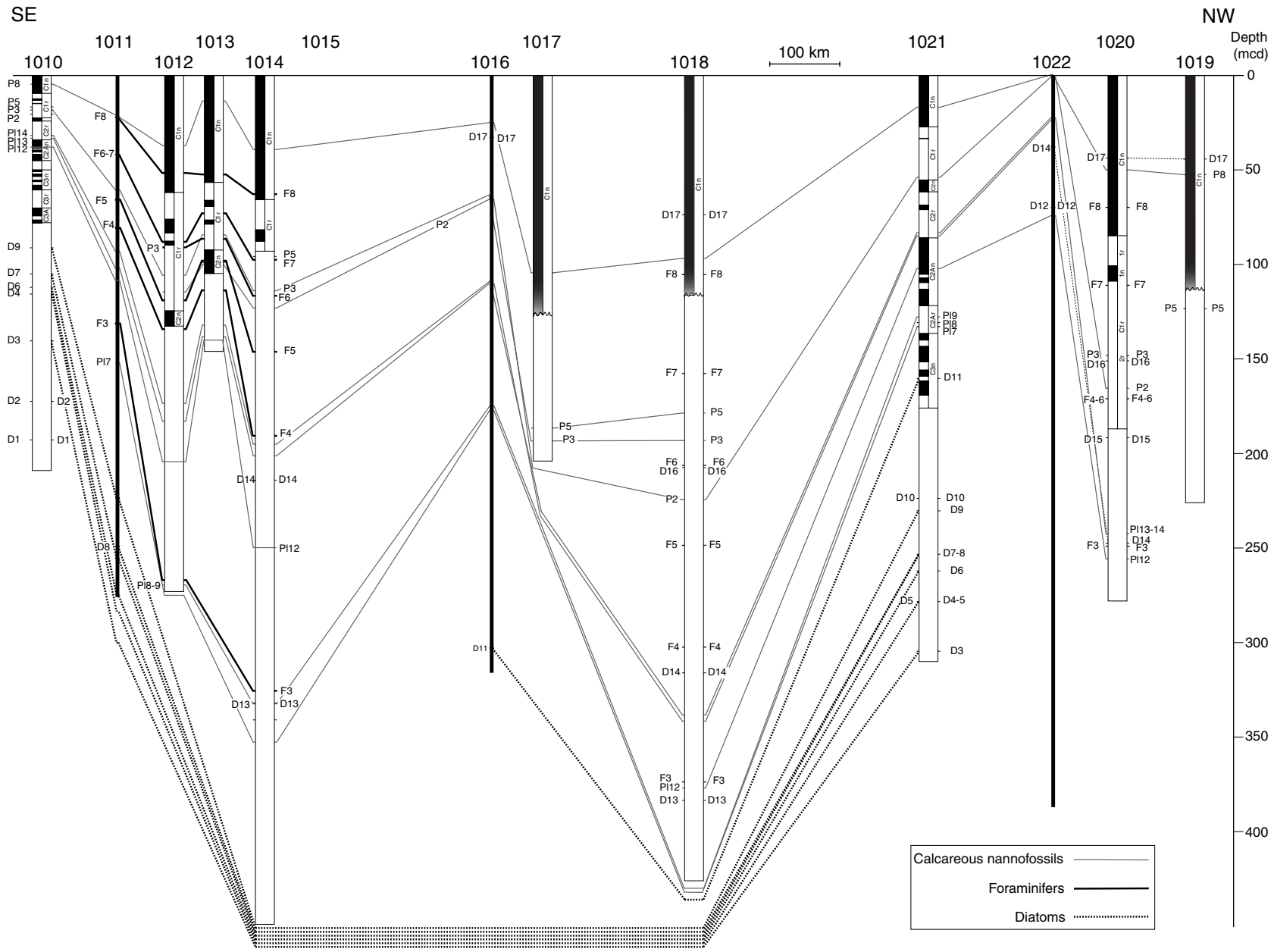

Figure 33. Summary fence diagram of biostratigraphic correlations in Leg 167. Magnetostratigraphies from Lyle, Koizumi, Richter, et al. (1997) and Hayashida et al. (1999).

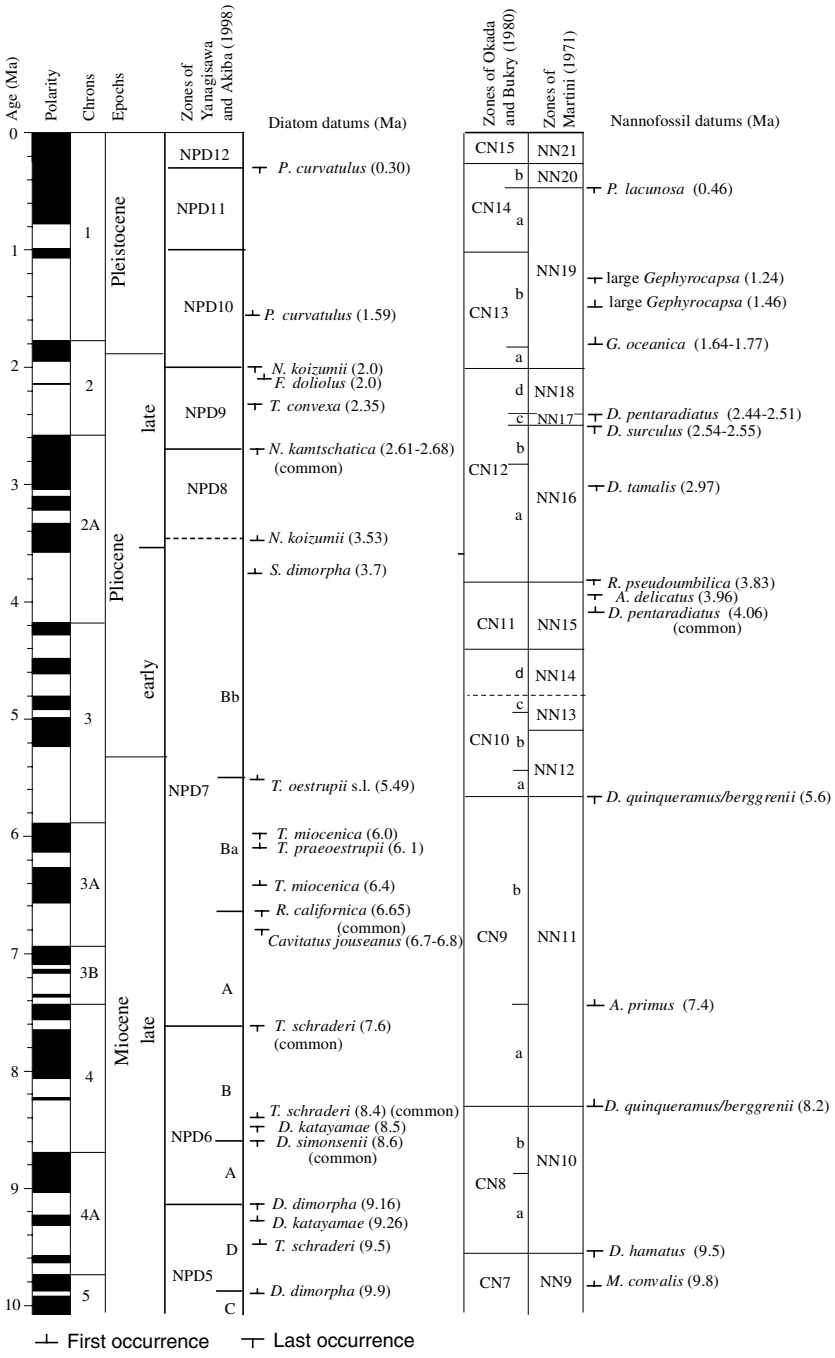

Figure 34. Biochronology of diatoms and calcareous nannofossils for the late Neogene and Quaternary (0–10 Ma) of the California margin (ODP Leg 167). The biostratigraphic datums are compared to the magnetochronostratigraphy of Cande and Kent (1995).

Planktonic Foraminifers

The planktonic foraminiferal assemblages are consistently dominated by few taxa. A total of seven biohorizons of evolutionary changes within the *Neogloboquadrina* plexus are broadly applicable in the interval from the late early Pliocene to the Quaternary (~3.5 Ma to present day) throughout the region (Kennett et al., Chap. 2, this volume): the LO and FO of *Neogloboquadrina pachyderma* A (dextral, inflated form), the FO of *N. pachyderma* B (sinistral, inflated form), the FO of *N. pachyderma* C, the LO of *N. kagaensis*, and the LO and FO of *N. asanoi* (Table 5; Figs. 33, 34). The FO of *Globorotalia inflata* (3.3 Ma) also appears to be useful for biostratigraphy. Older, biosiliceous-rich sediments in the sequences generally lack planktonic foraminifers.

Radiolarians

No radiolarian studies beyond those reported in the *Initial Reports* volume (Lyle, Koizumi, Richter, et al., 1997) were completed for this volume.

Stratigraphy and Physical Properties from the MST

We have observed that physical properties of sediments such as color are useful for high-resolution correlations in the Pleistocene section (Fig. 30). Profiles of physical properties will also prove useful to develop better correlations in the Neogene section as well (Fig. 36). The profiles have both megayear and high-frequency structure, which should be useful for basic correlations and for later high-reso-

lution tuning. Figure 36 is a comparison of GRAPE bulk density and 450–500 nm reflectance time series from Sites 1010, 1021, and 1022. It illustrates the strong variability on the million-year scale. Episodes of high reflectance and high bulk density occur about every 2 m.y. at Sites 1010 and 1021. We believe that the profiles are controlled by $CaCO_3$ variations, because $CaCO_3$ ranges from 0% to 60% at Site 1021 and from about 0% to 80% at Site 1010 (Lyle, Koizumi, Richter, et al., 1997), and because $CaCO_3$ is white throughout the visible spectrum. This hypothesis needs further confirmation, but would suggest that the high $CaCO_3$ event in the mid-Pliocene discussed by Ravelo et al. (1997) is not unique to the time immediately prior to Northern Hemisphere glaciation. It also appears that high $CaCO_3$ events were comparable in magnitude between the southern Site 1010 and the northern Site 1021 prior to ~8 Ma. After 8 Ma, north–south differences in $CaCO_3$ content were enhanced, perhaps as the latitudinal thermal gradient increased. Further work is needed to better define the high-resolution structure of these Miocene and early Pliocene events and to better constrain their timing.

Neogene Paleoceanographic Events

The multiple biostratigraphic events (biohorizons) along the California margin, after being placed within a chronological framework by integration with paleomagnetic stratigraphy, enables correlation between the Leg 167 drill sites. Comparison between drill sites identifies distinct biostratigraphic events in the California Current system which are placed within an absolute time frame.

During the middle Miocene through Quaternary paleoclimatic and paleoceanographic conditions varied considerably throughout the 29°N to 40°N latitudinal transect drilled during Leg 167. Subtropical and subarctic floras and faunas continually mixed along this zone with the result that standard microfossil zonations were not easily applicable (Fornaciari, Chap. 1, this volume; Maruyama, Chap. 3, this volume; Kennett et al., Chap. 2, this volume). For example, the North Pacific diatom zonation of Akiba (1986) and Yanagisawa and Akiba (1998) could not readily be applied in the latest Miocene through early late Pliocene (Maruyama, Chap. 3, this volume).

Middle Miocene and the Early Late Miocene

California margin sediments changed from biogenic silica oozes in the middle Miocene to essentially pure terrigenous clastics by the early Pliocene. The evolution is clearly seen in the opal records of Janecek (Chap. 16, this volume, Fig. 37) as well as the shipboard sediment descriptions. We hypothesize that the changes in biogenic silica mark events in nutrient availability to the California margin, and that the system gradually switches from high-nutrient surface waters in the latest middle Miocene to surface waters almost barren of nutrients for at least a short interval in the earliest Pliocene. We do not yet understand how the conditions evolved, or even exactly what conditions existed, and further study to understand the evolution of paleoproductivity at the California margin will prove fruitful to a broader understanding of biogeochemical cycles in the oceans and the paleoceanography of the North Pacific in the middle Miocene (Vincent and Berger, 1985).

The first big drop in biogenic opal burial occurs during the same time period as the late/middle Miocene $CaCO_3$ crash around the isthmus of Panama (Lyle et al., 1995; Roth et al., 2000). The late/middle Miocene boundary appears to represent a time that thermohaline circulation reorganized, partly because of the initial closing of the Panama gateway, but partly because of intensification of North Atlantic Deep Water (Roth et al., 2000). The peak opal burial along the California margin (~8–9.5 Ma) is older than peak burial in the equatorial Pacific (~5–7 Ma, Farrell et al., 1995), hinting at an out-of-phase relationship between nutrient supply to the northeastern Pacific and the equatorial Pacific during the late Miocene.

Table 6. Miocene biohorizons from Leg 167 before earliest paleomagnetic stratigraphy.

Event	CK95 (Ma)	Depth (mcd) Site 1010	Site 1011	Site 1021
LCO *R. californica*	6.65	NR	185.78	223.66
FO *A. primus*	7.4	83.67	213.76	210.30
LCO *T. schraderi*	7.6	91.23	223.44	230.26
LO *M. convallis*	7.7	91.03	225.26	NR
FO *D. quinqueramus/berggrenii*	8.2	88.17	241.12	217.03
FCO *T. schraderi*	8.4	Diachronous	249.24	253.29
LCO *D. simonsenii*	8.6	105.13	255.54	253.29
LO *D. dimorpha*	9.16	112.07	274.80	262.08
FO *T. schraderi*	9.5	Diachronous	—	278.29
LO *D. hamatus*	9.5	114.23	—	NR
FO *Minylitha convallis*	9.8	114.23	—	274.04
FO *D. dimorpha*	9.9	115.71	—	278.29
FO *D. hamatus*	10.4	132.66	—	NR
FO *D. bellus*	10.5	132.66	—	281.44?
FO *C. coalitus*	10.8	132.66	—	291.27?
LCO *D. praedimorpha*	11.5	140.40	—	304.61
LO *C. floridanus*	11.6	156.11	—	NR
FO *D. kugleri*	12.0	152.25	—	NR
LO *C. premacintyrei*	12.1	170.04	—	NR
FO *D. praedimorpha*	12.9	172.37	—	<325.61
FCO *D. simonsenii*	13.1	192.81	—	—
LO *S. heteromorphus*	13.6	203.65	—	—

Notes: CK95 = age following Cande and Kent (1995). NR = not recorded. Stratigraphic depths reported here represent a midpoint between constraining samples.

The high opal intervals in both Sites 1010 and 1021 are also high $CaCO_3$, at least at the coarse scale for which we now have data. Future work will be needed to determine whether at high resolution we will find an alternation between the plankton groups or fine-scale coherence.

Latest Miocene

At Sites 1010 and 1011 off Baja California and at Site 1021 off Northern California, the abundance of diatoms in the sediments declined during the latest Miocene to earliest Pliocene in a series of steps, beginning at about 7.5 Ma (base of NPD7) and continuing further at about 6.5 and 5.1 Ma (see Maruyama, Chap. 3, this volume; Janecek, Chap. 16, this volume; and smear-slide data in Lyle, Koizumi, Richter, et al., 1997). This offshore restriction in diatom productivity coincided with the progressive focusing of upwelling and biosiliceous productivity into the coastal regions (Isaacs, 1985; Barron, 1998).

Comparison to the Monterey and Sisquoc Formations

The opal-rich sediments discovered offshore in Leg 167 correspond to the well-known diatom-rich sediments of the middle and late Miocene Monterey Formation of southern and central California. There are major differences, however. In the Monterey formation, opal MAR actually increases upsection but is hidden by high influxes of terrigenous debris (Isaacs, 1985). Opal MAR in the Santa Barbara area increases in a series of steps from 10 Ma, for example, reaching the highest MARs between 6 and 4 Ma in the Sisquoc Formation. Offshore we have noted something of a reverse pattern—highest opal deposition prior to 11 Ma, a low period around 10 Ma, and high deposition between 7.5 and 9 Ma, followed by step-like drops at about 7.5 and 5 Ma. It would appear that upwelling along the California margin evolved from a relatively broad feature (Site 1021 was more than 300 km offshore and is not by any stretch of the imagination within the coastal upwelling zone) in the middle and early late Miocene to a system concentrated on the coast in the latest Miocene and early Pliocene. We have no understanding why this happened, and follow-up studies, especially those that stratigraphically link the outcrops onshore to the Leg 167 drilling, should prove to be a fruitful new avenue of research.

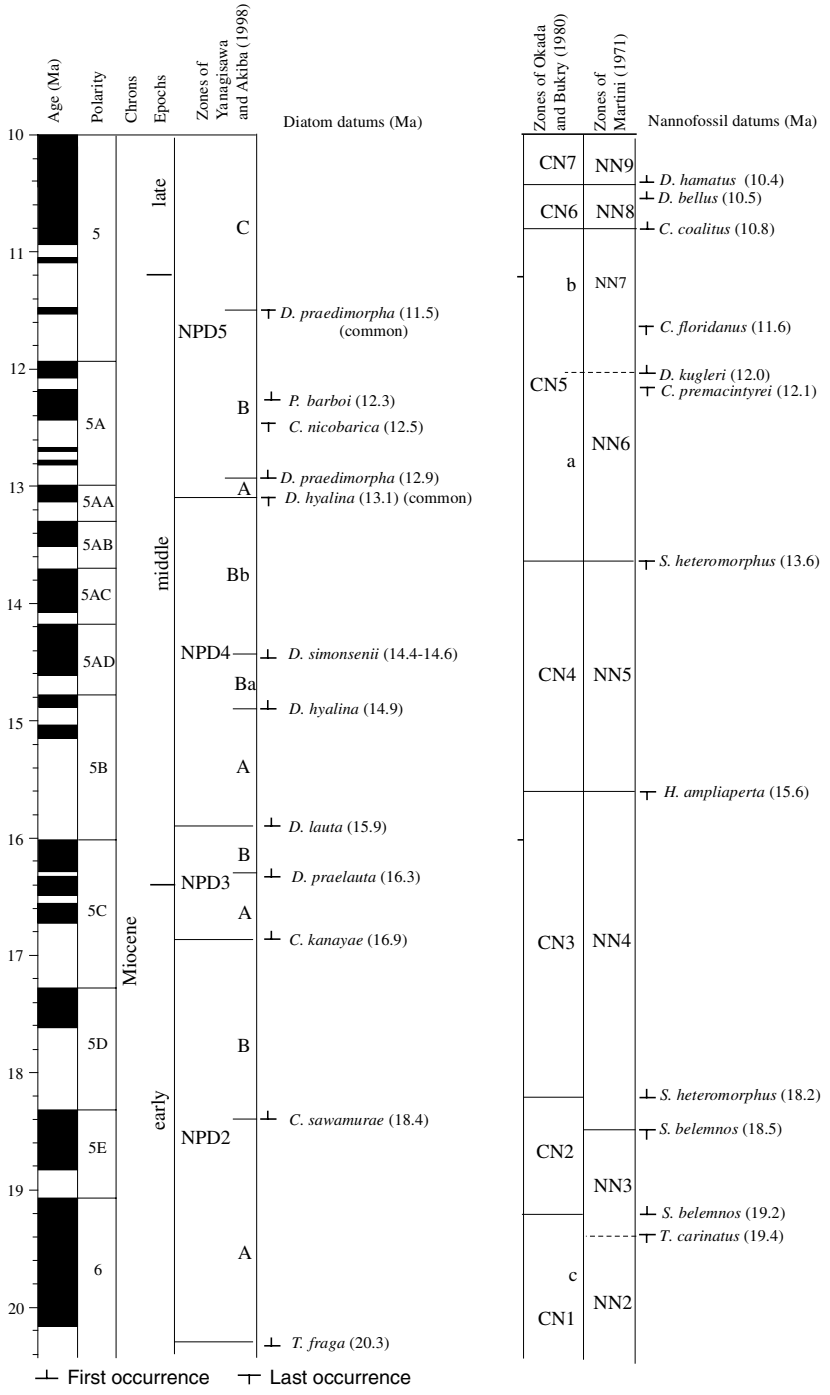

Figure 35. Biochronology of diatoms and calcareous nannofossils for the middle part of the Neogene (10–20 Ma) of the California margin (ODP Leg 167).The biostratigraphic datums are compared to the magnetochronostratigraphy of Cande and Kent (1995).

Pliocene

At about 4.5 Ma, coincident with the onset of a mid-Pliocene period of reduced latitudinal thermal gradients, diatom productivity virtually disappeared in the offshore waters of southern California (Barron, 1981; Maruyama, Chap. 3, this volume; Site 1016) and declined considerably at northern Site 1021 (Janecek, Chap. 16, this volume). The interval between about 5 and 4 Ma also tends to be an interval almost barren of foraminifers and calcareous nannofossils (Lyle, Koizumi, Richter, et al., 1997; Fornaciari, Chap. 1, this volume; Kennett et al., Chap. 2, this volume). This hiatus was also observed in Sites 467, 469, and 470 from DSDP Leg 63 (Barron, 1989).

Diatom productivity reappeared in strength only during the late Pliocene (at about 2.7–2.4 Ma) after a period of major high-latitude cooling led to enhanced upwelling along the California coast (Barron, 1998; Maruyama, Chap. 3, this volume; Janecek, Chap. 16, this volume). Latest Pliocene and Quaternary diatom assemblages in California waters are more comparable to those of the higher latitude North Pacific, and the zonation of Akiba (1986) and Yanagisawa and Akiba (1998) is applicable.

In contrast, high production of $CaCO_3$ appeared in the mid-Pliocene and dropped abruptly at 2.6 Ma (Ravelo et al., 1997), coincident to the major increase in ice rafting in the North Pacific associated with the formation of major Northern Hemisphere glaciers

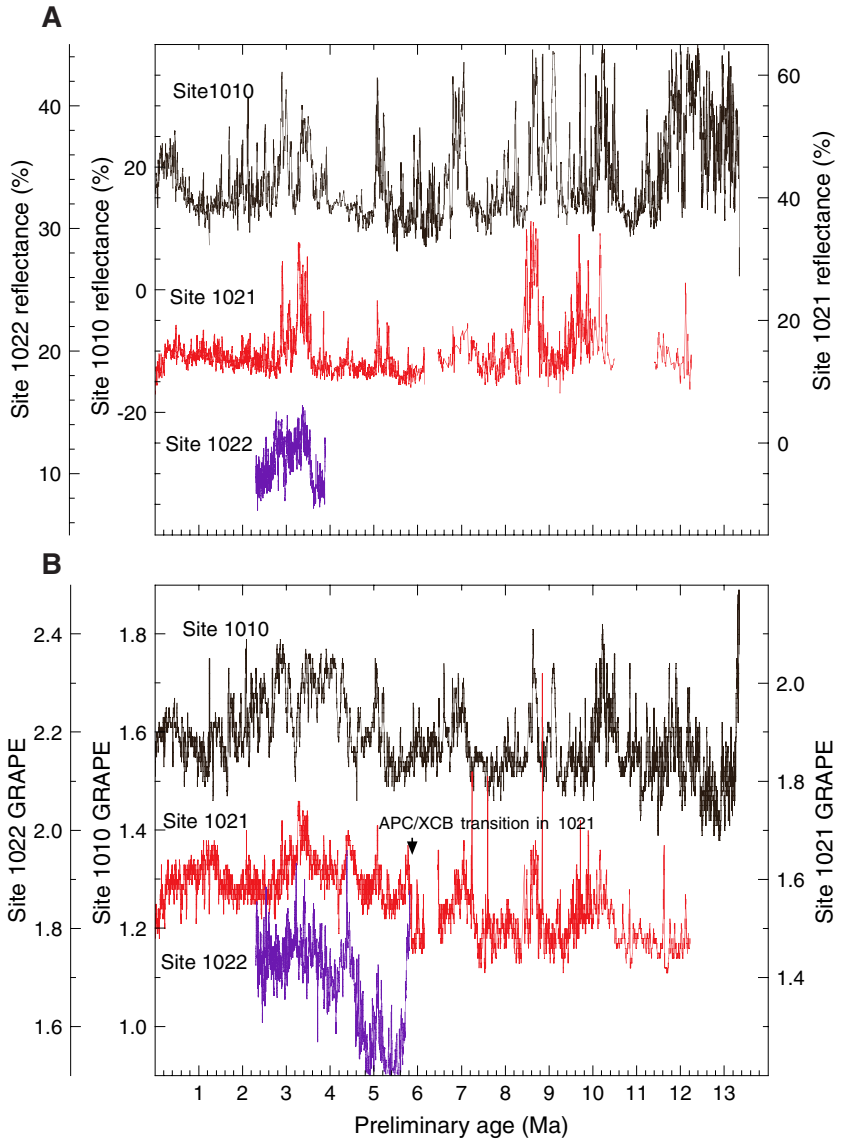

Figure 36. Comparison of (**A**) OSU SCAT reflectance data for the combined 450–500 nm (blue) channels and (**B**) GRAPE bulk density depth series from Sites 1010, 1021, and 1022 to show the potential of stratigraphies based upon physical properties.

(Krissek, 1995; Haug et al., 1995; Maslin et al., 1995). Ravelo et al. (1997) have concluded that the cause of the late Pliocene $CaCO_3$ event was high production, not low dissolution. There is a similarity in timing between the California margin event and the late Pliocene productivity pulse in the Alaska Gyre (Haug et al., 1995) that becomes less so to the south. Northern California margin sites (e.g., Sites 1020 and 1021) have a more abrupt termination at about 2.6 Ma. Southern California sites, in contrast, have a decrease in production at 2.6 Ma but continue to have high $CaCO_3$ burial until the Pliocene/Pleistocene boundary.

It is interesting to note that the late Pliocene $CaCO_3$ event is not unique along the California margin—events of similar intensity though not necessarily of similar duration can be found at roughly 5.2, 6.8, 8.8, 10, and 12–14 Ma (Fig. 36). The 5-Ma event may also be present in the North Pacific (Haug et al., 1995). It is uncertain why the North Pacific periodically becomes a major burial ground for $CaCO_3$, and it is worthy of further study.

The Tectonics–Climate Connection

One of the least explored research topics by Leg 167 researchers is the linkage of paleoceanographic and sedimentologic evolution of the northeastern Pacific with tectonic developments around the Pacific Basin. These include teleconnections from such events as the closure of the Panama Gateway and the uplift of the Himalaya Mountains. They also include the regional tectonics of western North America, because the formation of the Basin and Range and the uplift of the Sierra Nevada and the Cascade Range have probably affected basin configurations, runoff to the Pacific Ocean, and the strength and position of the northeast Pacific High (see Fig. 3). We will briefly explore some important issues here in the hopes of encouraging further research into the tectonic linkages.

Teleconnections

Three primary difficulties make it difficult to establish a definite link between a tectonic event (e.g., the rise of the Himalayas) and a major climate change. First and most important, there is rarely any good age control on the tectonic event so that it is usually difficult to prove conclusively that the tectonic and climate events happened at the same time. Second, tectonic events are long, and several important tectonic events may overlap. For example, the Panama Gateway closes during the same time interval in which the Himalayas are rising and the Indonesian Passage is closing. It is difficult to ascertain which event may be the critical factor for the climate change. Finally, climate may be sensitive not only to the final state but to some lesser threshold. For example, Lyle et al. (1995) have suggested that $CaCO_3$ burial was severely inhibited in the eastern Pacific Ocean when the

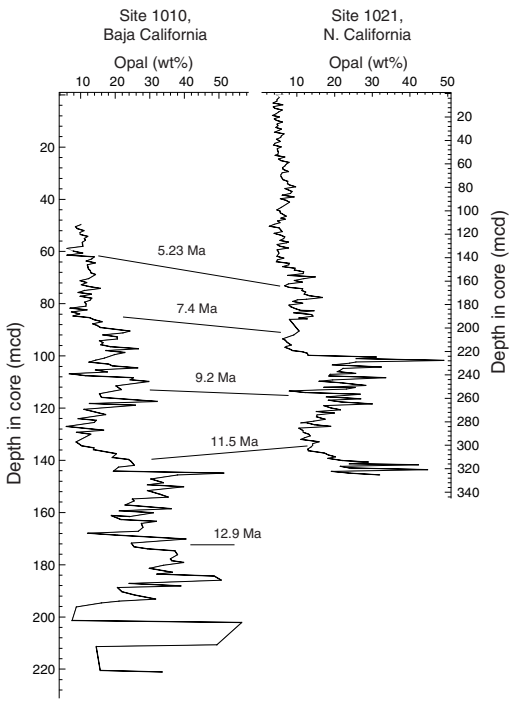

Figure 37. Biogenic silica abundance at Sites 1010 and 1021, from Janecek (Chap. 16, this volume). Correlations between the two drill sites are biostratigraphic. The change in environment from high opal deposition to low opal deposition is step-like, but the structure is not yet well understood.

deep-water connection through the Panama gateway was severed near the middle/late Miocene boundary, or about 7 m.y. before the final closure of the isthmus (Coates and Obando, 1996). A carbonate crash occurred on the Caribbean side of the Panama gateway also, but reached its peak extent about 2 m.y. before the Pacific side (Roth et al., 2000). A "simple" gateway closure can leave behind a complex sedimentary response.

The best way to come to an understanding of linkages between tectonics and climate is to continue to document events recorded in marine sediments and to improve our understanding of the timing of the tectonic processes.

The primary teleconnections that could be important to the development of the California Current system are the rise of the Himalayas, which could strengthen the Aleutian Low in the Subarctic North Pacific as the mountains rose (Kutzbach et al., 1993b); the closure of the Panama gateway, by modifying deep-water flow to the North Pacific (Haug and Tiedemann, 1998; Driscoll and Haug, 1998; and references therein); and closure of the Indonesian passage near the late/middle Miocene boundary, which should have enhanced heat transport northward in the western Pacific (Kennett et al., 1985; Romine and Lombari, 1985).

The uplift of the Himalayas, like all major orogenies, is a complex and long-lasting event. Initial uplift may have begun in the latest Oligocene, but there were two major later stages of mountain building in the Miocene and Pliocene (7.5–9 Ma and 3.5–4 Ma; Rea et al., 1998, and references therein). There is possibly a link between these mountain building events and (1) the loss of biogenic silica from Leg 167 sections around 8 Ma or (2) the beginning of the Pliocene $CaCO_3$ burial event on the California margin (~3.5–4 Ma; Ravelo et al., 1997). Any tie remains speculative without a specific hypothesis for the teleconnection between Himalayan uplift and productivity on the California margin, however.

There is little information on the closure of the Indonesian gateway, but oceanographic severance seems to have occurred in the period between 11.5 and 10 Ma, using modern age models with Romine and Lambari (1985) stratigraphy. Again this is enticingly close to a major decrease in biogenic silica content in the California margin sediments (~11.5 Ma; Fig. 37). However, this is also a period when it appears that the closure of the Panama Gateway cut off much of the deep-water exchange between the Caribbean and eastern Pacific Ocean (Lyle et al., 1995; Roth et al., 2000).

The closure of the Panama gateway is a favorite tectonic element to modify oceanographic conditions in both the Pacific and Atlantic Oceans in the period between the mid-Pliocene and the late/middle Miocene boundary. The timing of closure depends upon what one is tracing however. Closure times are about 9–11 Ma for deep-water exchange (Lyle et al., 1995), 8 Ma for a significant interoceanic biogeographic barrier (with a reopening around 6 Ma; Collins et al., 1996), 4.6–4.4 Ma for a surface-water barrier sufficient to make Caribbean surface water distinctive from Pacific surface water (Keigwin, 1982; Haug and Tiedemann, 1998, Billups et al., 1999), and 3.1–2.5 Ma for an uninterrupted land bridge and the initiation of mammal exchange between North and South America (Coates and Obando, 1996; Webb and Rancy, 1996).

Haug et al. (1998) have suggested that a strong teleconnection exists between the Panama gateway closure and North Pacific productivity and that this teleconnection caused the major Pliocene production event between 4.6 and 2.7 Ma. If there is a link, it should be shown in some manner along the California margin. Ravelo et al. (1997) have already pointed out the similarity between the mid-Pliocene carbonate burial event and the North Pacific production, because both end abruptly within the same interval. Further work to establish whether closure of the Panama gateway should produce these events should be a priority for late Neogene studies.

North American Region

The California margin of North America has had a complex tectonic history throughout the Neogene beginning with first the subduction of the Farallon Ridge in the Oligocene (Atwater and Stock, 1998; Bohannon and Parsons, 1995; and references in both papers) followed by the middle to late Miocene development of the Basin and Range province, a change in relative plate motions between the Pacific and North American plates in the late Miocene around 8 Ma (Atwater and Stock, 1998), the beginning of San Andreas fault motion around 6 Ma, and the uplift of the Sierra Nevada mountains since 10 Ma (1 km elevation at 10 Ma, 2 km elevation at 3 Ma, and 3 km elevation today; Huber, 1981). There are other, more speculative tectonic connections that might have affected the paleoceanographic evolution of the region. The most prominent of these is the possibility that the Mendocino Fracture Zone south of the Gorda spreading center may have been above sea level until about 5.5 Ma (Fisk et al., 1993). If the Mendocino Fracture Zone had been above sea level, it would have significantly altered California Current flow in the Miocene.

The Neogene records from Leg 167 potentially contain pertinent data on how local basins have responded to the changing tectonic regime, as well as how the regional tectonics have affected the climate and changed California Current circulation. Much if not all of this information has yet to be seriously studied. We note that a low-deposition event occurs throughout the California Borderlands (Sites 1011, 1012, and 1014) from the early Pliocene to late Miocene (>4 to perhaps 7 Ma; Fig. 38). This event is not found offshore (Fig. 39; Sites 1010, 1016, and 1021) and therefore appears to be regional to the California Borderlands. This may be linked to the initiation of the San Andreas fault system at about 6 Ma and a changing stress regime in the California Borderlands during the transition from movement on offshore faults to movement inshore of the borderlands region. More careful follow-up studies are needed to explore this possibility.

One would expect that uplift of the Sierra Nevada should have trapped more precipitation in western California and increased river gradients on the western slope of the Sierra Nevada Mountains. Both effects should cause an increased sediment load out of the mountain range from the Pliocene to the Holocene. Site 1018, because it lies

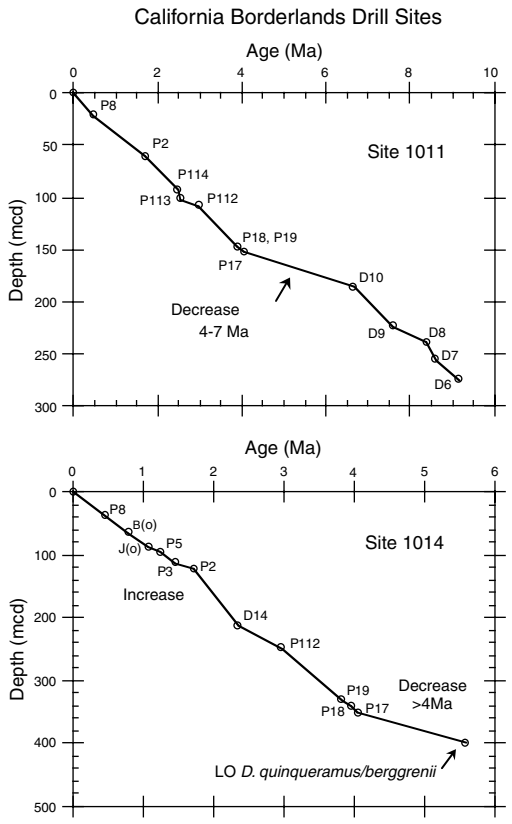

Figure 38. Age/depth plots for Sites 1011 and 1014 in the California Borderlands, illustrating the slowdown in sedimentation during the early Pliocene and late Miocene. Site 1013 (not shown) also had a hiatus in this interval.

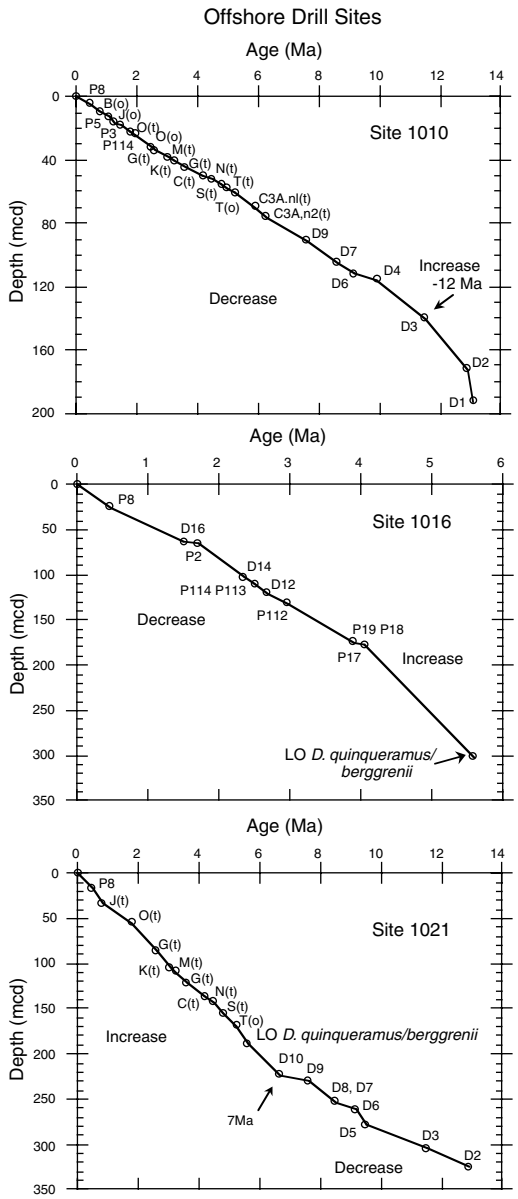

Figure 39. Age/depth plots for Sites 1010, 1016, and 1021 for the offshore drill sites along the California margin. The age/depth curves do not show the same pattern as sites around the California Borderland, indicating that the change in sedimentation in the borderlands reflects a regional process.

just south of the mouth of the Sacramento River drainage, should be the best place to monitor these changes. What we observe at the drill site shows no real trend since the late Pliocene, however. Instead, sedimentation rates average slightly less than 120 m/m.y. in the period from 2.4 to 0.46 Ma and jump to about 200 m/m.y. in the period from 0 to 0.46 Ma (Lyle, Koizumi, Richter, et al., 1997; Andreasen et al., Chap. 8, this volume). The upper sediment section has more coarse clastic debris and appears to have a higher deposition rate of terrestrial detritus. The major change in sedimentation at around 0.5 Ma may reflect the capture of sediments in the Great Valley of California prior to 0.5 Ma and their escape afterwards. Sarna-Wojcicki (1995) has suggested that a mid-Pleistocene lake ("Lake Clyde") existed up until about 0.6 Ma and drained to the ocean south of Site 1018. At 0.6 Ma, the lake cut an outlet through what is now San Francisco Bay, opening up the modern Sacramento River drainage. Thus, the record at Site 1018 may reflect not only climate and tectonics but also the geologic history of terrestrial sedimentary basins in California.

CONCLUSIONS

The first set of continuous sediment records older than the latest Pleistocene along the California margin were recovered during Leg 167. The recovery of these records and their assembly into continuous time series was one of the major shipboard accomplishments of the leg. Studies during Leg 167 and immediately postcruise have set the stage for a much more comprehensive understanding of the California current system and the sedimentary environment along the California margin.

Leg 167 studies have documented the high sensitivity of the California margin to millennial-scale climate forcing. There is a strong influence of Dansgaard-Oeschger events on surface-ocean conditions that suggests strong climate links between the northeastern Pacific Ocean and the North Atlantic. There is much yet to be done, however. Only a small percentage of the total available sediment column has been studied, so we do not yet have a sufficiently long historical perspective of the millennial-scale events or their relationship to orbitally forced insolation. We have not yet developed time series on sufficient numbers of different proxies to understand the cause of these events or the physical response of the North Pacific Ocean. We have not yet intercalibrated time scales to study the evolution of the millennial-scale events in a latitudinal sense.

We now have produced oxygen isotope stratigraphy for the late Pleistocene for seven drill sites, and alternate high-resolution stratigraphies based upon other sediment components are being developed. We have discovered that the California margin is highly sensitive to climate changes on orbitally forced time scales, and we have found that there is a major change in conditions about 400 ka, around MIS

11. Prior to this time we have much smaller variation of alkenone SST, and higher burial of biogenic remains along the northern California margin. These events do not seem as strong in the south, but we lack long high-resolution time series from the southern drill sites. There is also a need for better age control in Pleistocene sections older than about 200 ka for most of the Leg 167 drill sites. More long oxygen isotope profiles are needed for further work.

Orbitally forced insolation changes invoke a strong SST response along the California margin. SST measured by the alkenone $U^{k'}_{37}$ paleothermometer is highly coherent with the oxygen isotope record, being cold in glacials and much warmer in interglacials. By comparing northern and southern SST records it appears, somewhat paradoxically, that the glacial maxima were periods of weakest California current flow and the strong interglacials had strongest flow. Faunal and floral plankton assemblages vary strongly on the glacial–interglacial scale. Coastal plant communities show a glacial–interglacial variability that is most pronounced in the north, near the Cordilleran Ice Sheet.

We have identified but not really studied a series of major late Neogene oceanographic events. Opaline silica burial in the middle and upper Miocene sections of Sites 1010 and 1021 have step-like drops from high opal deposition in the middle Miocene. One major drop occurs at ~11 Ma. A second major drop occurs at about 7.5–8 Ma, equivalent in age to the end of the Monterey formation (Barron, 1998; other refs). A third drop occurs slightly younger than the end of the Miocene. We do not yet know why there is a disappearance of diatoms in the younger sections or periodic burial events. We have also identified $CaCO_3$ burial events at roughly 5.2, 6.8, 8.8, 10, and 12–14 Ma, coincident with but sometimes slightly offset from the opal peaks. We do not yet know the timing of these burial events with respect to each other nor the oceanographic dynamics that produced the sediment records.

A lower Pliocene interval, roughly from 5 to 4.2 Ma, is low in all biogenic components. It separates the Miocene high-opal sediments from upper Pliocene high-carbonate sediments. High $CaCO_3$ deposition occurred all along the entire California margin in the late Pliocene, but $CaCO_3$ burial dropped abruptly with the beginning of Northern Hemisphere glaciation (2.6 Ma).

The Neogene sections from Leg 167 are not well explored but indicate major periodic, poorly understood changes in oceanographic conditions since the middle Miocene. These sections represent the only detailed information we have to date on the temperate North Pacific Ocean and have the potential to provide valuable insights into global changes in Neogene paleoceanographic conditions and biogeochemical cycles.

ACKNOWLEDGMENTS

We thank the shipboard scientific party, the ODP technical support staff, and the captain and crew of the *JOIDES Resolution* for their outstanding efforts to make this leg so successful. Lyle was also supported by NSF Grant OCE-9811272 during the writing of this paper. We are also grateful to Mark Maslin for his review of the manuscript and suggestions that significantly improved the work.

REFERENCES

Akiba, F., 1986. Middle Miocene to Quaternary diatom biostratigraphy in the Nankai trough and Japan trench, and modified lower Miocene through Quaternary diatom zones for middle-to-high latitudes of the North Pacific. *In* Kagami, H., Karig, D.E., Coulbourn, W.T., et al., *Init. Repts. DSDP,* 87: Washington (U.S. Govt. Printing Office), 393–481.

Anderson, R.N., and Hobart, M.A., 1976. The relation between heat flow, sediment thickness, and age in the Eastern Pacific. *J. Geophys. Res.,* 81:2968–2989.

Atwater, T., and Stock, J., 1998. Pacific-North America plate tectonics of the Neogene southwestern United States: an update. *Int. Geol. Rev.,* 40:375–402.

Balsam, W.L., Otto-Bliesner, B.L., and Deaton, B.C., 1995. Modern and last glacial maximum eolian sedimentation patterns in the Atlantic Ocean interpreted from sediment iron oxide content. *Paleoceanography,* 10:493–507.

Barron, J.A., 1981. Late Cenozoic diatom biostratigraphy and paleoceanography of the middle-latitude eastern North Pacific, Deep Sea Drilling Project Leg 63. *In* Yeats, R.S., Haq, B.U., et al., *Init. Repts. DSDP,* 63: Washington (U.S. Govt. Printing Office), 507–538.

————, 1989. The late Cenozoic stratigraphic record and hiatuses of the northeast Pacific: results from the Deep Sea Drilling Project. *In* Winterer, E.L., Hussong, D.M., and Decker, R.W. (Eds.), *The Geology of North America* (Vol. N): *The Eastern Pacific Ocean and Hawaii.* Geol. Soc. Am., Geol. of North America Ser., 311–322.

————, 1992a. Neogene diatom datum levels in the equatorial and North Pacific. *In* Ishizaki, K., and Saito, T. (Eds.), *The Centenary of Japanese Micropaleontology:* Tokyo (Terra Sci. Publ.), 413–425.

————, 1992b. Paleoceanographic and tectonic controls on the Pliocene diatom record of California. *In* Tsuchi, R., and Ingle, J.C., Jr. (Eds.), *Pacific Neogene: Environment, Evolution, and Events:* Tokyo (Tokyo Univ. Press), 25–41.

————, 1998. Late Neogene changes in diatom sedimentation in the North Pacific. *J. Asian Earth Sci.,* 16:85–95.

Barron, J.A., and Gladenkov, A.Y., 1995. Early Miocene to Pleistocene diatom stratigraphy of Leg 145. *In* Rea, D.K., Basov, I.A., Scholl, D.W., and Allan, J.F. (Eds.), *Proc. ODP, Sci. Results,* 145: College Station, TX (Ocean Drilling Program), 3–19.

Behl, R.J., and Kennett, J.P., 1996. Brief interstadial events in the Santa Barbara Basin, NE Pacific, during the last 60 kyr. *Nature,* 379:243–246.

Billups, K., Ravelo, A.C., Zachos, J.C., and Norris, R.D., 1999. Link between oceanic heat transport, thermohaline circulation, and the Intertropical Convergence Zone in the early Pliocene Atlantic. *Geology,* 27:319–322.

Bohannon, R.G., and Parsons, T., 1995. Tectonic implications of post-30 Ma Pacific and North American relative plate motions. *Geol. Soc. Am. Bull.,* 107:937–959.

Bray, N.A., Keyes, A., and Morawitz, W.M.L., 1999. The California Current system in the Southern California Bight and the Santa Barbara Channel. *J. Geophys. Res.,* 104:7695–7714.

Brooks, J.M., Field, M.E., and Kennicutt, M.C., II, 1991. Observations of gas hydrates in marine sediments, offshore Northern California. *Mar. Geol.,* 96:103–108.

Brooks, R.R., Presley, B.J., and Kaplan, I.R., 1968. Trace elements in the interstitial waters of marine sediments. *Geochim. Cosmochim. Acta.,* 32:397–414.

Bukry, D., 1981. Pacific coast coccolith stratigraphy between Point Conception and Cabo Corrientes, Deep Sea Drilling Project Leg 63. *In* Yeats, R.S., Haq, B.U., et al., *Init. Repts. DSDP,* 63: Washington (U.S. Govt. Printing Office), 445–471.

Cande, S.C., and Kent, D.V., 1992. A new geomagnetic polarity time scale for the Late Cretaceous and Cenozoic. *J. Geophys. Res.,* 97:13917–13951.

————, 1995. Revised calibration of the geomagnetic polarity timescale for the Late Cretaceous and Cenozoic. *J. Geophys. Res.,* 100:6093–6095.

Cannariato, K.G., Kennett, J.P., and Behl, R.J., 1999. Biotic response to late Quaternary rapid climate switches in Santa Barbara Basin: ecological and evolutionary implications. *Geology,* 27:63–66.

Coates, A.G., and Obando, J.A., 1996. The geologic evolution of the Central American Isthmus. *In* Jackson, J.B.C., Budd, A.F., and Coates, A.G. (Eds.), *Evolution and Environment in Tropical America:* Chicago (Univ. of Chicago Press), 21–55.

Collins, L.S., Coates, A.G., Berggren, W.A., Aubry, M.-P., and Zhang, J., 1996. The late Miocene Panama isthmian strait. *Geology,* 24:687–690.

Dansgaard, W., Clausen, H.B., Gundestrup, N.S., Hammer, C.U., Johnsen, S.F., Kristinsdottir, P.M., and Reeh, N., 1982. A new Greenland deep ice core. *Science,* 218:1273–1277.

Dansgaard, W., Johnsen, S.J., Clausen, H.B., Dahl-Jensen, D., Gundestrup, N.S., Hammer, C.U., Hvidberg, C.S., Steffensen, J.P., Sveinbjörnsdottir, A.E., Jouzel, J., and Bond, G., 1993. Evidence for general instability of past climate from a 250-kyr ice-core record. *Nature,* 364:218–220.

Dean, W.E., and Gardner, J.V., 1998. Pleistocene to Holocene contrasts in organic matter production and preservation on the California continental margin. *Geol. Soc. Am. Bull.,* 110:888–899.

Dean, W.E., Gardner, J.V., and Piper, D.Z., 1997. Inorganic geochemical indicators of glacial-interglacial changes in productivity and anoxia on the California continental margin. *Geochim. Cosmochim. Acta,* 61:4507–4518.

Defense Mapping Agency Hydrographic/Topographic Center, 1989. *Sailing Directions (Planning Guide) for the North Pacific Ocean* (3rd ed.): DMA Publ., 152.

Doose, H., Prahl, F.G., and Lyle, M.W., 1997. Biomarker temperature estimates for modern and last glacial surface waters of the California Current system between 33° and 42°N. *Paleoceanography,* 12:615–622.

Driscoll, N.W., and Haug, G.H., 1998. A short circuit in thermohaline circulation: a cause for northern hemisphere glaciation? *Science,* 282:436–438.

Emery, K.O., 1960. *The Sea Off Southern California: A Modern Habitat of Petroleum:* New York (Wiley).

Farrell, J.W., Raffi, I., Janecek, T.C., Murray, D.W., Levitan, M., Dadey, K.A., Emeis, K.-C., Lyle, M., Flores, J.-A., and Hovan, S., 1995. Late Neogene sedimentation patterns in the eastern equatorial Pacific. *In* Pisias, N.G., Mayer, L.A., Janecek, T.R., Palmer-Julson, A., and van Andel, T.H. (Eds.), *Proc. ODP, Sci. Results,* 138: College Station, TX (Ocean Drilling Program), 717–756.

Field, M.E., and Kvenvolden, K.A., 1985. Gas hydrates on the California continental margin. *Geology,* 13:517–520.

Fisk, M.R., Duncan, R.A., Fox, C.G., and Witter, J.B., 1993. Emergence and petrology of the Mendocino Ridge. *Mar. Geophys. Res.,* 15:283–296.

Froelich, P.N., Klinkhammer, G.P., Bender, M.L., Luedtke, N.A., Heath, G.R., Cullen, D., Dauphin, P., Hammond, D., Hartman, B., and Maynard, V., 1979. Early oxidation of organic matter in pelagic sediments of the eastern equatorial Atlantic: suboxic diagenesis. *Geochim. Cosmochim. Acta,* 43:1075–1090.

Gallaway, P.J., 1997. Three-dimensional seismic mapping around Ocean Drilling Program Leg 167 Site 1019 (Site Survey CA-1): implications for sedimentation, deformation and evolution of the Eel River Basin [M.S. thesis]. Boise State Univ., Boise, Idaho.

Gardner, J.V., and Dartnell, P., 1995. Centennial-scale late Quaternary stratigraphies of carbonate and organic carbon from Santa Barbara Basin, Hole 893A, and their paleoceanographic significance. *In* Kennett, J.P., Baldauf, J.G., and Lyle, M. (Eds.), *Proc. ODP, Sci. Results,* 146 (Pt. 2): College Station, TX (Ocean Drilling Program), 103–124.

Gardner, J.V., Dean, W.E., and Dartnell, P., 1997. Biogenic sedimentation beneath the California Current system for the past 30 kyr and its paleoceanographic significance. *Paleoceanography,* 12:207–225.

Gardner, J.V., Heusser, L.E., Quinterno, P.J., Stone, S.M., Barron, J.A., and Poore, R.Z., 1988. Clear Lake record vs. the adjacent marine record: a correlation of their past 20,000 years of paleoclimatic and paleoceanographic responses. *In* Sims, J.D. (Ed.), *Late Quaternary Climate, Tectonism, and Sedimentation in Clear Lake, Northern California Coast Ranges.* Spec. Pap.—Geol. Soc. Am., 214:171–182.

Gieskes, J.M., Nevsky, B., and Chain, A., 1981. Interstitial water studies, Leg 63. *In* Yeats, R.S., Haq, B.U., et al., *Init. Repts. DSDP,* 63: Washington (U.S. Govt. Printing Office), 623–629.

Grootes, P.M., Stuvier, M., White, J.W.C., Johnsen, S., and Jouzel, J., 1993. Comparison of oxygen isotope records from the GISP2 and GRIP Greenland ice cores. *Nature,* 366:552–554.

Harris, S.E., Mix, A.C., and King, T., 1997. Biogenic and terrigenous sedimentation at Ceara Rise, western tropical Atlantic, supports Pliocene–Pleistocene deep-water linkage between hemispheres. *In* Shackleton, N.J., Curry, W.B., Richter, C., and Bralower, T.J. (Eds.), *Proc. ODP, Sci. Results,* 154: College Station, TX (Ocean Drilling Program), 331–345.

Haug, G.H., Maslin, M.A., Sarnthein, M., Stax, R., and Tiedemann, R., 1995. Evolution of northwest Pacific sedimentation patterns since 6 Ma (Site 882). *In* Rea, D.K., Basov, I.A., Scholl, D.W., and Allan, J.F. (Eds.), *Proc. ODP, Sci. Results,* 145: College Station, TX (Ocean Drilling Program), 293–314.

Haug, G.H., Sigman, D.M., Tiedemann, R., and Zahn, R., 1998. The Panamanian Isthmus formation, Atlantic Ocean circulation, and subarctic Pacific productivity: potential effects on Plio-Pleistocene climate. *Eos,* 79:F25.

Haug, G.H., and Tiedemann, R., 1998. Effect of the formation of the Isthmus of Panama on Atlantic Ocean thermohaline circulation. *Nature,* 393:673–676.

Hayashida, A., Verosub, K.L., Heider, F., and Leonhardt, R., 1999. Magnetostratigraphy and relative paleointensity of late Neogene sediments at ODP Leg 167 Site 1010 off Baja California. *Geophys. J. Int.*, 139:829–840.

Hendy, I.L., and Kennett, J.P., 1999. Latest Quaternary North Pacific surface water responses imply atmosphere-driven climate instability. *Geology,* 27:291–294.

Herbert, T.D., Schuffert, J.D., Thomas, D., Lange, K., Weinheimer, A., and Herguera, J.-C., 1998. Depth and seasonality of alkenone production along the California margin inferred from a core-top transect. *Paleoceanography,* 13:263–271.

Herbert, T.D., Yasuda, M., and Burnett, C., 1995. Glacial-interglacial sea-surface temperature record inferred from alkenone unsaturation indices, Site 893, Santa Barbara Basin. *In* Kennett, J.P., Baldauf, J.G., and Lyle, M. (Eds.), *Proc. ODP, Sci. Results,* 146 (Pt. 2): College Station, TX (Ocean Drilling Program), 257–264.

Heusser, L., 1998. Direct correlation of millennial-scale changes in western North American vegetation and climate with changes in the California Current system over the past ~60 kyr. *Paleoceanography,* 13:252–262.

Heusser, L.E., 1995. Pollen stratigraphy and paleoecologic interpretation of the 160-k.y. record from Santa Barbara Basin, Hole 893A. *In* Kennett, J.P., Baldauf, J.G., and Lyle, M. (Eds.), *Proc. ODP, Sci. Results,* 146 (Pt. 2): College Station, TX (Ocean Drilling Program), 265–279.

Hickey, B.M., 1979. The California Current System: hypotheses and facts. *Prog. Oceanogr.,* 8:191–279.

Hovland, M., Lysne, D. and Whiticar, M., 1995. Gas hydrate and sediment gas composition, Hole 892A. *In* Carson, B., Westbrook, G.K., Musgrave, R.J., and Suess, E. (Eds.), *Proc. ODP, Sci. Results,* 146 (Pt 1): College Station, TX (Ocean Drilling Program), 151–161.

Huber, N.K., 1981. Amount and timing of late Cenozoic uplift and tilt of the central Sierra Nevada, California: evidence from the upper San Joaquin River basin. *Geol. Surv. Prof. Pap. U.S.,* 1197:1–28.

Huyer, A., 1983. Coastal upwelling in the California Current system. *Prog. Oceanogr.,* 12:259–284.

Huyer, A., Korso, P.M., Fleischbein, J., Ramp, S.R., Stanton, T., Washburn, L., Chavez, F.P., Cowles, T.J., Pierce, S.D., and Smith, R.L., 1991. Currents and water masses of the coastal transition zone off northern California, June to August 1988. *J. Geophys. Res.,* 98:14809–14831.

Imbrie, J., Hays, J.D., Martinson, D.G., McIntyre, A., Mix, A.C., Morley, J.J., Pisias, N.G., Prell, W.L., and Shackleton, N.J., 1984. The orbital theory of Pleistocene climate: support from a revised chronology of the marine $\delta^{18}O$ record. *In* Berger, A., Imbrie, J., Hays, J., Kukla, G., and Saltzman, B. (Eds.), *Milankovitch and Climate* (Pt. 1), NATO ASI Ser. C, Math Phys. Sci., 126:269–305.

Isaacs, C.M., 1985. Abundance versus rates of accumulation in fine-grained strata of the Miocene Santa Barbara Basin, California. *Geo-Mar. Lett.,* 5:25–30.

Kastner, M., 1995. Data report: Chemistry of pore fluids in sediments of Hole 893A, Santa Barbara Basin. *In* Kennett, J.P., Baldauf, J.G., and Lyle, M. (Eds.), *Proc. ODP, Sci. Results,* 146 (Pt. 2): College Station, TX (Ocean Drilling Program), 331.

Kastner, M., Keene, J.B., and Gieskes, J.M., 1977. Diagenesis of siliceous oozes, I. Chemical controls on the rate of opal-A to opal-CT transformation—an experimental study. *Geochim. Cosmochim. Acta,* 41:1041–1059.

Kastner, M., Kvenvolden, K.A., Whiticar, M.J., Camerlenghi, A., and Lorenson, T.D., 1995. Relation between pore fluid chemistry and gas hydrates associated with bottom-simulating reflectors at the Cascadia Margin, Sites 889 and 892. *In* Carson, B., Westbrook, G.K., Musgrave, R.J., and Suess, E. (Eds.), *Proc. ODP, Sci. Results,* 146 (Pt 1): College Station, TX (Ocean Drilling Program), 175–187.

Keigwin, L., 1982. Isotopic paleoceanography of the Caribbean and East Pacific: role of Panama Uplift in late Neogene time. *Science,* 217:350–353.

Kennett, J.P., 1995. Latest Quaternary benthic oxygen and carbon isotope stratigraphy: Hole 893A, Santa Barbara Basin, California. *In* Kennett, J.P., Baldauf, J.G., and Lyle, M. (Eds.), *Proc. ODP, Sci. Results,* 146 (Pt. 2): College Station, TX (Ocean Drilling Program), 3–18.

Kennett, J.P., Baldauf, J.G., and Lyle, M. (Eds.), 1995. *Proc. ODP, Sci. Results,* 146 (Pt. 2): College Station, TX (Ocean Drilling Program).

Kennett, J.P., and Ingram, B.L., 1995. Paleoclimatic evolution of Santa Barbara basin during the last 20 k.y.: marine evidence from Hole 893A. *In* Kennett, J.P., Baldauf, J.G., and Lyle, M. (Eds.), *Proc. ODP, Sci. Results,* 146 (Pt. 2): College Station, TX (Ocean Drilling Program), 309–325.

Kennett, J.P., Keller, G., and Srinivasan, M.S., 1985. Miocene planktonic foraminiferal biogeography and paleoceanographic development of the Indo-Pacific region. *In* Kennett, J.P. (Ed.), *The Miocene Ocean: Paleoceanography and Biogeography.* Mem.—Geol. Soc. Am., 163:197–236.

Kennett, J.P., and Venz, K., 1995. Late Quaternary climatically related planktonic foraminiferal assemblage changes: Hole 893A, Santa Barbara Basin, California. *In* Kennett, J.P., Baldauf, J.G., and Lyle, M. (Eds.), *Proc. ODP, Sci. Results,* 146 (Pt. 2): College Station, TX (Ocean Drilling Program), 281–293.

Koizumi, I., 1992. Diatom biostratigraphy of the Japan Sea: Leg 127. *In* Pisciotto, K.A., Ingle, J.C., Jr., von Breymann, M.T., Barron, J., et al., *Proc.*

ODP, Sci. Results, 127/128 (Pt. 1): College Station, TX (Ocean Drilling Program), 249–289.

Krissek, L.A., 1995. Late Cenozoic ice-rafting records from Leg 145 sites in the North Pacific: late Miocene onset, late Pliocene intensification, and Pliocene–Pleistocene events. *In* Rea, D.K., Basov, I.A., Scholl, D.W., and Allan, J.F. (Eds.), *Proc. ODP, Sci. Results,* 145: College Station, TX (Ocean Drilling Program), 179–194.

Kutzbach, J.E., 1987. Model simulations of the climatic patterns during the deglaciation of North America. *In* Ruddiman, W.F., and Wright, H.E. Jr., (Eds.), *North America and Adjacent Oceans During the Last Deglaciation.* Geol. Soc. Am., Geol. of North Am. Ser., K:425–447.

Kutzbach, J.E., Guetter, P.J., Behling, P., and Selin, R., 1993a. Simulated climatic changes: results of the COHMAP climate-model experiments. *In* Wright, HE. Jr., Kutzbach, J.E., Webb, T., III., Ruddiman, W.F., Street-Perrott, F.A., Bartlein, P.J. (Eds.), *Global Climates since the last Glacial Maximum:* Minneapolis (Univ. Minn. Press), 24–94.

Kutzbach, J.E., Prell, W.L., and Ruddiman, W.F., 1993b. Sensitivity of Eurasian climate to surface uplift of the Tibetan Plateau. *J. Geol.,* 101:177–190.

Lawrence, J.R., and Gieskes, J.M., 1981. Constraints on water transport and alteration in the oceanic crust from the isotopic composition of pore water. *J. Geophys. Res.,* 86:7924–7934.

Levitus, S., and Boyer, T.P., 1994. *World Ocean Atlas 1994* (Vol. 4)*: Temperature.* NOAA Atlas NESDIS 4.

Lund, D.C., and Mix, A.C., 1998. Millennial-scale deep-water oscillations: reflections of the North Atlantic in the deep Pacific from 10 to 60 Ka. *Paleoceanography,* 13:10–19.

Lyle, M., 1998. Neogene carbonate burial in the Pacific Ocean. *Eos,* 79: F464.

Lyle, M., Dadey, K.A., and Farrell, J.W., 1995. The late Miocene (11–8 Ma) eastern Pacific carbonate crash: evidence for reorganization of deep-water circulation by the closure of the Panama Gateway. *In* Pisias, N.G., Mayer, L.A., Janecek, T.R., Palmer-Julson, A., and van Andel, T.H. (Eds.), *Proc. ODP, Sci. Results,* 138: College Station, TX (Ocean Drilling Program), 821–838.

Lyle, M., Koizumi, I., Richter, C., et al., 1997. *Proc. ODP, Init. Repts.,* 167: College Station, TX (Ocean Drilling Program).

Lyle, M., Zahn, R., Prahl, F., Dymond, J., Collier, R., Pisias, N., and Suess, E., 1992. Paleoproductivity and carbon burial across the California Current: the Multitracers Transect, 42°N. *Paleoceanography,* 7:251–272.

Lynch-Stieglitz, J., Curry, W.B., and Slowey, N., 1999. A geostrophic transport estimate for the Florida Current from the oxygen isotope composition of benthic foraminifera. *Paleoceanography,* 14:360–373.

Lynn, R.J., and Simpson, J.J., 1987. The California Current system: the seasonal variability of its physical characteristics. *J. Geophys. Res.,* 92:12947–12966.

MacKay, M.E., Jarrard, R.D., Westbrook, G.K., and Hyndman, R.D., 1994. Origin of bottom-simulating reflectors: geophysical evidence from the Cascadia accretionary prism. *Geology,* 22:459–462.

Madrid, V.M., Stuart, R.M., and Verosub, K.L., 1986. Magnetostratigraphy of the late Neogene Purisima Formation, Santa Cruz County, California. *Earth Planet. Sci. Lett.,* 79:431–440.

Mangelsdorf, K., Güntner, U., and Rullkötter, J., in press. Glacial-interglacial variability of climate and oceanographic conditions on the California continental margin during the last 160 kyr. *Org. Geochem.*

Maslin, M.A., Haug, G.H., Sarnthein, M., Tiedemann, R., Erlenkeuser, H., and Stax, R., 1995. Northwest Pacific Site 882: the initiation of Northern Hemisphere glaciation. *In* Rea, D.K., Basov, I.A., Scholl, D.W., and Allan, J.F. (Eds.), *Proc. ODP, Sci. Results,* 145: College Station, TX (Ocean Drilling Program), 315–329.

Mathews, M., 1986. Logging characteristics of methane hydrate. *The Log Analyst,* 27:26–63.

Mathews, M.A., and von Huene, R., 1985. Site 570 methane hydrate zone. *In* von Huene, R., Aubouin, J., et al., *Init. Repts. DSDP,* 84: Washington (U.S. Govt. Printing Office), 773–790.

McManus, J., Berelson, W.M., Coale, K.H., Johnson, K.S., and Kilgore, T.E., 1997. Phosphorus regeneration in continental margin sediments. *Geochim. Cosmochim. Acta,* 61:2891–2907.

McManus, J.F., Bond, G.C., Broecker, W.S., Johnsen, S., Labeyrie, L., and Higgins, S., 1994. High-resolution climate records from the North Atlantic during the last interglacial. *Nature,* 371:326–329.

Meese, D., Alley, R., Gow, T., Grootes, P.M., Mayewski, P., Ram, M., Taylor, K., Waddington, E., and Zielinski, G., 1994. Preliminary depth-age scale of the GISP2 ice core. *CRREL Spec. Rep.,* 94–1.

Mix, A.C., Lund, D.C., Pisias, N.G., Bodén, P., Bornmalm, L., Lyle, M., and Pike, J., 1999. Millenial-scale oscillations in the northeast Pacific: patterns and possible causes. *In* Webb, R.S., Clark, P.U., and Keigwin, L. (Eds.), *Mechanisms of Millennial-scale Global Climate Change.* Am. Geophys. Union, Geophys. Monogr. Ser., 112:127–149.

Moore, T.C., Jr., 1973. Late Pleistocene-Holocene oceanographic changes in the northeastern Pacific. *Quat. Res.,* 3:99–109.

Murray, D.W., Farrell, J.W., and McKenna, V., 1995. Biogenic sedimentation at Site 847, eastern equatorial Pacific Ocean during the past 3 m.y. *In* Pisias, N.G., Mayer, L.A., Janecek, T.R., Palmer-Julson, A., and van Andel, T.H. (Eds.), *Proc. ODP, Sci. Results,* 138: College Station, TX (Ocean Drilling Program), 429–459.

Norton, F.L., III, Hausman, E.D., and McElroy, M.B., 1997. Hydrospheric transports, the oxygen isotope record, and tropical sea surface temperatures during the last glacial maximum. *Paleoceanography,* 12:15–22.

Oeschger, H., Stauffer, B., Finkel, R., and Langway, C.C.J., 1985. Variations of the CO_2 concentration of occluded air and of anions and dust in polar ice cores. *In* Sundquist, E.T., and Broecker, W.S. (Eds.), The Carbon Cycle and Atmospheric CO2: Natural Variations Archean to Present. *Am. Geophys. Union, Geophys. Monogr.,* 32:132–143.

Okada, H., and Bukry, D., 1980. Supplementary modification and introduction of code numbers to the low-latitude coccolith biostratigraphic zonation (Bukry, 1973; 1975). *Mar. Micropaleontol.,* 5:321–325.

Omarzai, S.K., Coe, R.S., and Barron, J.A., 1993. Magnetostratigraphy: a powerful tool for high-resolution dating and correlation in the Miocene Monterey Formation of California: results from Shell Beach section, Pismo Basin. *In* Aissaoui, D.M., McNeill, D.F., and Hurley, N.F. (Eds.), *Applications of Paleomagnetism to Sedimentary Geology.* Spec. Publ.—Soc. Econ. Paleontol. Mineral., 49:95–111.

Ortiz, J.D., and Mix, A.C., 1997. Comparison of Imbrie-Kipp transfer function and modern analog temperature estimates using sediment trap and core top foraminiferal faunas. *Paleoceanography,* 12:175–190.

Ortiz, J., Mix, A., Hostetler, S., and Kashgarian, M., 1997. The California Current of the last glacial maximum: reconstruction at 42 degrees N based on planktonic foraminifera. *Paleoceanography,* 12:191–205.

Pares-Sierra, A., and O'Brien, J.J., 1989. The seasonal and interannual variability of the California Current system: a numerical model. *J. Geophys. Res.,* 94:3159–3180.

Paull, C.K., Matsumoto, R., Wallace, P.J., et al., 1996. *Proc. ODP, Init. Repts.,* 164: College Station, TX (Ocean Drilling Program).

Pike, J., Bodén, P., Lyle, M., Heusser, L., Mix, A., Bornmalm, L., and Alvarado, F., 1998. High-resolution deglacial climate record from Eel River Basin, Northern California margin, ODP Site 1019. *1st PAGES Open Sci. Meet.*

Prahl, F.G., Collier, R.B., Dymond, J., Lyle, M., and Sparrow, M.A., 1993. A biomarker perspective on prymnesiophyte productivity in the northeast Pacific Ocean. *Deep-Sea Res. Part A,* 40:2061–2076.

Prahl, F.G., Pisias, N., Sparrow, M.A., and Sabin, A., 1995. Assessment of sea-surface temperature at 42° N in the California Current over the last 30,000 years. *Paleoceanography,* 10:763–773.

Ravelo, A.C., Lyle, M., Koizumi, I., Caulet, J.P., Fornaciari, E., Hayashida, A., Heider, F., Hood., J., Hovan, S., Janecek, T., Janik, A., Stax, R., Yamamoto, M., and Leg 167 Scientific Party, 1997. Pliocene carbonate accumulation along the California margin. *Paleoceanography,* 12:729–741.

Rea, D.K., Snoeckx, H., and Joseph, L.H., 1998. Late Cenozoic eolian deposition in the North Pacific: Asian drying, Tibetan uplift, and cooling of the northern hemisphere. *Paleoceanography,* 13:215–224.

Reimers, C.E., Ruttenberg, K.C., Canfield, D.E., Christiansen, M.B., and Martin, J.B., 1996. Porewater pH and authigenic phases formed in the uppermost sediments of the Santa Barbara Basin. *Geochim. Cosmochim. Acta,* 60:4037–4057.

Roessler, C.S., and Chelton, D.B., 1987. Zooplankton variability in the California Current, 1951–1982. *Calif. Coop. Oceanic Fish. Invest. Repts.,* 28:59–96.

Romine, K., and Lombari, G., 1985. Evolution of Pacific circulation in the Miocene: radiolarian evidence from DSDP Site 289. *In* Kennett, J.P. (Ed.), *The Miocene Ocean: Paleoceanography and Biogeography.* Mem.—Geol. Soc. Am., 163:273–290.

Roth, J.M., Droxler, A.W., and Kameo, K., 2000. The Caribbean carbonate crash at the middle to late Miocene transition: linkage to the establishment of the modern global ocean conveyer. *In* Leckie, R.M., Sigurdsson, H., Acton, G.D., and Draper, G. (Eds.), *Proc. ODP, Sci. Results,* 165: College Station, TX (Ocean Drilling Program), 249–273.

Sabin, A.L., 1994. Holocene and latest Pleistocene paleoceanography of the northeast Pacific and its relationship to climate change in the Pacific Northwest [M.S. thesis]. Oregon State Univ., Corvallis, OR.

Sancetta, C., Lyle, M., Heusser, L., Zahn, R., and Bradbury, J.P., 1992. Late-glacial to Holocene changes in winds, upwelling, and seasonal production of the Northern California current system. *Quat. Res.,* 38:359–370.

Sarna-Wojcicki, A.M., 1995. Age, areal extent, and paleoclimatic effects of "Lake Clyde," a mid-Pleistocene lake that formed the Corcoran Clay, Great Valley, California. *Glacial History of the Sierra Nevada, California: a Symposium in Memorial to Clyde Wahrhaftig.*

Shaw, T.J., Gieskes, J.M., and Jahnke, R.A., 1990. Early diagenesis in differing depositional environments: the response of transition metals in pore water. *Geochim. Cosmochim. Acta,* 54:1233–1246.

Sholkovitz, E., 1973. Interstitial water chemistry of the Santa Barbara Basin sediments. *Geochim. Cosmochim. Acta,* 37:2043–2073.

Sowers, T., Bender, M., Labeyrie, L., Martinson, D., Jouzel, J., Raynaud, D., Pichon, J.J., and Korotkevich, Y., 1993. 135,000 year Vostok-SPECMAP common temporal framework. *Paleoceanography,* 8:737–766.

Spence, G.D., Minshull, T.A., and Fink, C., 1995. Seismic studies of methane gas hydrate, offshore Vancouver Island. *In* Carson, B., Westbrook, G.K., Musgrave, R.J., and Suess, E. (Eds.), *Proc. ODP, Sci. Results,* 146 (Pt 1): College Station, TX (Ocean Drilling Program), 163–174.

Stuiver, M., Grootes, P.M., and Braziunas, T.F., 1995. The GISP2 Delta 18-O climate record of the past 16,500 years and the role of the sun, ocean, and volcanoes. *Quat. Res.,* 44:341–354.

Talley, L.D., and Roemmich, D., 1991. Map Set for "Joseph L. Reid: a tribute in recognition of 40 years of contributions to Oceanography" special volume. *Deep-Sea Res.,* 38: Supp. 1A.

Thunell, R.C., and Mortyn, P.G., 1995. Glacial climate instability in the Northeast Pacific Ocean. *Nature,* 376:504–506.

Tréhu, A.M., Lin, G., Maxwell, E., and Goldfinger, C., 1995. A seismic reflection profile across the Cascadia subduction zone offshore central Oregon: new constraints on methane distribution and crustal structure. *J. Geophys. Res.,* 100:15101–15116.

Vincent, E., and Berger, W.H., 1985. Carbon dioxide and polar cooling in the Miocene: the Monterey Hypothesis. *In* Sundquist, E.T., and Broecker, W.S. (Eds.), *The Carbon Cycle and Atmospheric CO_2: Natural Variations Archean to Present.* Geophys. Monogr., Am. Geophys. Union, 32:455–468.

Webb, S.D., and Rancy, A., 1996. Late Cenozoic evolution of the neotropical mammal fauna. *In* Jackson, J.B.C., Budd, A.F., and Coates, A.G. (Eds.), *Evolution and Environment in Tropical America:* Chicago (Univ. of Chicago Press), 335–359.

Weber, M.E., Wiedicke, M., Riech, V., and Erlenkeuser, H., 1995. Carbonate preservation history in the Peru Basin: paleoceanographic implications. *Paleoceanography,* 10:775–800.

Yanagisawa, Y., and Akiba, F., 1998. Refined Neogene diatom biostratigraphy for the northwest Pacific around Japan, with an introduction of code numbers for selected diatom biohorizons. *J. Geol. Soc. Jpn.,* 104:395–414.

Yuan, T., Hyndman, R.D., Spence, G.D., and Desmons, B., 1996. Seismic velocity increase and deep-sea gas hydrate concentration above a bottom-simulating reflector on the northern Cascadia Continental Slope. *J. Geophys. Res.,* 101:13655–13671.

Date of initial receipt: 9 July 1999
Date of acceptance: 2 September 1999
Ms 167SR-238